

The National Academy of Sciences of Ukraine
The E.O. Paton Electric Welding Institute of the NAS of Ukraine
International Association «Welding»

Editor-in-Chief B.E. Paton

Editorial board:

Yu.S.Borisov V.F.Grabin
Yu.Ya.Gretskii A.Ya.Ishchenko
V.F.Khorunov
S.I.Kuchuk-Yatsenko
Yu.N.Lankin V.K.Lebedev
V.N.Lipodaev L.M.Lobanov
V.I.Makhnenko A.A.Mazur
L.P.Mojsov V.F.Moshkin
O.K.Nazarenko V.V.Peshkov
I.K.Pokhodnya I.A.Ryabtsev
V.K.Sheleg Yu.A.Sterenbogen
N.M.Voropai K.A.Yushchenko
V.N.Zamkov A.T.Zelnichenko

«The Paton Welding Journal»
is published monthly by the
International Association «Welding»

Promotion group:

V.N.Lipodaev, V.I.Lokteva
A.T.Zelnichenko (Exec. director)

Translators:

S.A.Fomina, I.N.Kutianova,
T.K.Vasilenko

Editorial and advertising offices
are located at PWI,
International Association «Welding»,
11, Bozhenko str., 03680,
Kyiv, Ukraine

Tel.: (38044) 227 67 57
Fax: (38044) 268 04 86
E-mail: tomik@mac.relc.com
E-mail: office@paton.kiev.ua

State Registration Certificate
KV 4790 of 09.01.2001

Subscriptions:

\$460, 12 issues, postage included

«The Paton Welding Journal» Website:
<http://www.nas.gov.ua/pwj>

CONTENTS

SCIENTIFIC AND TECHNICAL

- Makhnenko V.I., Shekera V.M., Kravtsov T.G. and Sevryukov V.V.** Effect of subsequent mechanical treatment on redistribution of residual stresses in surfaced shafts 2
- Trufyakov V.I., Shonin V.A., Mashin V.S. and Romanovsky D.S.** Application of high-frequency peening to improve the fatigue resistance of butt welded joints in aluminium alloys 6
- Labur T.M., Bondarev Andr.A., Lozovskaya A.V., Mashin V.S. and Poklyatsky A.G.** Influence of welding process on fracture resistance of joints in aluminium-lithium alloys 1420 and 1460 11
- Lazebnov P.P.** Statistic analysis of corrosion resistance of chromium-nickel deposited metal in alkali solutions 16
- Goncharov I.A., Paltsevich A.P. and Tokarev V.S.** Effect of hydrogen in low-alloyed weld metal on pore formation in submerged arc welding 20

INDUSTRIAL

- Tarasov N.M. and Kapustin S.S.** Arc spot welding of aluminium alloy thin-sheet elements using a drop dosing of electrode metal 24
- Barvinko Yu.P., Golinko V.M., Barvinko A.Yu., Perelmuter A.V. and Kuleba G.V.** Improvement of performance of vertical erection welded joints in the wall of cylindrical tanks made of coiled blanks 27
- Poklyatsky A.G. and Grinyuk A.A.** Effect of parameters of asymmetric and modulated currents on quality of aluminium alloy welded joints 33
- Yushchenko K.A., Kovalenko D.V. and Kovalenko I.V.** Application of activators for TIG welding of steels and alloys 37
- Radziyevsky V.N., Tkachenko G.G. and Gartsunov Yu.F.** Autovacuum brazing of steel impellers of centrifugal compressors 44
- Zyakhor I.V.** Modern equipment for friction welding 48
- ADVERTISING 53



EFFECT OF SUBSEQUENT MECHANICAL TREATMENT ON REDISTRIBUTION OF RESIDUAL STRESSES IN SURFACED SHAFTS

V.I. MAKHNENKO¹, V.M. SHEKERA¹, T.G. KRAVTSOV² and V.V. SEVRYUKOV³

¹The E.O. Paton Electric Welding Institute, NASU, Kyiv, Ukraine

²Mariupol Department of the Odessa State Marine Academy, Odessa, Ukraine

³Ministry of Transport of Ukraine, Kyiv, Ukraine

ABSTRACT

Residual stresses formed in surfaced shafts and influencing their cyclic loading resistance have been experimentally studied. It is shown that subsequent mechanical treatment of the shafts (roll burnishing, ultrasonic shock peening, explosion treatment) induces compressive stresses in the surface layer.

Key words: *surfacing, shaft model, residual stresses, roll burnishing, ultrasonic shock peening, calculation, experiment*

Surfacing is one of the most efficient methods for reconditioning of surfaces of parts and imparting them certain functional properties. The surfacing method is successfully used in water transport to impart corrosion resistance, e.g. in sea water, to different surfaces, such as parts of the type of shafts, different mechanisms and devices. However, in many cases the quality of a surfaced shaft may be determined not only by the corrosion resistance of its surface, but to a substantial degree by its resistance to cyclic loading. This problem is covered in sufficient detail in literature [1, 2, etc.]. So, here there is no need to dwell on it at length. What should be noted is just that the cyclic loading resistance of the surfaced shaft depends to a considerable degree upon geometrical and physical heterogeneities formed during the surfacing process and caused by corresponding micro- and macrodiscontinuities, microstructural defects and residual stresses. Therefore, the challenge in application of the surfacing technology is to decrease the degree of manifestation of the above factors by selecting rational parameters and conditions of surfacing and subsequent treatment of a surfaced part. In a number of cases the latter may favour a substantial increase in fatigue resistance through redistribution of residual stresses and changes in properties of the material of a surfaced part.

The subsequent treatment of the surfaced shafts may be of two types: heat and mechanical treatment. Both are aimed at improvement of microstructure and providing of favourable distribution of residual stresses, which eventually should lead to an increase in fatigue resistance. High tempering is the most common type of subsequent heat treatment. It leads to an essential relaxation of residual stresses after surfacing and, to a certain degree, to an improvement of microstructures of the HAZ metal under rather severe temperature conditions of surfacing, which cause formation of quenching structures. From this standpoint,

high tempering is undoubtedly a very efficient operation for improvement of fatigue resistance of the shafts made from ferritic-pearlitic steel, where the deposited layer is identical in its properties to the base metal, which is a characteristic feature of reconditioning surfacing.

In the case of deposition of a corrosion-protective layer of austenitic steel, differences in properties of the base and deposited metals lead to formation of new residual stresses after tempering. In this case a very high tensile stresses may be formed in the deposited layer near the fusion zone. It means that heat treatment of the surfaced shaft is of low efficiency in terms of decreasing residual stresses. In addition, it should be taken into account that holding of the surfaced shaft at temperatures of high tempering leads to a marked intensification of the processes of carbide formation and embrittlement of the material near the fusion zone, which may cause a substantial decrease in the fatigue strength at the presence of fatigue crack initiators. This is one of the main reasons of a wide interest of developers in different methods of mechanical treatment of the surfaced shafts, primarily in terms of producing a more favourable distribution of residual stresses and simultaneous strengthening due to cold working of the surface layer in which the fatigue cracks are initiated.

The most common methods of mechanical treatment are as follows: roll burnishing [3, 4, etc.], explosion treatment [5, etc.] and ultrasonic shock peening (USP) [6 – 8, etc.]. Unfortunately, no results of comparative investigations, on the basis of which it would be possible to evaluate advantages of this or that method of mechanical treatment for shafts with a deposited corrosion protective layer of austenitic steel, are available in the literature. The objective of this study was to clarify this issue.

For this purpose the comprehensive investigations were conducted to study distribution of residual stresses in a model of the shaft made from carbon St.35 (C – 0.33; Mn – 0.8; Si – 0.36; Cr – 0.07;

Variants of mechanical treatment of the shaft model of St.35 surfaced using wire Sv-05Kh20N9FBS

No. of variant	Sample index	Method of treatment
1	XV	Without mechanical treatment
2	I	Roll burnishing
3	XII	Same
4	VIII	»
5	XVIII	Explosion treatment
6	XVII	Same
7	XX	USP using a tool which was in service for some time
8	XI	Same
9	XXI	»
10	XVI	USP with preheating to 400 °C
11	XXII	Same

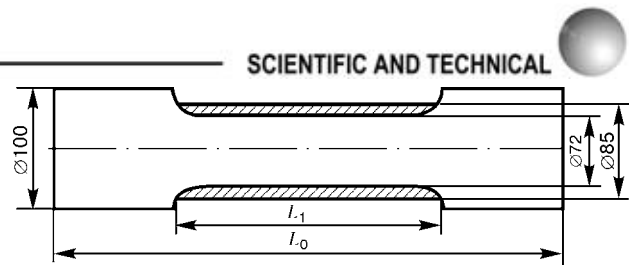


Figure 1. Schematic of surfacing of the shaft model used for fatigue tests

Ni – 0.06; S – 0.03; P – 0.01) surfaced by CO₂ arc welding using wire of the Sv-05Kh20N9FBS (C – 0.05; Cr – 20.0; Ni – 9.0; V – 0.7; Nb – 0.8; Si – 1.0 wt.%; Fe – balance) grade (Figure 1) on a small pitch spiral path. A layer 7 – 8 mm thick was deposited in several passes on a region with a diameter of 72 mm. Then the surface of this region with the deposited layer was treated by turning to a diameter of 85 mm, which corresponded to sizes of the shaft model fatigue tested without mechanical treatment. The sample thus produced (variant 1 from the Table) was used to investigate distribution of residual stresses. It was used as a reference to evaluate the contribution of different types of mechanical treatment applied to other samples of the same sizes (Table) to the distribution of residual stresses. Residual stresses were measured by the Sachs method [1]: disks 5 – 10 mm thick were cut out from the shaft model in a transverse direction to determine radial σ_{rr}^d and circumferential $\sigma_{\beta\beta}^d$ stresses. As cutting out of the disks leads to a complete relaxation of axial residual stresses σ_{zz} , this should exert a certain effect also on difference of measured stresses in the disk, σ_{rr}^d and σ_{zz}^d , from those in the shaft before it was cut into the disks.

The degree of this difference was determined by calculations on the basis of numerical modelling of thermomechanical processes occurring in surfacing of the shaft model [9]. Figure 2 shows the calculated data on distribution of residual stresses $\sigma_{\beta\beta}$ and σ_{zz} in different sections of the shaft model along the length of the layer 6 mm thick deposited in 4 passes. Figure 3, b shows distribution of calculated stresses $\sigma_{\beta\beta}^d$ and σ_{rr}^d in a disk, which corresponds to operation of cutting out of disks from the shaft, i.e. where conditions $\sigma_{zz} = \sigma_{rz} = 0$ are assigned for the end edges of the disk in sections 2 and 4 (Figure 2). Comparing the data on $\sigma_{\beta\beta}^d$ (curve 1) in Figure 3, b with the data in Figure 2, a (curves 2, 4) shows that cutting out of the disks has a comparatively small effect on the

value and character of distribution of circumferential stresses $\sigma_{\beta\beta}$, although this leads to a substantial change in stresses σ_{zz} (if we compare the data in Figure 2, b with $\sigma_{zz}^d \equiv 0$). Nevertheless, it should be taken into account that residual stresses $\sigma_{\beta\beta}$ in the deposited layer are at a level of 300 MPa for the shaft, while for the disk $\sigma_{\beta\beta}^d \approx 200$ MPa. The peak values of these stresses in the fusion zone vary from 650 MPa in the shaft to ≈ 520 MPa in the disk. Residual stresses σ_{rr} are characterized by a much less difference, as they are small as compared with $\sigma_{\beta\beta}$ and σ_{zz} .

Therefore, measurements of residual stresses in the disks cut out from the surfaced shaft give a sufficiently reliable picture of distribution of residual stresses and an approximate picture of the level of stresses $\sigma_{\beta\beta}$ and σ_{rr} in the respective sections of the shaft, which is acceptable for comparative estimations of the degree of the effect of a corresponding mechanical treatment of the surfaced shaft on residual stresses. Moreover, there could hardly be a more reliable experimental method for such purposes, except, probably, for the

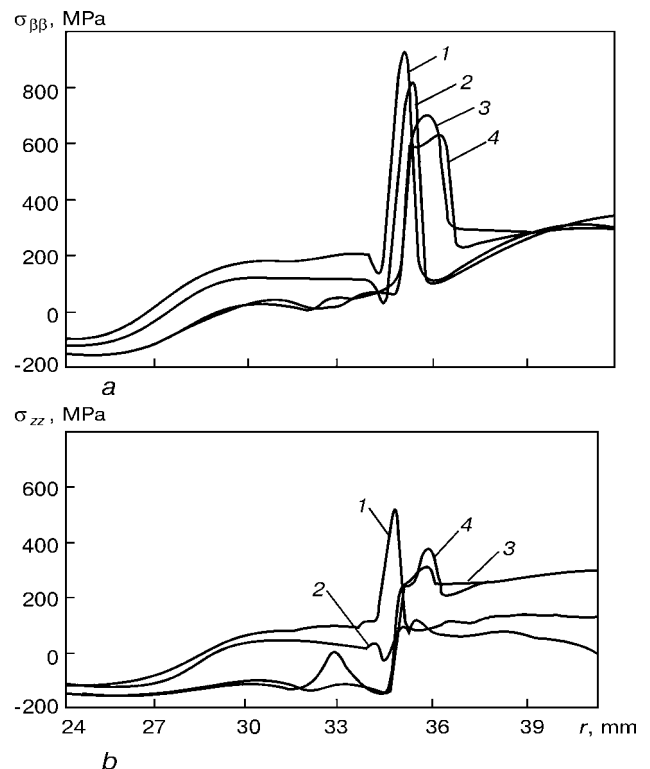


Figure 2. Distribution of calculated residual stresses $\sigma_{\beta\beta}$ (a) and σ_{zz} (b) in the surfacing zone of the model shaft of St.35: sections 1 and 2 correspond to the beginning, 3 and 4 – to the centre of a deposit; 1, 3 – along the shaft axis; 2, 4 – in the zone of overlapping of the neighbouring beads

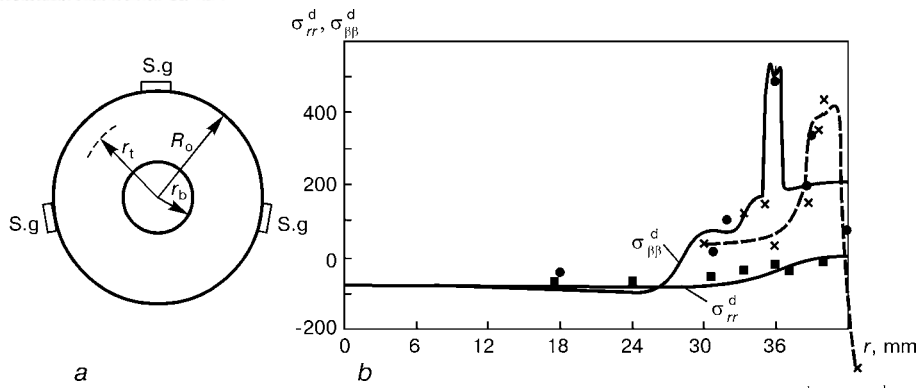


Figure 3. Diagram of boring of the disk using strain gauges (a) and distribution of residual stresses $\sigma_{\beta\beta}^d$ and σ_{rr}^d in this disk according to the calculated (solid lines) and experimental data (● — $\sigma_{\beta\beta}^d$; ■ — σ_{rr}^d) without treatment, as well as experimental data for $\sigma_{\beta\beta}^d$ after USP (×) (b)

methods of neutron [10] or synchronous [11] diffraction, which require a special expensive equipment.

Residual stresses in the disks, $\sigma_{\beta\beta}^d$ and σ_{rr}^d , were measured in the following sequence. The method of strain measurement using wire resistance gauges was used to fix the level of circumferential strains in a disk induced by boring and turning. Six or eight preliminarily calibrated strain gauges were placed on the outside surface of the disk with radius $r = R_o$ (Figure 3, a) to measure circumferential strains $\epsilon_{\beta\beta}(R_o)$. A hole with radius $r_b = r_0$ was drilled in the centre

of the disk and the first reading of strains $\epsilon_{\beta\beta}(R_o, r_b = r_0)$ was taken. Then this hole was bored to a size of $r_b = r_1$ and a new reading of $\epsilon_{\beta\beta}(R_o, r_b = r_1)$ was taken, etc. Boring of the base metal was done starting from $r_b = 10$ mm with subsequent removal of layers 2.5 – 3.0 mm thick. The value of $\epsilon_{\beta\beta}(R_o, r_b)$, taken with an opposite sign, determines an elastic change in circumferential strains $\epsilon_{\beta\beta}^d(R_o, r)$, depending upon radial residual stresses $\sigma_{rr}(r_b)$ acting on the surface with radius $r = r_b$. Therefore, the following relationship holds:

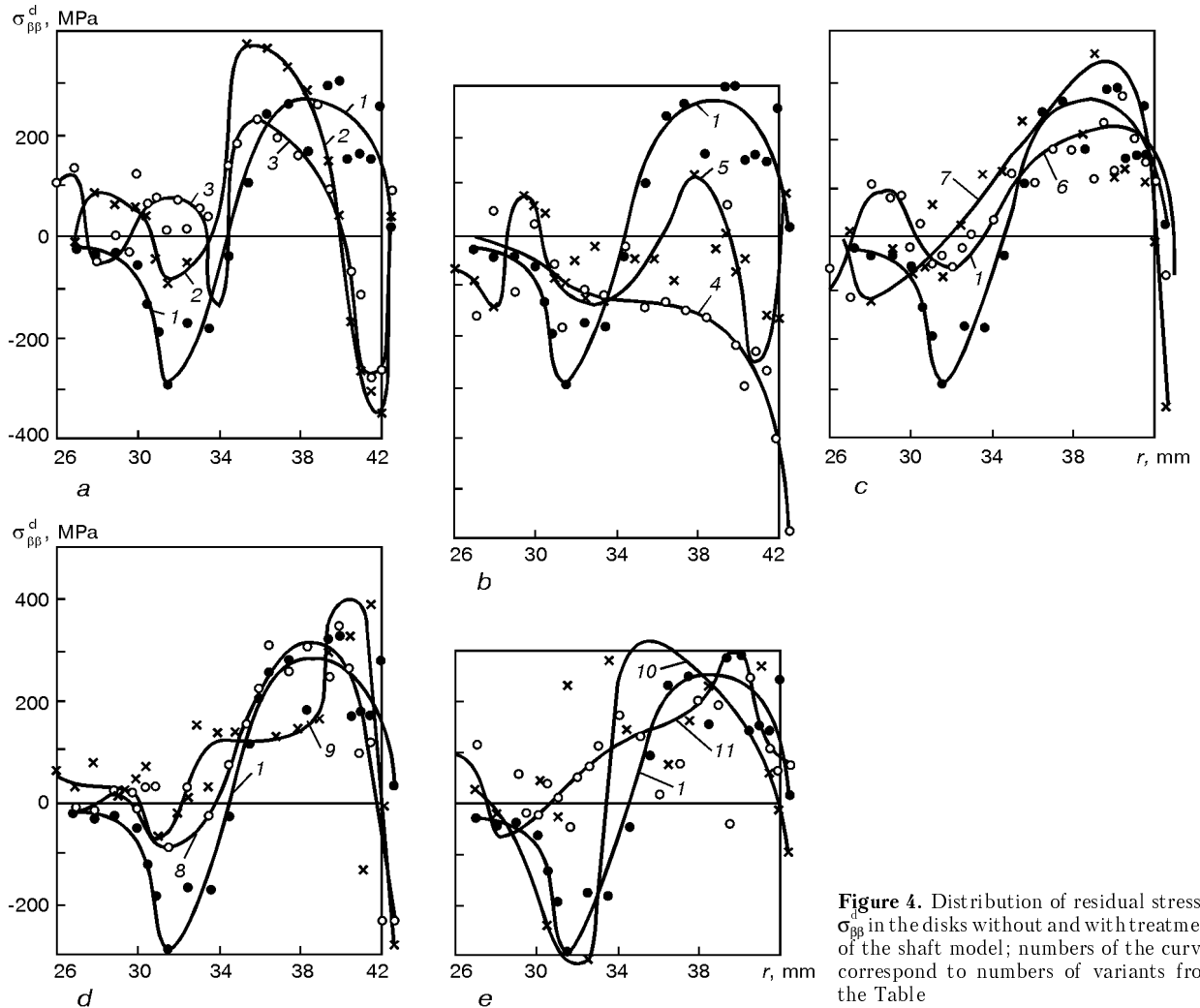


Figure 4. Distribution of residual stresses $\sigma_{\beta\beta}^d$ in the disks without and with treatment of the shaft model; numbers of the curves correspond to numbers of variants from the Table



$$\sigma_{rr}(r_b) = -\frac{E\varepsilon_{\beta\beta}^e(R_o)}{2} \left(\frac{R_o^2}{r_b^2} - 1 \right) \quad (1)$$

Boring was finished at $r_b = R_b \approx 0.5R_o$. Then the gauges for measuring circumferential stresses $\varepsilon_{\beta\beta}(R_b)$ were installed on the surface of radius $r_b = R_b$ and a layer-by-layer turning of the outside surface of the disk was done. Each of the turnings was finished at $r = r_t$, thickness of the removed layer being equal to 0.5 – 2.0 mm. Strain $\varepsilon_{\beta\beta}(R_b)$ taken with an opposite sign, which was measured after each turning allowing for the known values of stresses $\sigma_{rr}(R_b)$, made it possible to determine residual stresses $\sigma_{rr}(r_t)$ from the following relationship:

$$\sigma_{rr}(r_t) = \sigma_{rr}(R_b) \frac{R_b^2/R_o^2}{1 - R_b^2/R_o^2} \left[\frac{R_o^2}{r_t^2} - 1 \right] + \frac{E\varepsilon_{\beta\beta}^e(R_b)}{2} \left[\frac{r_t^2}{r_b^2} - 1 \right] \quad (2)$$

Here $\varepsilon_{\beta\beta}^e(R_b) = -\varepsilon_{\beta\beta}^e(R_b, r_t)$; $R_b < r_t < R_o$; E is the normal elasticity modulus of base and deposited metals equal to $2.06 \cdot 10^5$ and $1.91 \cdot 10^5$ MPa, respectively.

The approach described was used to the surfaced shaft models after appropriate mechanical treatment and without it (see the Table).

The experimental values of $\sigma_{\beta\beta}^d$ and σ_{rr}^d for variant 1 without mechanical treatment, shown in Figure 3, *b*, are in good agreement with the calculated data. Figure 4 (curve 1) shows the experimental values of $\sigma_{\beta\beta}^d$ after appropriate mechanical treatment in comparison with the data for variant 1. Despite a rather wide spread of the experimental data, which is partially associated with the procedural error (more so for boring and turning operations), the marked trend here is to formation of compressive stresses in the surface layer. Thickness of such a layer depends upon the type of treatment. Under conventional USP conditions (Figure 4, *c*, *d*) thickness of the surface layer with the negative values of stresses is not in excess of 0.5 mm, which is in a sufficiently good agreement with results of study [7]. The latter shows that thickness of the cold worked layer with such a treatment is close to the above value. Roll burnishing (Figure 4, *a*) under conventional conditions [3] increases the compression zone to 2 mm, while explosion treatment can substantially widen this zone depending upon the energy of explosion. Thus, at low values of the explosion energy this layer is about 2 mm thick, and at high values its thickness amounts to 15 mm (curves 5 and 4 in Figure 4, *b*, respectively). Therefore, studied was the possibility of increasing thickness of the cold worked layer in USP due to preheating of the shaft (prior to treatment) to a temperature of 400 °C (Figure 4, *e*). However, the efficiency of this heating

is very low. Moreover, in subsequent cooling, due to differences in properties of base and deposited metals the level of compressive stresses induced by treatment is partially lowered.

It follows from the abovesaid that it is best to perform mechanical treatment of the surfaced shaft at a sufficiently small thickness of the deposited layer, when the fusion zone, i.e. the zone of potential formation of fatigue cracks, is in a region of low or even compressive residual stresses. However, even at a relatively small thickness of the cold worked layer, like, for example, in USP, one can expect an increase in resistance to fatigue loads in the case where fatigue cracks are initiated in the surface layer without treatment.

CONCLUSIONS

1. Treatment of surfaced shafts (USP, roll burnishing and explosion treatment) promotes formation of compressive stresses in the surface layer. Thickness of the layer of compressive stresses in the austenitic steel deposit under conventional conditions of USP is not in excess of 0.5 mm, in roll burnishing it is about 2 mm, while in explosion treatment it can vary over wide ranges (2 – 15 mm) depending upon the level of distribution of the explosion energy.

2. Both USP and roll burnishing are efficient in terms of prevention of fatigue cracks initiated on the surface of the deposited layer.

REFERENCES

1. Kravtsov, T.G., Stalnichenko, O.I., Olejnik, N.V. (1994) *Reconditioning of parts by surfacing and evaluation of their strength*. Kyiv: Vyshecha Shkola.
2. Benua, F.A., Bogdanov, A.M. (1955) Investigation of residual stresses in surfaced ship shafts. *Rechn. Transport*, 2, 3 – 8.
3. Kudryavtsev, I.V., Savvina, N.M. (1972) Protection and reconditioning of large shafts by surfacing with subsequent cold working in relationship with their fatigue resistance. In: *Study of strengthening of machine parts*. Moscow: Mashinostroyeniye.
4. Kudryavtsev, I.V., Naumchenkov, N.E. (1976) *Fatigue of welded structures*. Moscow: Mashinostroyeniye.
5. Trufiyakov, V.I., Mikheev, P.P., Kudinov, V.I. et al. (1974) Increase in fatigue strength of welded joints by explosion loading. *Avtomaticheskaya Svarka*, 9, 29 – 32.
6. Statnikov, E.Sh., Shevtsov, E.M., Kulikov, V.F. (1977) Ultrasonic shock peening tool for strengthening of welds and decreasing of residual stresses. In: *New physical methods for intensification of technological processes*. Moscow: Metallurgia.
7. Makhnenko, V.I., Kravtsov, T.G. (1986) Thickness of a plate of the deformed layer in ultrasonic shock peening of surfaced parts. *Avtomaticheskaya Svarka*, 8, 28 – 30.
8. Kravtsov, T.G. (1981) Increase in fatigue strength of surfaced shafts by ultrasonic peening. *Ibid.*, 10, 35 – 38.
9. Makhnenko, V.I., Velikoiivanenko, E.A., Kravtsov, T.G. et al. (2001) Numerical investigation of thermomechanical processes in surfacing of shafts of ship mechanisms and devices. *The Paton Welding J.*, 1, 2 – 10.
10. (1989) *Measurement of residual and applied stress using neutron diffraction*. Ed. M. Hautching, A. Krawitz. Boston, London: Kluwer Akad. Publ. Dordrecht.
11. (1998) Evaluation of residual stresses in the bulk of materials by high energy synchrotron diffraction. *J. of Nondestructive Evaluation*, 3, 129 – 140.



INFLUENCE OF WELDING PROCESS ON FRACTURE RESISTANCE OF JOINTS IN ALUMINIUM-LITHIUM ALLOYS 1420 AND 1460

T.M. LABUR, Andr.A. BONDAREV, A.V. LOZOVSKAYA, V.S. MASHIN and A.G. POKLYATSKY
The E.O. Paton Electric Welding Institute, NASU, Kyiv, Ukraine

ABSTRACT

A dependence is established of fracture resistance of welded joints in Al–Li alloys 1420 and 1460 on the welding process (consumable or non-consumable electrode, electron beam). It is shown that different thermal conditions of welding lead to different degrees of HAZ metal softening. Application of a highly-concentrated heat source in electron beam welding, ensures a higher resistance to crack initiation and propagation. The metal of the fusion boundary of the weld with the base metal has the lowest fracture resistance of all the studied zones of welded joints, irrespective of the joining process.

Key words: fusion welding, Al–Li alloys, heat input, weld metal, fusion zone, HAZ, nominal breaking stress, specific work of crack propagation, critical stress intensity factor, J-integral, comparative analysis

Fast heating and subsequent slow cooling of the metal, concurrent with the thermal cycle of fusion welding, lead to the HAZ developing zones differing from each other by the degree of grain boundary partial melting and coarse particle precipitation, as a result of phase transformations [1]. Presence of a heterogeneous structure in the metal limits plastic deformation in the regions between the weld crystallite boundaries, thus promoting its localisation and development of a bulk-stressed state of the joints. Stress concentration is accompanied by initiation of microcracks that cause a lowering of welded joint metal strength (compared to that of the base metal) and premature failure of the joints.

The aim of this study is to establish a dependence of fracture resistance of the joints in high-performance Al–Li alloys 1420 and 1460 on the used processes of fusion welding that differ by the level of heat input and thermal impact in different regions of the HAZ, thus promoting base metal softening to different degrees. This was achieved using modern technologies of welding high-strength aluminium alloys, namely consumable and non-consumable argon-arc welding, as well as EBW that are the most widely applied in development of light-weight welded structures.

The object of experimental evaluation were 3.2 mm thick sheets after quenching and artificial ageing. Optimized welding modes provided a minimal level of the process heat input and a high quality of weld formation. Non-consumable electrode welding (TIG) was conducted in the pulsed-arc mode at square-wave asymmetrical current. Periodical nature of current impact on the weld pool ensured intensive stirring of the liquid metal and refinement of weld crystallites [1]. Lowering of thermal impact on the metal in welding and shortening of its duration were achieved by using consumable electrode welding (MIG) in a gas mixture of argon and helium [2]. EBW, unlike the arc processes (TIG and MIG) is characterized by a high specific power density (Table).

Low heat input values in EBW promote formation of a small volume of the liquid metal in the weld pool and a narrow HAZ [1]. EBW was performed with discrete scanning of the beam and programmed heat input by regulation of the beam holding time in its dwell points within the selected path that had the form of curves of the second kind [3]. Scan shape and parameters were controlled by an oscillograph. Change of the metal temperature condition during welding and distribution of the acting forces impart further dynamics to the weld pool, that against the background of continuous pumping down promotes formation of welded joints with a high density and fine-crystalline structure of weld metal [4].

Typical welding modes in joining Al–Li alloys

Welding process	Unit, power source	I_w, A	U_a, V	$v_w, m/h$	$q/v_w, kJ/cm$
Argon-arc					
TIG	I-126	275 – 289 (SP) 175 – 180 (RP)	12.0	11	30
MIG (50 % Ar + 50 % He)	«Fronius» TPS-450	115	19.2	35	63
EBW	Y-212	0.05	30000	60	120



The quality of the produced welded joints was determined by X-ray inspection. Its results confirmed the absence of such inner defects as pores or oxide films. Alloy 1420 was welded using Sv-AMg63 (Al-6.3Mg) filler wire, and alloy 1460 — using US wire 2319. Wire diameter in all the cases was 1.6 mm. In order to prevent defects in the weld metal, the edges were scraped to the depth of not less than 0.1 mm prior to welding.

Fracture resistance was evaluated by the results of testing by off-center tension flat samples with a sharp notch of 0.1 mm radius. The notch tip was located in the following structural zones of welded joints: weld axis, fusion zone and HAZ at 5 mm distance from the fusion boundary of the weld and the base metal. Tested for comparison were similar samples of base metal with transverse orientation of the rolled stock that is the least favourable in sheet semi-finished products of aluminium alloys. The theoretical coefficient of stress concentration in the studied samples was equal to 10 and was determined by a procedure described in [5].

Analysis of the fracture resistance values was based on physical principles of elasto-plastic fracture [6]. The stressed state and other stages of the process of sheet material fracture were simulated using certain sample dimensions and testing procedure. The diagram, recording all the fracture stages, allowed determination of the nominal breaking stress σ_f and specific work of crack propagation (SWCP). J -integral value was found from calculation of the function of deformation energy change, depending on crack length, using Merkle-Korten relationship [7]

$$J = U \{ [B(W - a_0) f(a_0/W)] \},$$

where U is the work of crack initiation, i.e. area under the curve of dependence of force on displacement; $f(a_0/W)$ is the function of geometrical ratio of crack length a_0 and size of tested sample W , that has the following form:

$$f(a_0/W) = 2 [(1 + \alpha)/(1 + \alpha^2)],$$

where

$$\alpha = \sqrt{[2\alpha_0/(W - a_0)]^2 + 2[2a_0/(W - a_0)] + 2 - [2a_0/(W - a_0) + 1]}.$$

Values of critical stress intensity factor K_c in different zones of welded joints of the studied alloys were evaluated by the linear dependence of K_c on SWCP that describes the crack propagation stage in fracture [5]

$$K_c = (4.35 \text{ SWCP} + 3.31) \cdot 10^{-4}.$$

Results of studying the welded joints showed that Al-Li alloys 1420 and 1460 differ from the base metal by lower (by 20 – 30 %) values of σ_f and K_c (Figure 1, *a, b*). Welds in alloy 1420 had 10 % higher σ_f values, irrespective of the welding process. K_c value in alloy 1460 was 15 % higher, than that of alloy 1420. Lower values of this characteristic are found in welded joints

of both the alloys produced by TIG process (Figure 1, *a, b*). The stress level at which welds in alloy 1420 failed, was 295 – 350 MPa, and in alloy 1460 — 280 – 315 MPa. Values of K_c in the first case were equal to 23.1 – 29.8, and in the second case to 25.2 – 34.6 MPa $\sqrt{\text{m}}$. Differences in fracture resistance values, determined in the studied alloys, can be attributed to the presence of stable strengthening phases. Composition of alloy 1460 includes such phases as δ' (Al₃Li), T_1 (Al₆CuLi) and S (Al₂CuLi) [1]. Alloy 1420, in addition to phase δ' , also contains phase S_1 (Al₂MgLi) [1].

Phase composition of the above alloys also affects the energy values of fracture resistance, describing the energy of initiation (J_c -integral) and subsequent growth (SWCP) of the crack. Their values in alloy 1460 are 30 – 40 % higher, than in alloy 1420 (Figure 1, *c, d*). This is indicative of the capability of 1460 alloy metal to undergo plastic deformation, that can be due to a smaller atomic diameter of copper (0.256 nm), compared to that of magnesium (0.32 nm), present in the composition of alloy 1420.

Different thermal conditions of fusion welding of the studied Al-Li alloys and metal cooling rates, concurrent with its solidification, lead to different degrees of softening of the HAZ metal. As a result, different values of σ_f and K_c are observed in the HAZ metal. Breaking stress of TIG welded joints in alloy 1420, is 382 to 397 MPa, and that of alloy 1460 — 320 – 373 MPa, this being lower than in the base metal (450 and 470 MPa, respectively). Lower σ_f values in alloy 1460 (compared to alloy 1420), are, possibly, due to the ability of copper, present in its composition, to lower the compositional stability of oversaturated solid solution, and cause its more intensive decomposition during process heating, including heating in welding [3]. Energy values of fracture (J -integral and SWCP) of welded joint metal in the HAZ are equal to 3.1 and 3.4 J/cm² in alloy 1420 and to 4.2 and 3.4 J/cm² in alloy 1460, respectively.

Comparison of fracture values of joints produced by different welding processes, revealed the characteristic for the studied alloys 1420 and 1460 tendency of σ_f and K_c lowering. TIG welds in alloy 1420 are characterised by the lowest values of breaking stress (300 – 315 MPa). K_c values for alloy 1420 are 23.1 MPa $\sqrt{\text{m}}$ and for alloy 1460 — 25.2 MPa $\sqrt{\text{m}}$. The noted regularity is due to thermal conditions of welding, under which the particles of the strengthening δ' (Al₃Li) phase do not have time to grow, as a result of the low rate of the solid solution decomposition [1]. Shortening of thermal impact duration in MIG, leads to 3 – 5 % higher values of σ_f and K_c , compared to a TIG weld.

Use of a highly-concentrated heat source in EBW results in higher values of σ_f (Figure 1), which in alloy 1420 increase by 60 MPa, and in alloy 1460 — by 30 MPa, compared to those in arc welding processes. Crack resistance factor K_c of welds in alloy 1420 is 29.8 MPa $\sqrt{\text{m}}$, and in alloy 1460 —

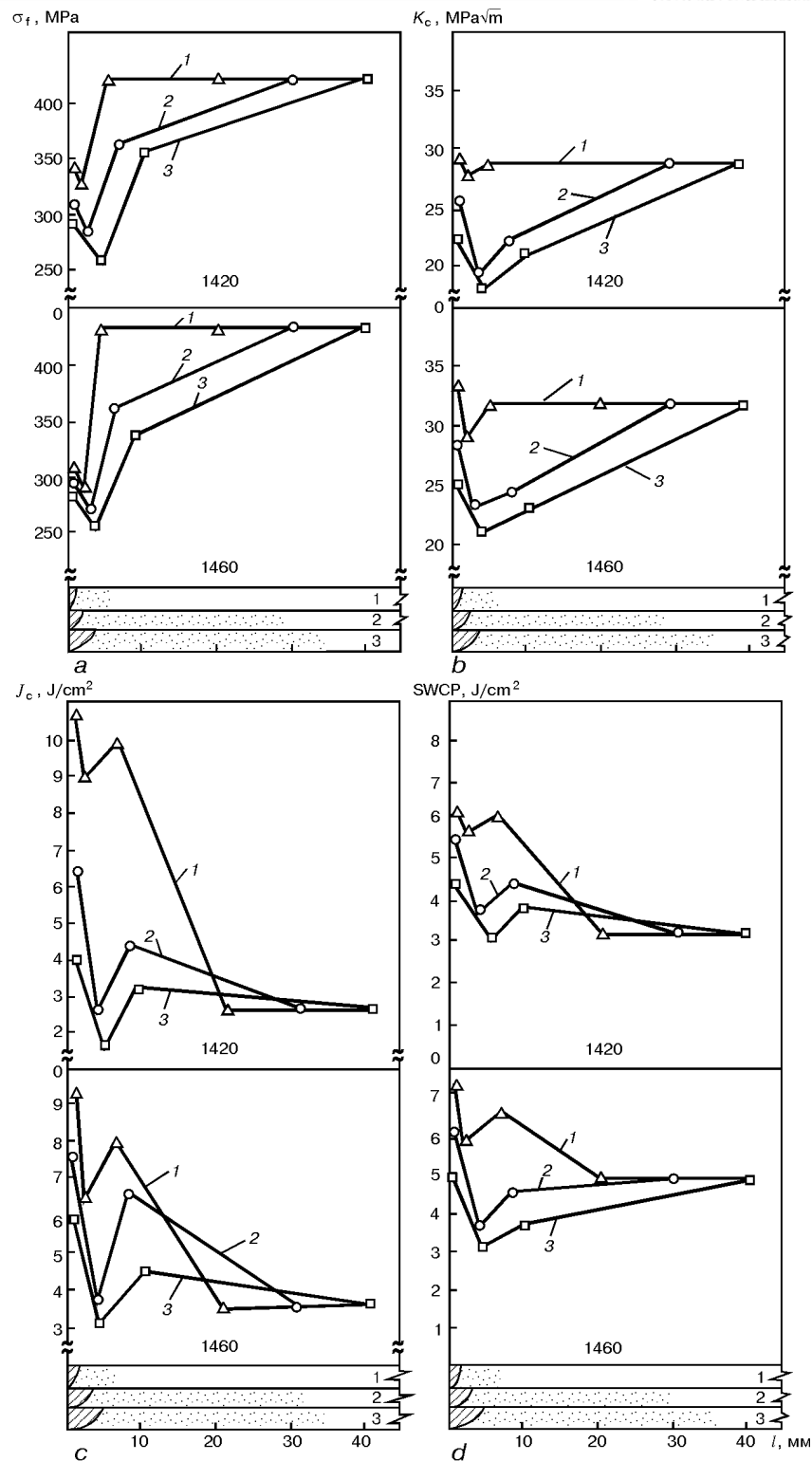


Figure 1. Influence of welding process on σ_f (a), K_c (b), J -integral (c) and SWCP (d) in different zones of Al-Li alloys 1420 and 1460: 1 – EBW; 2 – MIG; 3 – TIG; l – distance from the weld axis

34.6 MPa \sqrt{m} , this being by 30 – 35 % higher, than in the welds produced by the arc processes. In other welded joint regions, K_c values change by 7 and 10 MPa \sqrt{m} , respectively, depending on the welding heat input. In EBW, the welds in alloy 1420 are characterised by J -integral values, equal to 11.4 J/cm 2 , this being approximately 2 – 3 times higher, than in the welds produced by the arc processes. Welds in alloy 1460 in this case differ from

such welds in alloy 1420 by 2.0 – 2.5 J/cm 2 smaller values of J -integral. A similar dependence is found also for SWCP values (Figure 1, d). Welds in both the studied alloys are characterised by its highest level (5.9 and 6.0 J/cm 2 , respectively). This is promoted by thermal conditions of welding by the electron beam, when the short-term processes of heating and cooling limit the development of phase transformations that can lead to embrittlement of intermetallic

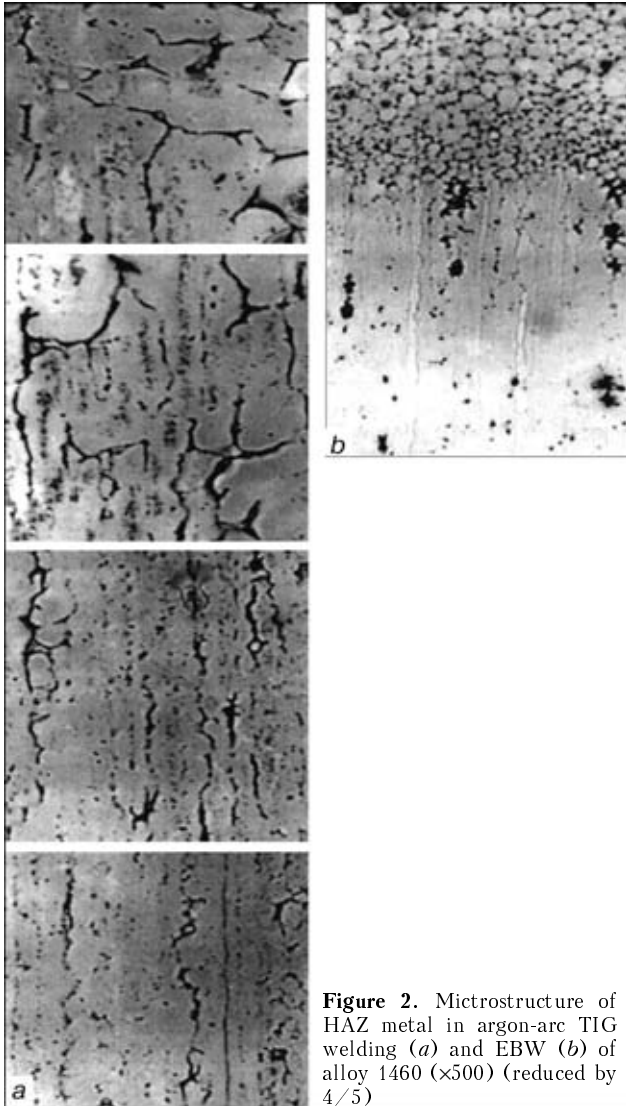


Figure 2. Microstructure of HAZ metal in argon-arc TIG welding (a) and EBW (b) of alloy 1460 (x500) (reduced by 4/5)

inclusions along the grain boundaries. MIG joints have 5 – 15 % lower fracture resistance, and in TIG joints this value is lower by 25 – 30 %, this, however, being higher, compared to that of the base metal (2.9 J/cm²). This is promoted by formation of a fine-crystalline structure of the weld metal. Macrostructural analysis of welded joints reveals that the thickness of the crystal layer and intergranular layers is 2.0 and 1.5 times smaller in EBW weld metal, than in TIG weld metal, respectively.

It should be noted that irrespective of the welding heat input, the fusion zone of joints in alloys 1420 and 1460, is characterized by minimal values of σ_f , K_c , J -integral and SWCP, unlike other structural zones (Figure 1). A higher heat input in TIG yields lower values of σ_f and K_c , compared to other welding processes studied (Figure 1). The values of the above properties of 1420 alloy welded joints are equal on average to 265 MPa and 21.2 MPa \sqrt{m} .

A higher susceptibility of 1460 alloy joints to quasibrittle fracture, is indicative of lower (by 55 MPa and 1.4 MPa \sqrt{m}) values of σ_f and K_c . The above is attributable not only to the structural inhomogeneity of the metal in this zone, resulting from the alloy

softening under the impact of the thermal cycle of welding, but also to coagulation, as well as embrittlement of the phases located along the grain boundaries. This is also brought about by the presence of tensile stresses, induced by phase transformations and coagulation of inclusions in the regions along the grain boundaries in the fusion zone. Development of stresses is promoted by a high heat input and low cooling rate, concurrent with the process of fusion welding of aluminium alloys [2].

Study of different processes of joining Al–Li alloys demonstrated a dependence of J -integral energy value on the welding heat input. Lower values are characteristic of joints, produced by TIG welding, with higher values for EBW. The range of J -integral variation for 1420 alloy is 1.9 – 9.2 J/cm², and for alloy 1460 – 3.2 – 6.4 J/cm². SWCP characteristic in the fusion zones of both of the studied alloys, has close values of 2.5 and 2.1 J/cm², respectively (Figure 1, d). Values of J -integral and SWCP in 1420 alloy joints are close to those of the base metal, and in alloy 1460 they are lower by 10 to 15 %. The established dependence can be related to formation on 1460 alloy grain boundaries of a greater volume fraction of coarse particles of stable $T_1(Al_6CuLi)$ and $S(Al_2CuLi)$ phases, compared to alloy 1420, as well as their higher brittleness under non-uniform plastic strain, that is due to their nature and development of considerable tensile stresses in welding. Presence of the above inclusions in testing the welded joints leads to crack initiation near the brittle structural fragments in the intergranular regions. A greater rigidity of the inclusions of strengthening phases (δ' , T_1 and S), than that of the matrix, causes initiation of microcracks in the plane of their contact, that is visible in the fractures of broken samples. Analysis of the fractures provides evidence in favor of the supposition of grain boundary cohesion strength lowering during welding as a result of phase transformations and coagulation of phase inclusions.

In MIG welded joints the metal fracture resistance values on the boundary of the weld fusion with the base metal, are also lower, than in other structural zones. The short-term action of welding heating in MIG, compared to TIG, provides an increase in all the fracture resistance values of alloy 1420 by 25 – 30 % and of alloy 1460 – 1.5 times in the fusion zone.

A similar tendency of the studied fracture characteristics changing is also found in the joints of both the alloys after EBW, but the nature of their change is different. Compared to the joints produced by arc welding processes, σ_f value rises by 5 to 15 %. K_c value in the fusion zone of alloy 1420 increases by 50 % and that of alloy 1460 by 35 %. SWCP value is almost doubled in both the alloys, and J -integral value increases 4 times in alloy 1420 and 2.5 times in alloy 1460 (Figure 1, c). This is due to a lower level of the metal softening under the impact of a low heat input in EBW, and the resultant lower probability



of appearance of coarse grain boundary intermetallic inclusions in the fusion zone.

Metallographic examination of the joints in the vicinity of the boundary with the weld, showed that in this zone the base metal becomes overheated during welding under the impact of non-equilibrium solidus temperature. A characteristic partial melting of the structural constituents with formation of liquid inclusions in the solid metal bulk is an indication of it (Figure 2). In arc welding processes, the fusion zone structure reveals thicker grain boundaries, their triple junctions and a considerable amount of partially melted phases. In EBW a predominantly polyhedral structure with minor inclusions of partially-melted phases is observed.

Thus, in order to provide a favourable combination of the load and energy values of fracture resistance, it is desirable to perform welding at a lower heat input, this promoting elimination or limitation of the degree of embrittlement of intermetallic phase inclu-

sions along grain boundaries and having a considerable positive effect on improvement of welded joints performance in high-strength Al-Li alloys.

REFERENCES

1. Rabkin, D.M., Lozovskaya, A.V., Sklyabinskaya, I.E. (1982) *Metals science of welding aluminium and its alloys*. Kyiv: Naukova Dumka.
2. Ishchenko, A.Ya. (1991) Welding of light alloys and metallic composite materials. *Avtomaticheskaya Svarka*, **6**, 26 – 31.
3. Bondarev, A.A., Bondarev, Andr.A. (1996) Investigation of physico-metallurgical processes and process features of electron beam welding of aluminium alloys. In: *Col. of pap. on Increasing Welding Production Effectiveness*. Lipetsk.
4. Ishchenko, A.Ya., Bondarev, A.A., Nazarenko, S.V. et al. (2000) Technology of electron beam welding of high-strength aluminium alloys stringer panels. *The Paton Welding J.*, **6**, 27 – 30.
5. Kishkina, S.I. (1981) *Fracture resistance of aluminium alloys*. Moscow: Metallurgia.
6. Khertsberg, R.V. (1989) *Deformation and fracture mechanics of structural materials*. Moscow: Metallurgia.
7. (1986) *Static strength and fracture mechanics of steels*. Ed. by V. Dal, V. Anton. Moscow: Metallurgia.



STATISTIC ANALYSIS OF CORROSION RESISTANCE OF CHROMIUM-NICKEL DEPOSITED METAL IN ALKALI SOLUTIONS

P.P. LAZEBNOV

Zaporizhya State Technical University, Zaporizhya, Ukraine

ABSTRACT

Results of comparative corrosion tests of Cr–Ni deposited metal in alkali solutions are given. Correlation and regression analyses are made, thus examining the interrelation between the input (δ -ferrite in welds) and output (rate of metal corrosion) parameters.

Key words: regression and correlation analyses, deposited metal, corrosion rate, sodium hydroxide, cooking liquor, correlation

The equipment for chemical industry is subjected to the corrosion processes. In one cases these processes lead to a uniform fracture of steels and alloys, while in others — to the corrosion cracking and other types of corrosion of structures, which are operating in contact with aggressive media. Thus, in 1980 a cooking boiler «Kamyur» of 1100 t/day capacity at the pulp-and-paper mill «McMillan Blodel» (USA) exploded because of a corrosion failure of a butt welded joint of the upper conical part with a vessel cylinder [1]. After three-year inspection of work of boilers of a continuous cooking at the sulphate-pulp factories of the USA, the results of inspection were summarized and presented at the International Congress in Toronto (Canada) [2, 3] and the following conclusions were made.

Among 107 boiling apparatuses, more than 40 of them had cracks in welded joints of an impregnation zone located in casing metal. They were mainly observed in welded joints of vessels made from carbon and bimetal steels and also Inconel-plated steels.

The crack initiation is observed in structures passed heat treatment and without it. Boilers with a full treatment are less sensitive to the corrosion cracking than the apparatuses with a local «normalizing» of welded joints.

In all the boilers the corrosion processes are provoked by a main component of the cooking liquor — NaOH.

The industrial solutions, in which the sulphate cellulose is cooked, are the complex systems. Table 1 gives characteristics of the cooking liquors used.

At designing of technological complexes of the pulp-and-paper industry, the Cr–Ni steels were successfully used for many decades (cooking boilers of companies «Kamyur», «Pandia», KMW, steaming towers, etc.). Coming from technical-economical tasks the vessels are manufactured from a bimetal sheet rolled stock. The bimetal has a base layer (boiler steels of type 17Mn4 and analogs of steels 20K, 22K) which is clad with corrosion-resistant steels of types 10Kh18N10T (C — 0.1; Cr — 18.0; Ni — 10.0; Ti — 0.6 wt.%), 08Kh17N15M2T (C — 0.08; Cr — 17.0; Ni — 15.0; Mo — 2.0; Ti — 0.6 wt.%). Analysis of condition of the boilers park showed that, as a result of long-time service, the protective layer of the apparatuses underwent a significant corrosion action.

The study of corrosion-active and inhibiting ingredients of the sulphate liquor plays a large role in fighting with the corrosion. It was established that the carbonate- and silicate-ions have inhibiting action, while the chloride-, sulphite- and sulphate-ions have activating action on the corrosion processes. As it follows from [5], sodium chloride NaCl and sodium thiosulphate Na₂S₂O₃ contribute to the initiation of a pitting corrosion in stainless steels, the sodium sulphate Na₂SO₄ brakes it remarkably, while the sodium sulphite Na₂SO₃ is neutral (Table 2).

Corrosion action of the sulphate liquor on steel 10Kh18N10T and 10Kh17N13M2T (C — 1.0; Cr — 17.0; Ni — 13.0; Mo — 2.0; Ti — 0.6 wt.%) increases with increase in temperature (reaching maximum at

Table 1. Composition of white liquors

Sulphate factory	Concentration of elements in solution, C, g/l						
	NaOH	Na ₂ S	Na ₂ CO ₃	Na ₂ SO ₄	NaCl	Na ₂ S ₂ O ₃	Na ₂ SO ₃
CIS	75.0 – 90.0	11.0 – 35.0	10.0 – 11.0	0.9 – 2.8	0.2	2.0 – 5.0	0.20
Canada [4]	≤ 95.2	39.2	26.6	6.5	6.5	5.2	0.99



Table 2. Single-factor effect of anions of white sulphate liquor on corrosion rate, R_c , of steel 10Kh18N10T [5]

<i>NaCl</i>		<i>Na₂SO₄</i>		<i>Na₂S₂O₃</i>		<i>Na₂SO₃</i>	
<i>C, g/l</i>	<i>R_c mm/year</i>	<i>C, g/l</i>	<i>R_c mm/year</i>	<i>C, g/l</i>	<i>R_c mm/year</i>	<i>C, g/l</i>	<i>R_c mm/year</i>
–	0.063	2.7	0.064	2.0	0.067	0.1	0.065
0.2	0.084	4.0	0.046	3.0	0.069	0.5	0.066
0.5	0.122	5.0	0.045	4.0	0.068	1.0	0.066
1.0	0.176	6.0	0.043	5.0	0.067	2.0	0.068
1.5	0.192	7.0	0.040	7.0	0.232	3.0	0.069
2.0	0.209	8.0	0.039	8.0	0.235	4.0	0.070

Note: Specimens were tested at 100 °C temperature in a model solution of liquor, g/l: NaOH – 86.40; Na₂S – 30.40; Na₂SO₄ – 2.70; Na₂S₂O₃ – 2.00; Na₂CO₃ – 1.00; Na₂SO₃ – 0.09.

130 – 160 °C) depending on concentration of active alkali and decreases as a result of dilution with a black liquor (in accordance with technological regulations of sulphate-pulp factories).

In study of general corrosion resistance of Cr–Ni metals of different systems of alloying in sodium hydroxide and industrial white liquor (NaOH – 35 – 60; Na₂S – 15; Na₂CO₃ – 11; Na₂S₂O₃ and Na₂SO₄ – 0.2 g/l) of boiler «Kamyur» at the Arkhangelsk pulp-and-paper mill a similar regularity of corrosion rate on temperature differed only by quantitative characteristics is observed. To confirm the right use of NaOH for accelerating tests of solutions in the development of welding materials used in alkali media of pulp-and-paper industry a statistic processing of data of corrosion resistance of specimens in laboratory and real conditions was made (Table 3).

The methods of correlation and regression analysis make it possible to study the relation between the input and output parameters. Often, a coefficient of

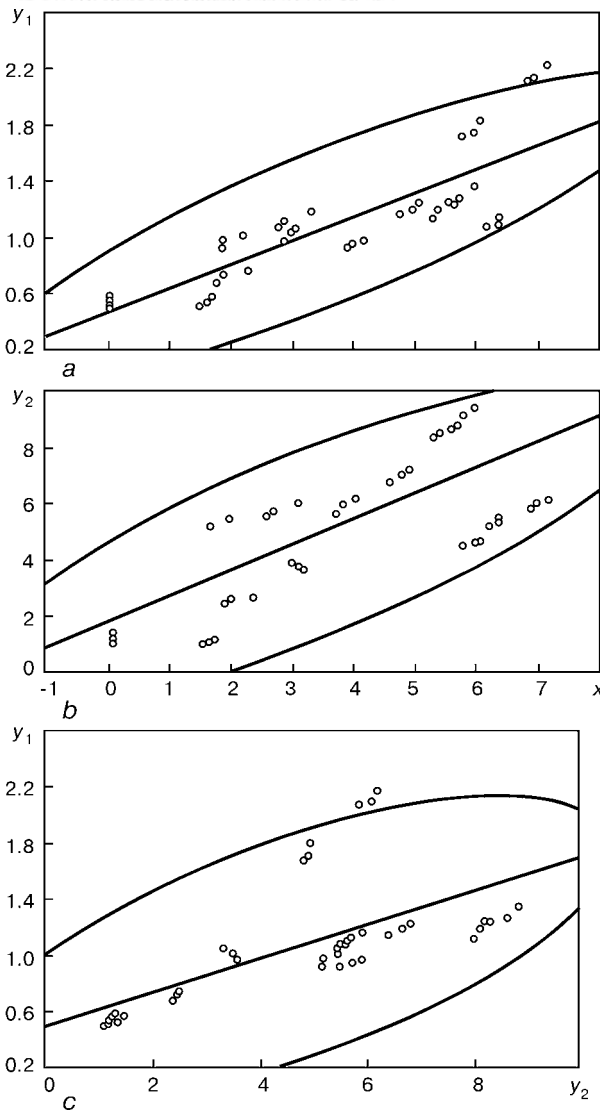
correlation r_{yx} (in case of a linear relation) is characteristics of closeness of relation between two random values [6, 7]. At a sufficient closeness of distribution of examining variables x, y to a normal law r_{yx} is a characteristic of degree of interrelation closeness. The given situation is typical of a linear relation (probability of plotting a hypothetical line of regression in a correlation field).

A regression analysis of a series of experiments (see Table 3) was made at an input parameter x (mass share of δ -ferrite, %) and output parameters y_1, y_2 (corrosion rate during real R_{c1} and laboratory R_{c2} tests). On the basis of Table data, a statistic processing of results was made. A graphical pair correlation of two cases $y_1:x$ and $y_2:x$ was made preliminary which allows setting of correlation between y_1, y_2 and x , and also its form. In accordance with data of Table 3, the points whose set forms a correlation field (Figure, *a, b*), are plotted in coordinates $y_1:x$ and $y_2:x$. On this basis, a hypothesis was assumed that

Table 3. Corrosion resistance of Cr–Ni deposited metal

<i>Number of specimen</i>	<i>Grade of welding electrode</i>	<i>Type of deposited metal</i>	<i>Mass content of δ-ferrite, %</i>	<i>Rate of corrosion at tests, g/(m²·h)</i>	
				<i>full-scale R_{c1}</i>	<i>laboratory R_{c2}</i>
				<i>x</i>	<i>y₁</i>
1 – 3	OZL-8	07Kh20N9	6.9; 7.0; 7.2	0.0209; 0.0212; 0.0220	0.0589; 0.0611; 0.0623
4 – 6	TsL-11	08Kh20N10G2	6.2; 6.4; 6.4	0.0106; 0.0108; 0.0113	0.0544; 0.0560; 0.0570
7 – 9	ZIO-3	07Kh19N10G2B	5.8; 6.0; 6.1	0.0170; 0.0173; 0.0182	0.0485; 0.0492; 0.0499
10 – 12	NIAT-1	08Kh19N11M2G2	5.7; 5.8; 6.0	0.0124; 0.0128; 0.0135	0.0836; 0.0864; 0.0884
13 – 15	NZh-13	08Kh19N10M2B	5.3; 5.4; 5.6	0.0112; 0.0119; 0.0124	0.0800; 0.0814; 0.0824
16 – 18	EA-400/10u	07Kh19N11M3G2F	4.8; 5.0; 5.1	0.0115; 0.0119; 0.0123	0.0642; 0.0669; 0.0681
19 – 21	OZL-6	10Kh25N13G2	3.9; 4.0; 4.2	0.0092; 0.0094; 0.0096	0.0549; 0.0575; 0.0589
22 – 24	EA-395/9	11Kh15N25M6G2	–	0.0050; 0.0051; 0.0055	0.0110; 0.0115; 0.0120
25 – 27	EA-981/15	09Kh15N25M6G2F	–	0.0052; 0.0057; 0.0059	0.0117; 0.0125; 0.0129
28 – 30	Pilot	09Kh20N10 (0.01% Y)	2.9; 3.0; 3.1	0.0096; 0.0103; 0.0107	0.0357; 0.0347; 0.0332
31 – 33	Same	07Kh20N10 (0.02% Y)	1.5; 1.6; 1.7	0.0052; 0.0053; 0.0057	0.0133; 0.0135; 0.0146
34 – 35	»	08Kh20N10 (0.027% Y)	1.8; 1.9; 2.3	0.0067; 0.0073; 0.0076	0.0236; 0.0243; 0.0246
36 – 38	OKR.6 (Sweden)	06Kh19N9M3	2.8; 2.9; 3.3	0.0108; 0.0111; 0.0117	0.0552; 0.0566; 0.0592
39 – 42	832MVR (Sweden)	04Kh21N10G2	1.9; 1.9; 2.2	0.0092; 0.0098; 0.0101	0.0517; 0.0520; 0.0542

Notes. 1. Full-scale tests of boiler «Kamyur» were performed at 120 – 170 °C and pressure 1.2 MPa in a cooking liquor during 15100 h.
2. Laboratory tests of autoclave were performed at 130 °C and pressure 0.2 MPa in 30 % solution of NaOH during 240 h.



Regression and correlation analyses of results of experiments: *a* – full-scale tests of specimens of deposited metal in a cooking liquor and sodium hydroxide ($y_1 = 0.165x + 0.462$); *b* – same, the laboratory tests ($y_2 = 0.852x + 1.617$); *c* – correlation relation $y_1 = f(y_2)$ ($y_1 = 0.119y_2 + 0.509$)

there is a linear relation between the parameters examined, and, consequently, the regression lines are straight.

Initial data for regression analysis are given below (summing of results from 42 experiments):

$$\begin{aligned} \sum x &= 155.0; \sum y_1 = 47.83; \sum y_2 = 204.44; \\ \sum xy_1 &= 211.20; \sum x^2 = 784.50; \sum y_1^2 = 64.58; \\ \sum xy_2 &= 933.70; \sum y_2^2 = 1225.50. \end{aligned}$$

Using these data the coefficients of correlation between parameters $y_1:x$ and $y_2:x$ are determined according to formulae [7]

$$r_1 = \frac{n \sum xy_1 - \sum x \sum y_1}{\sqrt{n \sum x^2 - (\sum x)^2} \sqrt{n \sum y_1^2 - (\sum y_1)^2}} = 0.84, \quad (1)$$

Table 4. Results of correlation and regression analyses of parameters $y_1:x$, $y_2:x$ and $y_1:y_2^*$

Characteristic	Numerical value		
	<i>x</i>	<i>y</i> ₁	<i>y</i> ₂
Confidence probability, <i>P</i>	0.95	0.95	0.95
Coefficient of correlation:			
<i>r</i> ₁	–	0.84	–
<i>r</i> ₂	–	–	0.79
Interval for a strong relation:			
table		[0.7; 0.9]	
calculation		[0.79; 0.84]	
Mathematical expectation, <i>M</i> (arithmetic mean)	3.66	1.07	4.73
Limits of interval:			
lower (–0.95)	2.95	0.94	3.99
upper (+0.95)	4.37	1.21	5.48
Value of parameter at the limit of a confidence interval:			
maximum	7.20	2.20	8.84
minimum	0	0.50	1.10
Range	7.20	1.70	7.74
Dispersion, <i>S</i>	5.21	0.20	5.74
Standard deviation, $\sigma_{y/x}$ (root-mean-square)	2.28	0.44	2.40
Equations of regression:			
$y_1 = f(x)$		$y_1 = 0.165x + 0.462$	
$y_2 = f(x)$		$y_2 = 0.852x + 1.617$	
$y_1 = f(y_2)$		$y_1 = 0.119y_2 + 0.509$	
Confidence zones of linear regression, $\Delta_{y/x}$		$y_1 = 0.165x + 0.462 \pm \Delta_{y/x}$	
		$y_2 = 0.852x + 1.617 \pm \Delta_{y/x}$	
		$y_1 = 0.119y_2 + 0.509 \pm \Delta_{y/x}$	

*Number of experiments (selection) was 42.

$$r_2 = \frac{n \sum xy_2 - \sum x \sum y_2}{\sqrt{n \sum x^2 - (\sum x)^2} \sqrt{n \sum y_2^2 - (\sum y_2)^2}} = 0.79. \quad (2)$$

The values r_1 and r_2 are within the interval $0.7 \leq r \leq 0.9$ that characterizes the condition of a strong interrelation between two random parameters. Relation $y_1 = f(x)$ is presented by the equation

$$y_1 = a_1x + b_1, \quad (3)$$

whose coefficient was determined by the least-squares method [7]. Substituting numerical values of variables from data of regression analysis we shall obtain a system of normal equations. After their solution we shall find coefficients a_1 and b_1 :

$$\begin{cases} (\sum x)a_1 + nb_1 = \sum y_1, & a_1 = 0.165, \\ (\sum x^2)a_1 + (\sum x)b_1 = \sum xy_1, & b_1 = 0.462. \end{cases} \quad (4)$$

The equation of regression line (3) will take form

$$y_1 = 0.165x + 0.462. \quad (5)$$



Similarly, we shall calculate the coefficient of regression line $y_2 = f(x)$:

$$y_2 = a_2x + b_2, \tag{6}$$

$$\begin{cases} (\sum x)a_2 + nb_2 = \sum y_2, & a_2 = 0.852, \\ (\sum x^2)a_2 + (\sum x)b_2 = \sum xy_2, & b_2 = 1.617. \end{cases} \tag{7}$$

The equation (6) will take form

$$y_2 = 0.852x + 1.617. \tag{8}$$

In accordance with (5) and (8) the calculation lines of regression are plotted (see Figure, *a, b*). After solution of these equations we shall find a correlation relation of functions $y_1 = f(y_2)$:

$$\begin{cases} y_1 = 0.165x + 0.462, \\ y_2 = 0.852x + 1.617, \end{cases} \tag{9}$$

$$y_1 = 0.119y_2 + 0.509.$$

A calculation regression line is shown in Figure, *c*. It follows from graphs that the parameters y_1 and y_2 (results of real and laboratory tests, respectively) are mutually correlated.

To determine a confidence zone of the linear regression we shall use the formula from [8]

$$\Delta_{y/x} = t\sigma_{y/x}, \tag{10}$$

where $\Delta_{y/x}$ is the linear deviation of experimental point \tilde{y}_i from corresponding point y_i at the regression line; t is the nominal deviation; $\sigma_{y/x} = \sqrt{\frac{\sum(y_i - \tilde{y}_i)^2}{n - 2}}$ is the standard deviation.

The processing of experiment results (see Table 3) by the above-described procedure was realized in the computer using special programs. The mutual correlation of the parameters y_1 and y_2 results from the given graphs plotted on the basis of equations (5), (8) and (9). The confidence zones reflect limits, i.e. ellipses of correlation fields. The main describing statistics are given in Table 4.

The above results make it possible to state that the complex of experiments using solutions NaOH can be determining also for the industrial liquors. This factor outlines the right application of sodium hydroxide as a model medium in investigation of corrosion of materials operating in alkali media used in the pulp-and-paper industry.

REFERENCES

1. Smith, K. (1981) Explosion of a continuous cooking boiler. *Pulp and Paper*, **10**, 66 – 69.
2. Singbeil, D., Garner, A. (1984) Stress corrosion cracking of Kraft continuous digesters. In: *Proc. of Int. Congr. on Met. Corr.*, Toronto, June 3 – 7. Ottawa.
3. Chakrapani, D.G. *et al.* (1984) Pulp digester cracking afflicts a variety of alloys. *Ibid.*
4. Mueller, D.A. (1967) Corrosion studies of carbon steel in alkaline pulping liquors by potential time and polarization – gurvo-reteds. *TAPPI*, **3**, 139 – 140.
5. Shkolnikov, E.V., Ananieva, G.F., Smirnov, V.D. (1988) How to decrease corrosion of cooking boilers. *Bumazhn. Promyshlennost*, **12**, 32 – 34.
6. Kolemaev, V.A., Staroverov, O.V., Turundayevsky, V.B. (1997) *Theory of probability and mathematical statistics*. Moscow: Vysshaya Shkola.
7. Rumshinsky, L.Z. (1971) *Mathematical processing of results of experiments*. Moscow: Nauka.
8. Lakin, G.F. (1983) *Biometry*. Moscow: Vysshaya Shkola.



STATISTIC ANALYSIS OF CORROSION RESISTANCE OF CHROMIUM-NICKEL DEPOSITED METAL IN ALKALI SOLUTIONS

P.P. LAZEBNOV

Zaporizhya State Technical University, Zaporizhya, Ukraine

ABSTRACT

Results of comparative corrosion tests of Cr–Ni deposited metal in alkali solutions are given. Correlation and regression analyses are made, thus examining the interrelation between the input (δ -ferrite in welds) and output (rate of metal corrosion) parameters.

Key words: regression and correlation analyses, deposited metal, corrosion rate, sodium hydroxide, cooking liquor, correlation

The equipment for chemical industry is subjected to the corrosion processes. In one cases these processes lead to a uniform fracture of steels and alloys, while in others — to the corrosion cracking and other types of corrosion of structures, which are operating in contact with aggressive media. Thus, in 1980 a cooking boiler «Kamyur» of 1100 t/day capacity at the pulp-and-paper mill «McMillan Blodel» (USA) exploded because of a corrosion failure of a butt welded joint of the upper conical part with a vessel cylinder [1]. After three-year inspection of work of boilers of a continuous cooking at the sulphate-pulp factories of the USA, the results of inspection were summarized and presented at the International Congress in Toronto (Canada) [2, 3] and the following conclusions were made.

Among 107 boiling apparatuses, more than 40 of them had cracks in welded joints of an impregnation zone located in casing metal. They were mainly observed in welded joints of vessels made from carbon and bimetal steels and also Inconel-plated steels.

The crack initiation is observed in structures passed heat treatment and without it. Boilers with a full treatment are less sensitive to the corrosion cracking than the apparatuses with a local «normalizing» of welded joints.

In all the boilers the corrosion processes are provoked by a main component of the cooking liquor — NaOH.

The industrial solutions, in which the sulphate cellulose is cooked, are the complex systems. Table 1 gives characteristics of the cooking liquors used.

At designing of technological complexes of the pulp-and-paper industry, the Cr–Ni steels were successfully used for many decades (cooking boilers of companies «Kamyur», «Pandia», KMW, steaming towers, etc.). Coming from technical-economical tasks the vessels are manufactured from a bimetal sheet rolled stock. The bimetal has a base layer (boiler steels of type 17Mn4 and analogs of steels 20K, 22K) which is clad with corrosion-resistant steels of types 10Kh18N10T (C — 0.1; Cr — 18.0; Ni — 10.0; Ti — 0.6 wt.%), 08Kh17N15M2T (C — 0.08; Cr — 17.0; Ni — 15.0; Mo — 2.0; Ti — 0.6 wt.%). Analysis of condition of the boilers park showed that, as a result of long-time service, the protective layer of the apparatuses underwent a significant corrosion action.

The study of corrosion-active and inhibiting ingredients of the sulphate liquor plays a large role in fighting with the corrosion. It was established that the carbonate- and silicate-ions have inhibiting action, while the chloride-, sulphite- and sulphate-ions have activating action on the corrosion processes. As it follows from [5], sodium chloride NaCl and sodium thiosulphate Na₂S₂O₃ contribute to the initiation of a pitting corrosion in stainless steels, the sodium sulphate Na₂SO₄ brakes it remarkably, while the sodium sulphite Na₂SO₃ is neutral (Table 2).

Corrosion action of the sulphate liquor on steel 10Kh18N10T and 10Kh17N13M2T (C — 1.0; Cr — 17.0; Ni — 13.0; Mo — 2.0; Ti — 0.6 wt.%) increases with increase in temperature (reaching maximum at

Table 1. Composition of white liquors

Sulphate factory	Concentration of elements in solution, C, g/l						
	NaOH	Na ₂ S	Na ₂ CO ₃	Na ₂ SO ₄	NaCl	Na ₂ S ₂ O ₃	Na ₂ SO ₃
CIS	75.0 – 90.0	11.0 – 35.0	10.0 – 11.0	0.9 – 2.8	0.2	2.0 – 5.0	0.20
Canada [4]	≤ 95.2	39.2	26.6	6.5	6.5	5.2	0.99



Table 2. Single-factor effect of anions of white sulphate liquor on corrosion rate, R_c , of steel 10Kh18N10T [5]

<i>NaCl</i>		<i>Na₂SO₄</i>		<i>Na₂S₂O₃</i>		<i>Na₂SO₃</i>	
<i>C, g/l</i>	<i>R_c mm/year</i>	<i>C, g/l</i>	<i>R_c mm/year</i>	<i>C, g/l</i>	<i>R_c mm/year</i>	<i>C, g/l</i>	<i>R_c mm/year</i>
–	0.063	2.7	0.064	2.0	0.067	0.1	0.065
0.2	0.084	4.0	0.046	3.0	0.069	0.5	0.066
0.5	0.122	5.0	0.045	4.0	0.068	1.0	0.066
1.0	0.176	6.0	0.043	5.0	0.067	2.0	0.068
1.5	0.192	7.0	0.040	7.0	0.232	3.0	0.069
2.0	0.209	8.0	0.039	8.0	0.235	4.0	0.070

Note: Specimens were tested at 100 °C temperature in a model solution of liquor, g/l: NaOH – 86.40; Na₂S – 30.40; Na₂SO₄ – 2.70; Na₂S₂O₃ – 2.00; Na₂CO₃ – 1.00; Na₂SO₃ – 0.09.

130 – 160 °C) depending on concentration of active alkali and decreases as a result of dilution with a black liquor (in accordance with technological regulations of sulphate-pulp factories).

In study of general corrosion resistance of Cr–Ni metals of different systems of alloying in sodium hydroxide and industrial white liquor (NaOH – 35 – 60; Na₂S – 15; Na₂CO₃ – 11; Na₂S₂O₃ and Na₂SO₄ – 0.2 g/l) of boiler «Kamyur» at the Arkhangelsk pulp-and-paper mill a similar regularity of corrosion rate on temperature differed only by quantitative characteristics is observed. To confirm the right use of NaOH for accelerating tests of solutions in the development of welding materials used in alkali media of pulp-and-paper industry a statistic processing of data of corrosion resistance of specimens in laboratory and real conditions was made (Table 3).

The methods of correlation and regression analysis make it possible to study the relation between the input and output parameters. Often, a coefficient of

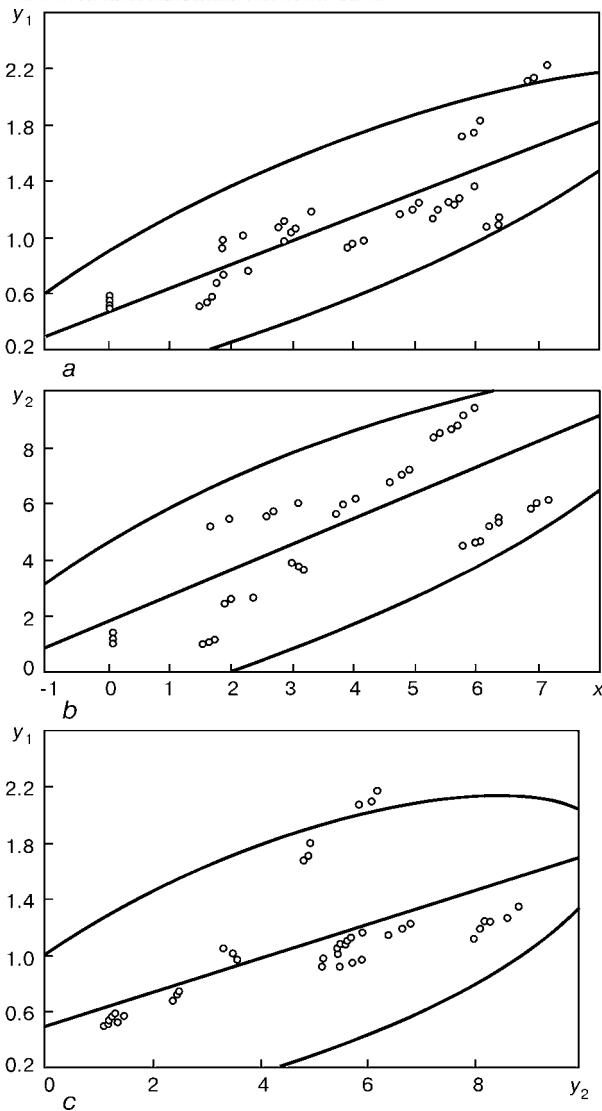
correlation r_{yx} (in case of a linear relation) is characteristics of closeness of relation between two random values [6, 7]. At a sufficient closeness of distribution of examining variables x, y to a normal law r_{yx} is a characteristic of degree of interrelation closeness. The given situation is typical of a linear relation (probability of plotting a hypothetical line of regression in a correlation field).

A regression analysis of a series of experiments (see Table 3) was made at an input parameter x (mass share of δ -ferrite, %) and output parameters y_1, y_2 (corrosion rate during real R_{c1} and laboratory R_{c2} tests). On the basis of Table data, a statistic processing of results was made. A graphical pair correlation of two cases $y_1:x$ and $y_2:x$ was made preliminary which allows setting of correlation between y_1, y_2 and x , and also its form. In accordance with data of Table 3, the points whose set forms a correlation field (Figure, *a, b*), are plotted in coordinates $y_1:x$ and $y_2:x$. On this basis, a hypothesis was assumed that

Table 3. Corrosion resistance of Cr–Ni deposited metal

<i>Number of specimen</i>	<i>Grade of welding electrode</i>	<i>Type of deposited metal</i>	<i>Mass content of δ-ferrite, %</i>	<i>Rate of corrosion at tests, g/(m²·h)</i>	
				<i>full-scale R_{c1}</i>	<i>laboratory R_{c2}</i>
			<i>x</i>	<i>y₁</i>	<i>y₂</i>
1 – 3	OZL-8	07Kh20N9	6.9; 7.0; 7.2	0.0209; 0.0212; 0.0220	0.0589; 0.0611; 0.0623
4 – 6	TsL-11	08Kh20N10G2	6.2; 6.4; 6.4	0.0106; 0.0108; 0.0113	0.0544; 0.0560; 0.0570
7 – 9	ZIO-3	07Kh19N10G2B	5.8; 6.0; 6.1	0.0170; 0.0173; 0.0182	0.0485; 0.0492; 0.0499
10 – 12	NIAT-1	08Kh19N11M2G2	5.7; 5.8; 6.0	0.0124; 0.0128; 0.0135	0.0836; 0.0864; 0.0884
13 – 15	NZh-13	08Kh19N10M2B	5.3; 5.4; 5.6	0.0112; 0.0119; 0.0124	0.0800; 0.0814; 0.0824
16 – 18	EA-400/10u	07Kh19N11M3G2F	4.8; 5.0; 5.1	0.0115; 0.0119; 0.0123	0.0642; 0.0669; 0.0681
19 – 21	OZL-6	10Kh25N13G2	3.9; 4.0; 4.2	0.0092; 0.0094; 0.0096	0.0549; 0.0575; 0.0589
22 – 24	EA-395/9	11Kh15N25M6G2	–	0.0050; 0.0051; 0.0055	0.0110; 0.0115; 0.0120
25 – 27	EA-981/15	09Kh15N25M6G2F	–	0.0052; 0.0057; 0.0059	0.0117; 0.0125; 0.0129
28 – 30	Pilot	09Kh20N10 (0.01% Y)	2.9; 3.0; 3.1	0.0096; 0.0103; 0.0107	0.0357; 0.0347; 0.0332
31 – 33	Same	07Kh20N10 (0.02% Y)	1.5; 1.6; 1.7	0.0052; 0.0053; 0.0057	0.0133; 0.0135; 0.0146
34 – 35	»	08Kh20N10 (0.027% Y)	1.8; 1.9; 2.3	0.0067; 0.0073; 0.0076	0.0236; 0.0243; 0.0246
36 – 38	OKR.6 (Sweden)	06Kh19N9M3	2.8; 2.9; 3.3	0.0108; 0.0111; 0.0117	0.0552; 0.0566; 0.0592
39 – 42	832MVR (Sweden)	04Kh21N10G2	1.9; 1.9; 2.2	0.0092; 0.0098; 0.0101	0.0517; 0.0520; 0.0542

Notes. 1. Full-scale tests of boiler «Kamyur» were performed at 120 – 170 °C and pressure 1.2 MPa in a cooking liquor during 15100 h.
2. Laboratory tests of autoclave were performed at 130 °C and pressure 0.2 MPa in 30 % solution of NaOH during 240 h.



Regression and correlation analyses of results of experiments: *a* – full-scale tests of specimens of deposited metal in a cooking liquor and sodium hydroxide ($y_1 = 0.165x + 0.462$); *b* – same, the laboratory tests ($y_2 = 0.852x + 1.617$); *c* – correlation relation $y_1 = f(y_2)$ ($y_1 = 0.119y_2 + 0.509$)

there is a linear relation between the parameters examined, and, consequently, the regression lines are straight.

Initial data for regression analysis are given below (summing of results from 42 experiments):

$$\begin{aligned} \sum x &= 155.0; \sum y_1 = 47.83; \sum y_2 = 204.44; \\ \sum xy_1 &= 211.20; \sum x^2 = 784.50; \sum y_1^2 = 64.58; \\ \sum xy_2 &= 933.70; \sum y_2^2 = 1225.50. \end{aligned}$$

Using these data the coefficients of correlation between parameters $y_1:x$ and $y_2:x$ are determined according to formulae [7]

$$r_1 = \frac{n \sum xy_1 - \sum x \sum y_1}{\sqrt{n \sum x^2 - (\sum x)^2} \sqrt{n \sum y_1^2 - (\sum y_1)^2}} = 0.84, \quad (1)$$

Table 4. Results of correlation and regression analyses of parameters $y_1:x$, $y_2:x$ and $y_1:y_2^*$

Characteristic	Numerical value		
	<i>x</i>	<i>y</i> ₁	<i>y</i> ₂
Confidence probability, <i>P</i>	0.95	0.95	0.95
Coefficient of correlation:			
<i>r</i> ₁	–	0.84	–
<i>r</i> ₂	–	–	0.79
Interval for a strong relation:			
table		[0.7; 0.9]	
calculation		[0.79; 0.84]	
Mathematical expectation, <i>M</i> (arithmetic mean)	3.66	1.07	4.73
Limits of interval:			
lower (–0.95)	2.95	0.94	3.99
upper (+0.95)	4.37	1.21	5.48
Value of parameter at the limit of a confidence interval:			
maximum	7.20	2.20	8.84
minimum	0	0.50	1.10
Range	7.20	1.70	7.74
Dispersion, <i>S</i>	5.21	0.20	5.74
Standard deviation, $\sigma_{y/x}$ (root-mean-square)	2.28	0.44	2.40
Equations of regression:			
$y_1 = f(x)$		$y_1 = 0.165x + 0.462$	
$y_2 = f(x)$		$y_2 = 0.852x + 1.617$	
$y_1 = f(y_2)$		$y_1 = 0.119y_2 + 0.509$	
Confidence zones of linear regression, $\Delta_{y/x}$		$y_1 = 0.165x + 0.462 \pm \Delta_{y/x}$	
		$y_2 = 0.852x + 1.617 \pm \Delta_{y/x}$	
		$y_1 = 0.119y_2 + 0.509 \pm \Delta_{y/x}$	

*Number of experiments (selection) was 42.

$$r_2 = \frac{n \sum xy_2 - \sum x \sum y_2}{\sqrt{n \sum x^2 - (\sum x)^2} \sqrt{n \sum y_2^2 - (\sum y_2)^2}} = 0.79. \quad (2)$$

The values r_1 and r_2 are within the interval $0.7 \leq r \leq 0.9$ that characterizes the condition of a strong interrelation between two random parameters. Relation $y_1 = f(x)$ is presented by the equation

$$y_1 = a_1x + b_1, \quad (3)$$

whose coefficient was determined by the least-squares method [7]. Substituting numerical values of variables from data of regression analysis we shall obtain a system of normal equations. After their solution we shall find coefficients a_1 and b_1 :

$$\begin{cases} (\sum x)a_1 + nb_1 = \sum y_1, & a_1 = 0.165, \\ (\sum x^2)a_1 + (\sum x)b_1 = \sum xy_1, & b_1 = 0.462. \end{cases} \quad (4)$$

The equation of regression line (3) will take form

$$y_1 = 0.165x + 0.462. \quad (5)$$



Similarly, we shall calculate the coefficient of regression line $y_2 = f(x)$:

$$y_2 = a_2x + b_2, \tag{6}$$

$$\begin{cases} (\sum x)a_2 + nb_2 = \sum y_2, & a_2 = 0.852, \\ (\sum x^2)a_2 + (\sum x)b_2 = \sum xy_2, & b_2 = 1.617. \end{cases} \tag{7}$$

The equation (6) will take form

$$y_2 = 0.852x + 1.617. \tag{8}$$

In accordance with (5) and (8) the calculation lines of regression are plotted (see Figure, *a, b*). After solution of these equations we shall find a correlation relation of functions $y_1 = f(y_2)$:

$$\begin{cases} y_1 = 0.165x + 0.462, \\ y_2 = 0.852x + 1.617, \end{cases} \tag{9}$$

$$y_1 = 0.119y_2 + 0.509.$$

A calculation regression line is shown in Figure, *c*. It follows from graphs that the parameters y_1 and y_2 (results of real and laboratory tests, respectively) are mutually correlated.

To determine a confidence zone of the linear regression we shall use the formula from [8]

$$\Delta_{y/x} = t\sigma_{y/x}, \tag{10}$$

where $\Delta_{y/x}$ is the linear deviation of experimental point \tilde{y}_i from corresponding point y_i at the regression line; t is the nominal deviation; $\sigma_{y/x} = \sqrt{\frac{\sum(y_i - \tilde{y}_i)^2}{n-2}}$ is the standard deviation.

The processing of experiment results (see Table 3) by the above-described procedure was realized in the computer using special programs. The mutual correlation of the parameters y_1 and y_2 results from the given graphs plotted on the basis of equations (5), (8) and (9). The confidence zones reflect limits, i.e. ellipses of correlation fields. The main describing statistics are given in Table 4.

The above results make it possible to state that the complex of experiments using solutions NaOH can be determining also for the industrial liquors. This factor outlines the right application of sodium hydroxide as a model medium in investigation of corrosion of materials operating in alkali media used in the pulp-and-paper industry.

REFERENCES

1. Smith, K. (1981) Explosion of a continuous cooking boiler. *Pulp and Paper*, **10**, 66 – 69.
2. Singbeil, D., Garner, A. (1984) Stress corrosion cracking of Kraft continuous digesters. In: *Proc. of Int. Congr. on Met. Corr.*, Toronto, June 3 – 7. Ottawa.
3. Chakrapani, D.G. *et al.* (1984) Pulp digester cracking afflicts a variety of alloys. *Ibid.*
4. Mueller, D.A. (1967) Corrosion studies of carbon steel in alkaline pulping liquors by potential time and polarization – gurvo-reteds. *TAPPI*, **3**, 139 – 140.
5. Shkolnikov, E.V., Ananieva, G.F., Smirnov, V.D. (1988) How to decrease corrosion of cooking boilers. *Bumazhn. Promyshlennost*, **12**, 32 – 34.
6. Kolemaev, V.A., Staroverov, O.V., Turundayevsky, V.B. (1997) *Theory of probability and mathematical statistics*. Moscow: Vysshaya Shkola.
7. Rumshinsky, L.Z. (1971) *Mathematical processing of results of experiments*. Moscow: Nauka.
8. Lakin, G.F. (1983) *Biometry*. Moscow: Vysshaya Shkola.



EFFECT OF HYDROGEN IN LOW-ALLOYED WELD METAL ON PORE FORMATION IN SUBMERGED ARC WELDING

I.A. GONCHAROV, A.P. PALTSEVICH and V.S. TOKAREV
The E.O. Paton Electric Welding Institute, NASU, Kyiv, Ukraine

ABSTRACT

The content of diffusive and residual hydrogen in the deposited and weld metal was determined using the method of a gas chromatography in welding with fused manganese-silicate fluxes of AN-348A, AN-60 and AN-60SM grades. It was established that the critical content of hydrogen in weld during SAW at which the pores are formed, does not depend on the flux grade and amounts to $12 - 14 \text{ cm}^3 \text{ H}_2 / 100 \text{ g}$ of weld metal that is equal to the hydrogen solubility in δ -iron at melting temperature and 10^5 Pa pressure.

Key words: fused flux, deposited metal, weld metal, pores, diffusive hydrogen, residual hydrogen

Assurance of sound welds is one of main requirements specified to welding fluxes. To evaluate the resistance of welds to pore formation, a method was suggested by K.V. Lyubavsky, which consists in a bead deposition on a plate with a V-shaped groove, filled preliminary with a portion of a rust [1]. Criterion of evaluation is a minimum amount of the rust (in grams per 100 mm of weld), at which the external pores are formed.

Due to its simplicity the method of Lyubavsky was widely spread in testing of welding fluxes. However, as was noted by the author, the rust composition is changed depending on the conditions of its producing and storage. Naturally, here, the critical amount of the rust is changed causing the pore formation in the welds. In addition, depending on the sizes of plates, groove, steel grade, wire diameter and welding conditions the resistance against the pore formation during welding is greatly changed [2, 3]. It seen from Table 1 that the results of testing fluxes by the Lyubavsky's method carried out by us at different surfacing conditions are comparative and suitable for evaluation within one series of experiments with the same welding conditions, sizes of samples and rust composition. Actually, the flux properties and welding technology peculiarities are evaluated by this method from the point of view of prevention of porosity caused by hydrogen.

It is known from the literature [3, 4] that the main cause of the weld porosity in SAW is an increased content of hydrogen and abrupt drop of its solubility during metal solidification. The most valid data about the hydrogen solubility within the range of temperature of iron melting T_m are given in [5, 6] and they amount to $12 - 14$ for a solid iron and $27 - 28 \text{ cm}^3 / 100 \text{ g}$ for the molten iron.

Data about hydrogen content and pore formation in welds during the SAW are not numerous and con-

tradictory. The authors of [3] showed that the welds are sound at hydrogen content up to 6.5 and porous — at $7.6 \text{ cm}^3 / 100 \text{ g}$. According to [7], the samples for hydrogen analysis in welding with flux AN-30 contained $[\text{H}]_{\text{diff}} + [\text{H}]_{\text{res}} > 17.3 \text{ cm}^3 / 100 \text{ g}$. It should be noted that flux before welding was calcinated at $300 \text{ }^\circ\text{C}$ temperature for 3 h and the defects were not observed in the samples. The contradiction of data is due to the imperfection of methods of sampling and analysis. Moreover, low values of the diffusion hydrogen in the deposited metal in SAW ($0.8 - 2.8 \text{ cm}^3 / 100 \text{ g}$) given in works [8, 9] are explained by the imperfection of the method of analysis and not precise terminology. As a matter of fact the question is about the weld metal when the authors produce a «pencil» sample by pouring the weld pool metal to a copper mould.

To obtain the objective data about the hydrogen content in the deposited and weld metal in SAW and their comparison with a hydrogen solubility in iron at the melting temperature, the chromatographic method of analysis of $[\text{H}]_{\text{diff}}$ by GOST 23338-91 using a gas analyzer OB-2178 was used. Samples for the analysis were manufactured from X-70 (C — up to 0.12; Mn — 1.6; Si — 0.3; Nb — 0.04; N — 0.07 wt.%; Fe — balance) type steel. The welding wire of Sv-10GN (C — 0.1; Mn — 1.0; Ni — 0.8 wt.%; Fe — balance) grade of 4 mm diameter was cleaned from copper plating and degreased before welding. The surfacing was performed at the following conditions: $I_w = 550 - 600 \text{ A}$, $U_a = 32 - 34 \text{ V}$, $v_w = 36 \text{ m/h}$. The hydrogen content in welds varied by introducing different amount of rust to the $2.5 \times 2.5 \text{ mm}$ grooves on the samples.

After measuring the $[\text{H}]_{\text{diff}}$ content in the deposited and weld metal the samples of 4 – 5 mm diameter and 15 mm length were cut from welds to determine the content of $[\text{H}]_{\text{res}}$ by the method of a gas chromatography using equipment described in [10]. The samples were degassed at temperature $800 \text{ }^\circ\text{C}$ until stoppage of the residual hydrogen evolution.

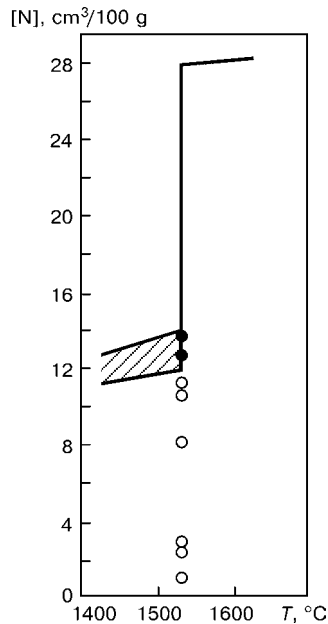


Table 1. Results of testing welding fluxes by the Lyubavsky's method

Surfacing conditions (DCRP)	Amount of introduced rust, g/100 mm of weld	Pores in welds in submerged arc surfacing		
		AN-348A	AN-60SM	AN-60
Steel 09G2 (C — 0.09; Mn — 2.0 wt.%; Fe — balance), wire Sv-08GA (C < 0.1; Mn — 0.8 — 1.0 wt.%; Fe — balance) 3 mm dia., $v_w = 70$ m/h, $U_a = 34$ V, $I_w = 450$ A	0.1	None	—	—
	0.15	Chain	—	—
	0.2	Same	None	None
	0.3	—	Chain	Single
	0.4	—	—	Chain
Steel 10G2 (C — 0.1; Mn — 2.0 wt.%; Fe — balance), wire Sv-08A (C — 0.1; Si — 0.03; Mn — 0.35 — 0.65 wt.%; Fe — balance) 4 mm dia., $v_w = 36$ m/h, $U_a = 32$ V, $I_w = 600$ A	0.2	None	—	—
	0.3	Single	—	—
	0.4	Chain	None	—
	0.5	Continuous	Single	—
	0.6	—	Chain	—
	0.7	—	—	None
	0.8	—	—	Single
	0.9	—	—	Chain
	0.9	—	—	Chain
St.3 (C — 0.14 — 0.22; Mn — 0.3 — 0.6 wt.%; Fe — balance), wire Sv-08A 4 mm dia., $v_w = 24$ m/h, $U_a = 38$ V, $I_w = 650$ A	0.7	None	—	—
	0.8	Chain	—	—
	1.3	—	None	—
	1.4	—	Chain	—
	1.8	—	—	None
	2.0	—	—	Single
	2.0	—	—	Single

Table 2. Hydrogen content in submerged arc welding

Flux	Amount of introduced rust, g/100 mm of weld	Pores in weld	Content of $[H]_{diff}$ in deposited metal, $cm^3/100$ g	Hydrogen content in weld metal, $cm^3/100$ g		
				$[H]_{diff}$	$[H]_{res}$	$[H]_{total}$
AN-348A	0	None	9.3; 11.0; 9.1 9.8	2.8; 3.3; 2.6 2.9	0.2	3.1
	0.2	Same	37.2; 41.0; 37.3 38.5	9.7; 11.3; 10.3 10.4	0.2	10.6
	0.3	Many	50.9; 40.5; 28.3 39.9	16.6; 14.6; 10.0 13.7	0.3	14.0
AN-60SM	0	None	2.4; 2.3; 3.2 2.6	1.0; 0.8; 1.0 0.9	0.1	1.0
	0.3	Same	34.8; 35.7; 31.9 34.1	9.4; 12.8; 10.8 11.0	0.2	11.2
	0.4	Single	38.4; 35.9; 43.4 38.0	11.6; 12.4; 13.8 12.6	0.3	12.9
AN-60	0	None	6.1; 6.2; 5.6 6.0	2.1; 2.1; 2.0 2.1	0.3	2.4
	0.4	Same	19.6; 19.2; 16.8 18.5	9.3; 7.7; 7.0 8.0	0.2	8.2
	0.5	Many	43.5; 35.1; 30.4 36.3	15.4; 13.2; 12.6 13.7	0.3	14.0



Effect of hydrogen concentration in weld metal at melting temperature on pore formation in welds: ○ — sound metal; ● — pores in metal

The fluxes AN-60, AN-348A and AN-60SM were used for investigations, which are close in chemical composition and belonged to the same slag system $MnO-SiO_2-CaF_2$, but differed by a mechanism of prevention of hydrogen absorption by the weld pool. In welding with a pumicious flux AN-60 a significant amount of silicon tetrafluoride is evolved, binding the hydrogen in the zone of welding into HF which is insoluble in steel. In welding with a glass-type flux AN-348A the surface of grains is less developed and SiF_4 evolution is less intensive. As a result the hydrogen in the zone of welding has a poor binding. Flux AN-60SM, which has a glass-crystalline structure of grains, evolves a lower amount of SiF_4 as compared with flux AN-348A during heating in the welding process. At similar conditions the air sampling from the zone of welding the evolution of silicon tetrafluoride amounts to 0.51 mg/m^3 in flux AN-60SM and 0.73 mg/m^3 in AN-348A flux. In [11] we have established that flux AN-60SM is differed from flux AN-348A and AN-60 by a lower content of the potential hydrogen and lower temperature of its desorption during heating.

Table 2 gives the results of measurement of content of the diffusive hydrogen in the deposited and weld metal and also residual hydrogen in SAW with fluxes AN-60, AN-348A and AN-60SM. It is seen from the given data that the critical content of hydrogen in weld at which the pores begin to form for all three types of fluxes is approximately similar and amounts to $12 - 14 \text{ cm}^3/100 \text{ g}$ of weld metal.

The results obtained are well correlated with experimental data of [12] where it was stated that the critical concentration of hydrogen for the pore formation in a pure iron is $13 \text{ cm}^3/100 \text{ g}$ of iron and also of [13] where it was outlined that pores appear in

weld at $12 - 14 \text{ cm}^3/100 \text{ g}$ of weld metal in welding with coated electrodes of the calcium fluoride type.

In Figure the data obtained by us are combined with a fragment of a diagram of Fe-H₂ solubility within the range of temperature of solid iron melting for the better visual presentation. As is seen, the pores are formed in metal during the SAW, if the hydrogen content in it at the moment of solidification is equal to the solubility limit.

The knowledge of this fact makes it possible to use the difference between the critical content of hydrogen in weld causing the pore formation ($12 \text{ cm}^3/100 \text{ g}$) and hydrogen content in weld during welding with this flux as a criterion of resistance of welds to the pore formation in SAW. From data of Table 2 resistance limit of welds to the pore formation in SAW with flux AN-60SM is highest ($12.0 - 1.0 = 11.0 \text{ cm}^3/100 \text{ g}$). Welds, produced with flux AN-60 ($12.0 - 2.4 = 9.6 \text{ cm}^3/100 \text{ g}$), occupy the intermediate position. Welds, produced with flux AN-348A ($12.0 - 3.1 = 8.9 \text{ cm}^3/100 \text{ g}$) have the lowest resistance to the pore formation.

The data obtained about the diffusive hydrogen content in the deposited metal makes it possible, except the feasibility of assessment of the weld resistance to pore formation by the hydrogen content in the latter, to use the standard classification of IIW by the levels of hydrogen in welds, developed relative to welding with electrodes, to the welding fluxes [14]. Flux AN-60SM provides a sufficiently low level of hydrogen (up to $5 \text{ cm}^3/100 \text{ g}$ of deposited metal), and fluxes AN-60 and AN-348A belong to the materials which provide the low level of hydrogen ($5 - 10 \text{ cm}^3/100 \text{ g}$ of deposited metal).

CONCLUSIONS

1. Critical content of hydrogen in weld during SAW, at which the pores are formed, is $12 - 14 \text{ cm}^3/100 \text{ g}$ of weld metal for the manganese-silicate fluxes, that is equal to the hydrogen solubility in δ -iron at melting temperature and pressure 10^5 Pa .

2. It was suggested that the difference between the critical content of hydrogen in weld causing the pore formation ($12 \text{ cm}^3/100 \text{ g}$) and hydrogen content in weld during welding with the flux examined can be used as a criterion of weld resistance to pore formation in SAW. In SAW with AN-60SM the resistance limit of welds to pore formation is highest. Welds produced with flux AN-60 occupy the intermediate position. Welds produced with flux AN-348A have the lowest resistance to the pore formation.

REFERENCES

1. Lyubavsky, K.V. (1948) Metallurgy of automatic submerged arc welding of low-carbon steel. In: *Problems of theory of welding processes*. Moscow: TsNIITMASH.
2. Frumin, I.I. (1956) Prevention of pores in submerged arc welding and surfacing. *Avtomaticheskaya Svarka*, **6**, 1 - 30.
3. Frumin, I.I., Kirido, I.V., Podgayetsky, V.V. (1949) Pore formation in welds and effect of flux composition on susceptibility to pores. *Avtogennoye Delo*, **10**, 1 - 11.



4. Podgayetsky, V.V. (1970) *Pores, inclusions and cracks in welds*. Kyiv: Tekhnika.
5. Shapovalov, V.I., Trofimenko, V.V. (1979) Hydrogen solubility in delta-iron. *Izv. Vuzov, Chern. Metallurgia*, **8**, 89 – 91.
6. Galaktionova, N.A. (1967) *Hydrogen in metals*. Moscow: Metallurgia.
7. Potapov, N.N., Lyubavsky, K.V. (1970) Hydrogen in deposited metal in submerged arc welding. *Svarochnoye Proizvodstvo*, **7**, 4 – 5.
8. Kovach, Ya., Petrov, G.L. (1974) Investigation of hydration and dehydration of acid fluxes for the automatic arc welding of steels. In: *Welding fluxes and slags*. Kyiv: Naukova Dumka.
9. Kasatkin, B.S., Vakhnin, Yu.N., Tsaryuk, A.K. *et al.* (1988) Effect of total content of hydrogen in flux An-17M on concentration of diffusive hydrogen in deposited metal. *Avtomaticheskaya Svarka*, **2**, 14 – 16.
10. Paltsevich, A.P. (1999) Chromatographic method of determination of hydrogen in components of electrode coatings. *Ibid*, **6**, 45 – 48.
11. Goncharov, I.A., Tokarev, V.S., Paltsevich, A.P. (1998) About the effect of method of production of welding fluxes on their quality. In: *Abstracts of papers of Int. Sci.-Techn. Seminar on Submerged Arc Welding Today and Tomorrow*, Zaporizhyya, Sept. 3 – 6. Kyiv: PWI.
12. (1976) Effect of hydrogen on blowhole formation in pure iron during solidification. *J. of the Iron and Steel of Japan*, **1**, 62 – 71.
13. Paltsevich, A.P. (1983) Experimental investigation of pore formation in welds caused by hydrogen in welding with electrodes with a basic coating. In: *Abstracts of papers of All-Union Conf. on Welding Consumables*, Cherepovets, Oct. 1 – 14. Kyiv: PWI.
14. (1973) Weld metal hydrogen levels and the definition of hydrogen-controlled electrodes. *IIW Doc. 11-682-73*.

ARC SPOT WELDING OF ALUMINIUM ALLOY THIN-SHEET ELEMENTS USING A DROP DOSING OF ELECTRODE METAL

N.M. TARASOV and S.S. KAPUSTIN
 Kharkov National Aerospace University, Kharkov, Ukraine

ABSTRACT

The technology of joining thin elements (0.8 – 2.0 mm), made from aluminium alloys, by the argon-arc welding with use of a drop dosing of the electrode metal, is described. The process of arc welding is presented, its main parameters are given and the strength of the joints is examined. Recommendations are given on the selection of conditions of butt joint welding.

Key words: argon-arc welding, aluminium alloys, thin-sheet elements, drop dosing, drop formation, joint, strength, stability

In some branches of engineering (aircraft, instrument, etc.) the thin-sheet structures from aluminium and its alloys found a wide application. Housings, chassis, covers of different instruments, pipelines, tanks are manufactured from thin (0.8 – 2.0 mm) sheets of aluminium alloys. The difficulties in welding of thin-sheet aluminium alloy structures are caused by the presence of a refractory oxide film on the surface of workpieces, a low rigidity of edges being welded and their susceptibility to distortion during the process of arc heating, as well as a high ratio of surface tension forces to the body force [1, 2]. The inaccuracy in assembly and distortion of edges in welding cause a local increase in gaps in the butt and change the nature of a heat dissipation that increases the probability of burn-through formation [3], complicates the technol-

ogy of welding, increases the expenses for the manufacture of components.

To improve the process of joint formation is possible by using a short-time local heating of the workpiece and a drop dosing of a filler metal [4].

The peculiarity of the mentioned process (Figure 1) is the fact that the spot welding is performed by a single drop of the molten metal of a preset mass and temperature. The elements to be welded are heated by arc at a reverse polarity current in argon. To localize heating and to reduce the consumption of gas the diameter of the outlet orifice of an outer nozzle 1 is selected close to the diameter of a weld spot, and the nozzle edge is located at a small distance from the workpiece surface. For this purpose, a support bushing 3 is fed closely to this surface. The drop mass is selected coming from the thicknesses of elements being welded. Each drop is formed from an electrode cut (stickout) of length l_e located at the edge of a massive heat-dissipating internal nozzle 2. During the drop formation and workpiece heating the electrode and the internal nozzle are fixed. A more flexible adjustment of the workpiece heating is provided with the

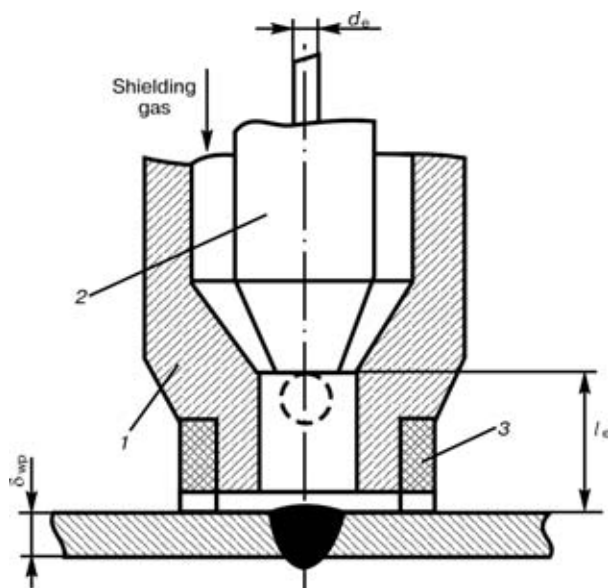


Figure 1. Schematic diagram of arc spot welding: 1 – outer nozzle; 2 – heat-dissipating internal nozzle; 3 – supporting bushing

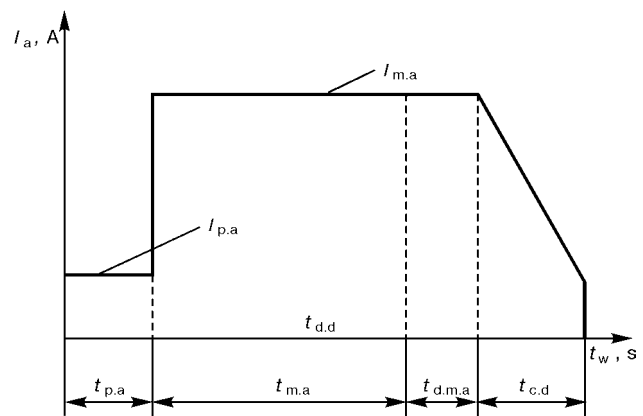


Figure 2. Cyclogram of welding current in formation and deposition of a drop: $I_{p.a}$ – pilot arc current; $I_{m.a}$ – main arc current; $t_{p.a}$ – time of pilot arc burning; $t_{m.a}$ – time of main arc burning; $t_{d.d}$ – moment of drop detachment; $t_{d.m.a}$ – time of main arc delay; $t_{c.d}$ – time of current drop

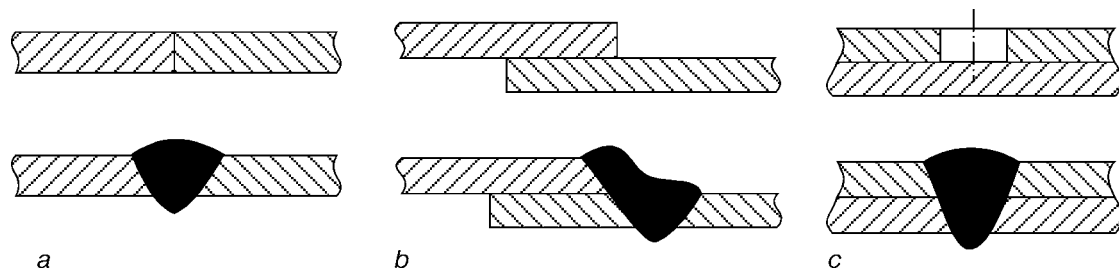


Figure 3. Preparation of edges and types of joints: *a* – butt; *b* – overlap; *c* – with a hole in one sheet

help of the heat-dissipating nozzle. After the drop formation the further arc burning is used for the workpiece heating. Here, the drop mass is not changed. It depends on the electrode diameter d_e , and also its stickout l_e and in case of the aluminium alloys, the mass can be adjusted within 0.03 – 0.12 g. The electrode diameter is selected coming from the workpiece thickness δ_{wp} . Thus, at $\delta_{wp} = 0.8 - 1.2$ mm $d_e = 1.6$ mm, at $\delta_{wp} = 1.2 - 2.0$ mm $d_e = 2.0$ mm. The detachment of a molten drop and its deposition on the workpiece are performed using a forced gas-dynamic method [4].

To provide the stability of the welding process a programming change in the arc current is used (Figure 2). At the beginning of the cycle during the arc exciting with a short-circuiting a pilot arc current $I_{p,a}$ is preset in a low value, then it is increased up to the operating value of a main arc current $I_{m,a}$. The mean temperature of drop is adjusted within 800 – 1700 °C by changing the electrode diameter and arc current. To improve the process of solidification and filling the crater after the drop detachment a delay in arc power current is used with a gradual its decreasing. To increase a space stability of the arc and to increase the degree of its constriction, the pulses of a unipolar current of 150 Hz frequency are used [5].

The main parameters of the welding process are the diameter d_e and stickout l_e , current of pilot arc $I_{p,a}$ and main arc $I_{m,a}$, time of burning of pilot arc $t_{p,a}$ and main arc $t_{m,a}$, the time of delay of a power current of main arc after the drop detachment $t_{d,m,a}$, consumption of argon.

The technology of arc spot welding of thin-sheet elements has been developed using the above-mentioned procedures. Experimental investigations showed that in this case the welded spots are produced similar in appearance, main sizes and strength. The deposited electrode metal is joined reliably to the workpieces to be welded. The developed technology makes it possible to perform welding of components

from aluminium alloys AMts (Al–Mn), AMg (Al–Mg), AK (Al–Cu–Mg–Mn), etc. Welding can be performed both without any backings and also on a removable backing using the different types of the joints: butt, overlap, including those with a hole in one sheet (Figure 3). Joints of type *b* are preferable at a small overlapping.

The mechanism of formation of joints and their characteristics were studied in changing different parameters and factors of the welding process. In particular, the effect of arc current I_a ($I_{m,a}$) and time of welding t_w ($t_{m,a}$) on the strength of butt joints and sizes of its main design elements were studied.

Standard AMts alloy specimens of 20 mm width and 1.2 mm thickness were butt welded by a single spot using equipment which provided a local heating and stepless adjustment of the arc current I_a and time of welding t_w within the wide ranges. The welding was performed by a special welding gun, with the help of which a dosed deposition of the molten metal is realized. As a filler metal a wire Sv-AMts of 2 mm diameter was used. The mass of the deposited drop was constant, i.e. $m_d = 90$ mg.

Two variants of welding were performed, using a removal backing and without any backings. A single-spot joints were tested in rupture test machine (three specimens at each condition) and a rupture strength P_r of a spot was determined. Main parameters of the welded spot were also measured (Figure 4): spot diameter d_s , height of upper reinforcement h , diameter of melting zone from reversed side d_1 and height of sagging h_1 .

In welding on a removable backing the value of P_r depends mainly on the sizes and shape of a cast weld nugget, which are determined by t_w and I_a . With increase in t_w and I_a the rupture force increases, reaching a maximum value, which depends on the mass of the deposited drops, thickness and material of the elements joined. The further increase in I_a and t_w at preserving high strength of the joint made by arc spot

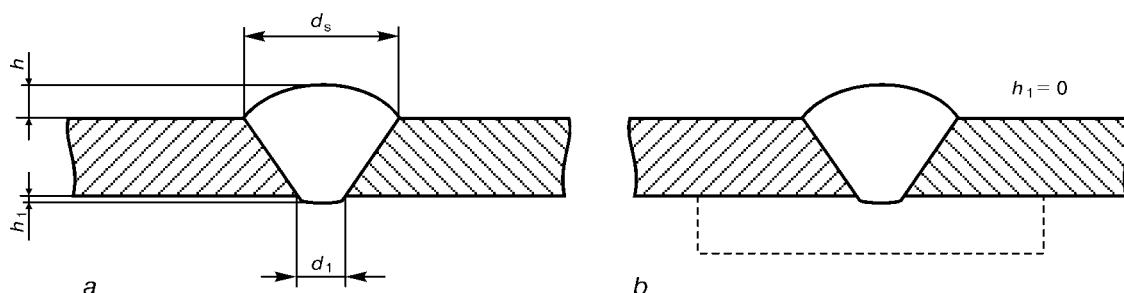


Figure 4. Main parameters of a welded spot in welding without backings (*a*) and on a removable backing (*b*)

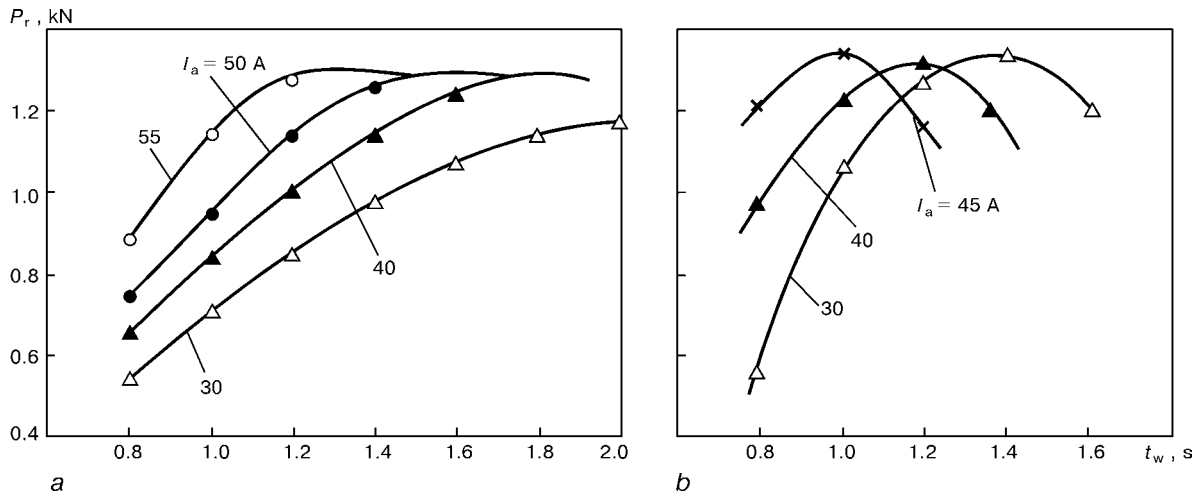


Figure 5. Dependence of rupture strength P_r on t_w at different values of I_a : *a* – welding on a removable backing; *b* – same, without backing

welding (Figure 5, *a*) leads to a deterioration of the appearance because of the molten metal overheating.

In welding without any backings the sagging formation is provided by a surface tension of film at the lower surface of the elements being welded. In this case the change in values I_a and t_w affect greatly on strength of welded spot joints. At low values I_a and t_w the non-fusion of elements is observed. In case of an excessive heating a large sagging (up to 5 mm) is observed from the lower side of the sheets. In addition, the spots are produced without the upper reinforcement and have a concave surface. The strength of such joints is small. The satisfactory welded spots in appearance have a negligible sagging from the lower side of sheet, resembling the shape of a rivet cap. Here, the maximum value P_r is 1.2 – 1.3 kN (Figure 5, *b*).

The fracture of welded specimens occurs with a tear of metal in one of the sheets. The deviation of values t_w for more than 0.2 s promotes unquality joint, while in welding on a removable backing the same increase in t_w leads only to the increase in sizes of the cast zone at high spot preserved strength. Consequently, in welding without any backings it is necessary to set values I_a and t_w more precisely and to keep constant.

The stability of characteristics of the produced joint and, first of all, strength is of a great importance. The strength of joints was examined in tensile test of AMts alloy specimens of 1.2 mm thickness and 20 mm width welded by a single spot without any backings at the following optimum conditions: $I_a = 40$ A; $t_w = 1.2$ s; $d_e = 2.0$ mm; $m_d = 90$ mg. AMts alloy was used for electrode. The number of test specimens was 100 pcs in a batch. To prevent the effect of parent

metal properties on the strength of joints, all the specimens for welding were cut from one sheet. The surface of specimens was degreased preliminary with acetone and cleaned with a metal brush. The test results were processed using the methods of a mathematical statistics.

The test results obtained showed that the mean value of the rupture force (mathematical expectation) for the welded spot of 7 mm diameter was 1.2 kN, the deviation of a rupture force from the mean value did not exceed ± 10 %. The separation of one of the sheets around the spot is observed. The results obtained prove a sufficiently high level of final setting-up of the arc spot welding process with a dosed electrode metal. Here, the quality of welding depends negligibly on the skill of the welder, as the process is fulfilled automatically.

The investigations made it possible to issue the well-grounded recommendations for the selection of conditions of welding, providing the quality spot joints with a stable strength.

REFERENCES

1. (1998) *Welding in aircraft construction*. Ed. by B.E. Paton. Kyiv: MIIVTs.
2. Lozovsky, V.P., Timoshenko, A.N. (1987) Arc spot welding of aluminium alloy thin-sheet overlap joints. *Avtomaticheskaya Svarka*, **7**, 49 – 51.
3. Slavin, G.A., Petrov, A.V., Smirnova, S.V. et al. (1965) Automatic non-consumable electrode pulsed-arc welding of thin-sheet aluminium alloys. *Svarochnoye Proizvodstvo*, **12**, 18 – 20.
4. Tarasov, N.M., Tulin, V.M. (1982) Control of electrode metal transfer by a short-time increase in rate of a shielding gas flowing. *Ibid.*, **8**, 23 – 25.
5. Tarasov, N.M., Rogachev, E.P., Grebennikov, A.V. (1997) Source of unipolar pulses of 150 Hz frequency and peculiarities of arc welding with its use. *Avtomaticheskaya Svarka*, **6**, 37 – 40.



IMPROVEMENT OF PERFORMANCE OF VERTICAL ERECTION WELDED JOINTS IN THE WALL OF CYLINDRICAL TANKS MADE OF COILED BLANKS

Yu.P. BARVINKO¹, V.M. GOLINKO¹, A.Yu. BARVINKO¹, A.V. PERELMUTER² and G.V. KULEBA³

¹The E.O. Paton Electric Welding Institute, NASU, Kyiv, Ukraine

²Ukrainian Institute of Environmental and Resources Studies, Kyiv, Ukraine

³GAO «Pridrenprovsky Main Pipelines», Kremenchug, Ukraine

ABSTRACT

The paper analyses different methods of making vertical erection joints in tanks built of coiled blanks. It is suggested that in repair of erection joints in the currently used tanks and in construction of new tanks, the butt joint should be made by welding-in special sheet inserts. Theoretical estimation of local stresses in the tank wall after welding-in the inserts is presented, allowing for actual radial distortions of the wall.

Key words: steel tanks, coiled blanks, vertical erection joints of walls, angular deformations, end portions of walls, inserts, hoop stresses

Quality and performance of vertical erection welded joints in the wall of tanks, built of coiled blanks, are inherently connected with development and improvement of the welding process. The coiling method, suggested in 1944 by G.V. Raevsky, Dr. of Sci. (Eng.) at the PWI [1], has been successfully applied since 1950 in construction of 100 – 5000 m³ tanks with up to 10 mm walls. The walls were made in the factory in the form of one panel, welded of separate sheets by automatic welding from both sides. During the wall mounting, just the operations of uncoiling the coil, fit-up and welding of one vertical erection joint were performed. This method of tank construction was a breakthrough in improvement of the quality of welded joints, shortening the tank construction period, reduction of their cost and was well suited to satisfy the needs of the post-war period [2]. This technology has become well-established with time and is extensively applied now in Ukraine and Russia.

Subsequent mastering of the technology of construction of 10000, 20000, 30000 and 50000 m³ tanks of coiled blanks, required creation of production facilities, allowing fabrication of coils of high-strength steels (plate thickness up to 17 mm) and development of special technologies of assembly and welding of erection joints. Making sound erection joints became the determinant technological operation in construction of such tanks [3].

Shaping of the wall end portions, their assembly and welding in site of an aligned vertical butt of tanks of up to 5000 m³ volume inclusive, were successfully mastered by specialised mounting organisations. This allowed a very quick transition to welding only butt joints.

In mounting larger volume tanks with 12 – 17 mm thickness of the wall lower horizontal section of

09G2S (C – 0.09 – 0.1; Mn – 1.5; Si – 0.4 wt.%) and 16G2AF (C – 0.16; Mn – 2.0; N – 0.04; V – 0.4 wt.%; Fe – balance) steels, the problem of reliability of vertical erection joints in the wall matching that of the respective factory-made butt joints, was becoming ever more urgent. The results of technical diagnostics of vertical erection joints of the wall in 20000 m³ tanks, built of coiled blanks with 16 mm thickness of the wall lower horizontal section of 09G2S steel, revealed their poor quality. This was manifested in the presence of inadmissible high angular deformations and considerable misalignment of the edges, that markedly lowered the tank performance under low-cycle loading [4]. The operating codes [5] for tank construction did not directly specify the angular deformations. Angular deformations were limited indirectly by tolerances for the tank wall deflection from the vertical. This, in a certain sense, resulted from the monopoly of the coiling process of tank fabrication in the absence of any alternative in the form of construction of the wall from individual sheets. With the availability of specialised factories fitted with highly efficient mills for coiled blank fabrication [2], a simultaneous introduction of more stringent requirements to erection joints in the wall of tanks of 10000 m³ and greater volume, would have meant interrupting the functioning of the entire tank construction industry for a certain time. Therefore, improvement of the erection joint quality became a lengthy step-by-step process that resulted in part of the built tanks having butt joints of a rather low quality. With time this caused a critical condition of tanks exposed to intensive low-cycle loading (regular 1 – 2 times a day filling-discharge) [6].

Analysis of the existing designs of vertical erection joints. Practical experience showed that development of a technology that would allow achieving the geometrical shape of a more than 12 mm wall in a section of an aligned erection joint, meeting the



requirements of foreign standards [7], is a complicated task. Many organisations [8] have been trying to find its optimal solution for more than 20 years now. As a temporary measure, special instructions have been developed for reinforcement of defective walls in PVS-20 tanks that allowed operating tanks with angular deformations [4]. Depending on the values of angular deformations, determined by the tank wall deflection from the design shape, based on 500 mm length, it was proposed to mount on part of the joint length, special horizontal stiffeners, relieving the welded joint stressed state.

Another solution of the problem of operational safety of tanks with considerable angular deformations in erection joints, can consist in the use a differentiated approach to the number of their loading cycles, i.e. can be based on co-ordinating the «angularity» with the admissible number of the tank filling–discharge cycles during its subsequent service. Such a work was performed at the PWI, using special samples [9, 10]. It resulted in adding to the codes [11], a table indicating the number of admissible cycles of the wall loading, depending on angular deformation of the welded joint, steel grade and sheet thickness. The dependence given in the table allows assessment of fatigue life of the considered butt joints in newly constructed tanks and determination of the residual life of tanks after a certain period of service. Testing also confirmed that if the requirements to angular deformations in welded joint and edge misalignment, allowed by the codes [7], are met, at low-cycle loading the fatigue crack develops in them at cycle number of not less than $5 \cdot 10^4$, i.e. the butt joint performance is actually provided during the entire operating life of the tanks. The issue of the method for repairing the defects in vertical butt joints of the walls after they have stood the admissible number of loading cycles, was not considered.

However, intensive cracking in vertical erection joints of the considered tank walls after 15 – 20 years of service [12], made it necessary to look for new technologies, both to improve the quality of butt joints in the newly constructed tanks, and to restore the performance of butt joints that developed cracks.

In order to improve the quality of erection joints in the newly constructed tanks, a special technology was developed for making these joints [13]. In this technology, special shaping devices are used to give the end portions of the coils a geometrical shape, close to the design shape, prior to welding. The shaping devices are attached to a trussed ladder around which the panel was coiled. After attachment of the wall edges to them along the entire height, their end portions are shaped to the required curvature by subsequent rotation of the trussed ladder. Practical experience shows that application of the developed technology does not guarantee stable results in terms of providing the required shape of the end portions. This is due to the difference in wall thickness in different horizontal sections and higher compliance of the panel.

In view of the above disadvantages, a technology was proposed with a rigid punch–die system [14], in which the shaping was performed successively in each horizontal section of the wall. The punch was hydraulically driven by a special oil pumping plant. During the work performance, the entire device was moved by the crane to the required horizontal section. The technology was designed for multiple use of the device. Considering that the tanks are individual structures, the work on the punch–die system was limited to experiments on several tanks.

Another area of studies to improve the geometrical shape of a vertical erection joint, is change of the panel end portion design. As one of the variants it is proposed to make the butt joint not aligned, but «staggered» by the horizontal sections. Making the panel end portions in the form of «combs» (with oppositely located protrusions and recesses) and their subsequent joining during erection [14], should have completely eliminated all the drawbacks, inherent in the typical geometry of a butt, aligned in the horizontal sections along one vertical line. When the above method is used, it is necessary to join the start of one and end of another coil in each butt joint. If the coil weight is 60 tons, a certain sagging of the foundation will always be observed in the area of placing the coil on the bottom. This circumstance, in combination with the presence of deformations in welded panels up to 18 m high, makes it difficult to achieve accurate fit-up of the «comb» sheets for welding, and requires reducing the joint line shifting to 200 – 300 mm. The «comb» method has lately found application in Russia in construction of large-volume tanks.

The PWI is developing a more versatile, in the authors' opinion, method of making the vertical erection joints by welding in special sheet inserts (Figure 1), providing the required quality. It is anticipated that such a geometry of the erection joint will be primarily suitable for repair of the currently operating and, later on, also of the newly constructed tanks, made of coiled blanks. The insert height should equal to the horizontal section height (except for the first one from the bottom). Alternation of inserts of different height allows production of a vertical «staggered» weld by the horizontal sections along the entire height of the wall. If required, inserts for several horizontal sections can be joined together to produce a larger piece.

Features of the technology of butt joint repair, developed at the PWI. Welding-in of inserts is a complicated technological problem. So, in the tanks, constructed by sheet-by-sheet method, the designed wall curvature is given to each sheet by forge-rolling. Now, the tank wall, produced by forced deployment of the coil panel to the design radius, with its subsequent fastening to rigid discs below and on top, continuously is in the pre-stressed condition during service (Figure 2), under the impact of inner equilibrium bending moments. If an opening for the insert is cut in such a wall, the formed free edges will start



Figure 1. General view of a section of 20000 m³ tank wall with special inserts used instead of a straight-line erection joint

moving inside the tank under the impact of the moments. Therefore, prior to welding-in each insert, it is first necessary to ensure the design position of the edge along the entire length of the cut-out opening, and then shape the insert to fit it.

When welding-in the inserts, the wall pre-tension applied by moments M_1 , M_2 should be taken into account, and a special technology should be used for welding the inserts into the «rigid» contour. As is seen from Figure 1, two vertical welds and one horizontal weld are made in mounting each insert. At the design thicknesses of the horizontal wall sections, transverse shrinkage of each weld during welding (from measurement data) is equal to 1.5 – 2.0 mm. If no special measures are taken, transverse shrinkage will be compensated through an increase of the curvature of the adjacent wall regions with formation of inadmissible depressions (dents). Therefore, the insert length should be specified, allowing for transverse shrinkage (deformation) of vertical welds. The direction of longitudinal shrinkage of vertical welds is in the plane of maximal rigidity of the wall and does not lead to its noticeable distortion. Appearance of a depression in the wall, results from transverse and longitudinal deformations of horizontal welded joints in cooling of the weld metal. Welding deformations induced by horizontal welds are reduced by applying special welding technologies and geometries.

All the above facts were taken into account in development by the PWI of a new technology for repair of vertical butt joints in the wall. It is assumed that after repair the straight-line erection joint, will be replaced by a regular butt joint of the wall with the vertical butt «staggered» along the entire horizontal section height. Local deflections of the wall in the butt plane will meet the requirements of the codes in force in Ukraine [15].

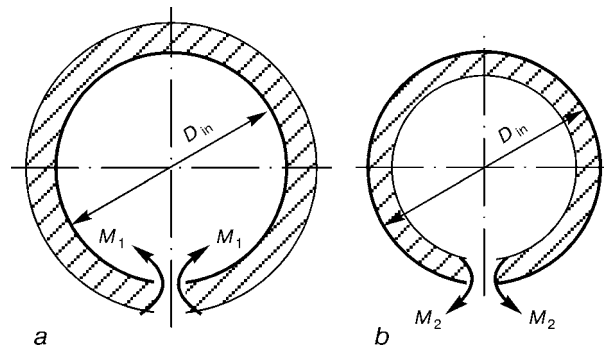


Figure 2. Schematic of the tank wall pre-tension at $R_{res} > R_d$ (a) and $R_{res} < R_d$ (b): R_{res} – residual curvature radius of the coiled blank; R_d – design radius of the tank wall; D_{in} – inner diameter of the tank

The developed technology was used in 1999 to repair three erection joints in the wall of 20000 m³ tank No.4 in «Snigirevka» pumping plant (Figure 1). Analysis of wall distortions during repair and after its completion revealed that with the actual absence of angular deformations or misalignment of the butt joint edges, the cylindrical surface of welded-in inserts does not always match the design shape of the wall within the tolerances of the currently operating codes. It was also found that the current code requirements do not fully allow for the features of the repair technology and do not permit a sufficient degree of control over their geometrical shape. Measurements showed that local deformations of the wall in the vicinity of the inserts should be evaluated not only by the dimensions of the gap between the horizontal gauge or the vertical bar and the wall, but also by deviation Δf (on the level of horizontal welds and in the sheet middle) of the actual value of deflection f from the design value, allowing for the tank design radius, determined by Δf value (Figure 3). If Δf dependence on hoop stresses σ_h is found for the considered regions of the wall, it is possible to introduce the admissible Δf values, at which condition $\sigma_{h,l} < \sigma_y$ will be satisfied ($\sigma_{h,l}$ are the values of hoop stresses, allowing for local deflection of the wall geometrical shape from the design shape; σ_y is the standardised yield point of rolled sheets in the considered horizontal section of the wall).

Criterion $\sigma_{h,l} < \sigma_y$ can be accepted taking into account the fact that during the tank filling with the product for storage, its wall gradually acquires the design shape and Δf values tend to zero.

Such tolerances for mounting the inserts will provide certain guarantees of tank performance during operation. It is natural that as experience of operation of 20000 m³ tanks after repair is gained and their

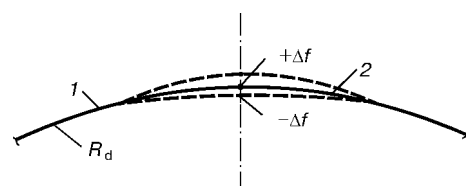


Figure 3. Possible positions of sheet inserts after welding-in: 1 – design position of tank wall; 2 – sheet insert

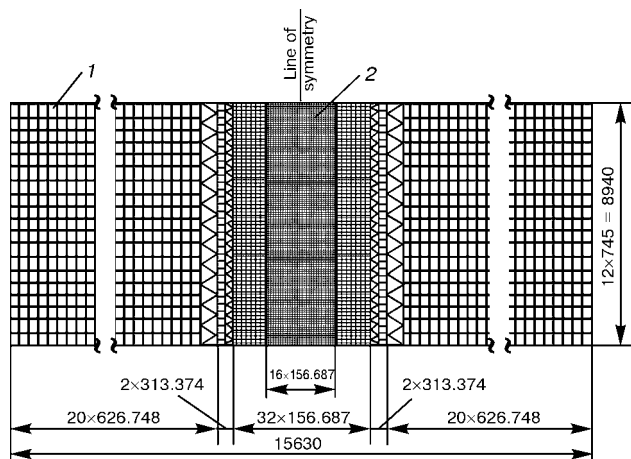


Figure 4. Schematic of finite elements of wall sections 1 and 2 (reinforced area is high-lighted)

repair technology is improved, Δf values will be further determined more precisely.

Theoretical evaluation of local stresses in the tank wall after welding-in the inserts. The sought dependence of Δf was derived using an all-purpose computing program system SCAD, complemented by a procedure for allowing for the initial geometrical imperfections of the model. The required initial data were taken from measurements made during repair of three vertical erection joints of the above tank No.4 in «Snigirevka» pumping plant. The diameter of this tank was 39.9 m and the wall height was 18 m. The computational scheme of the tank was determined by the finite element model of the wall and the method of assigning its geometrical shape.

In view of the structure symmetry, calculation was made for one fourth of the tank. In this case, the first six horizontal sections (starting from the bottom) were considered, as they are the most active sections of the wall. The conditions of rigid restraint in the wall-to-bottom joint were accepted for the wall lower boundary, which contributes to a certain reliability margin. Freedom of linear displacements with limitation of the angle of the guide turning was provided on the upper edge, that approximately corresponds to the conditions in the wall middle. Boundary conditions resulting from the problem symmetry, were defined along the vertical edges of the considered fragment.

Computation was performed by a finite element model, including rectangular and triangular shell elements. The size of these elements did not exceed 627 mm along a horizontal and 745 mm along a vertical for the wall region removed for the repaired area, with subsequent four times reduction in the insert region. The schematic of the wall breaking up into finite elements is presented in Figure 4. The width of inserts in the circular direction was assumed to be the average over their actual length (2000 and 3000 mm) and was equal to 2500 mm. The thickness of the sheet inserts and wall elements was assumed in keeping with Table 1.

Table 1. Thickness of sheet inserts for different horizontal sections of the wall

Section number	Wall, mm	Reinforcement (insert), mm
I	16	16
II	15	16
III	14	16
IV	12	14
V	11	12
VI	10	12

Calculation was performed, allowing for elastic loading of the wall material, having the following characteristics: modulus of elasticity $E = 2.0 \cdot 10^5$ MPa; Poisson's ratio $\mu = 0.3$.

The wall of the considered reference tank with the assumed distortions, practically corresponded to the actual wall structure of tank No.4 after repair. Characteristic regions along two verticals were selected on it, where special inserts were welded in.

The distorted shape of the tank was determined by measurement of maximal deflections from the design shape, taken on the level of horizontal welds in points, located in the middle of the sheet inserts. Measurement results are given in Table 2.

Considering, that the measurements were taken with a certain error, their results were «smoothed» by solving the problem of the best mean-root-square approximation. The following relationships were derived, for wall regions 1 and 2, respectively:

$$\Delta(x) = 4185.36x^5 - 10507.9x^4 + 8657.32x^3 - 2471.16x^2 + 128.509x - 9.11538,$$

$$\Delta(x) = 916502x^5 + 124.144x^4 - 895.411x^3 + 1019.66x^2 - 356.115x - 5.465035,$$

where x is the co-ordinate ($\text{mm} \cdot 10^4$).

Table 2. Value of deflection f from the design shape along height h of the wall, mm

h, mm	Section 1	Section 2
0	-5	-9
1490	-41	-22
2980	-40	-31
4470	-35	-23
5960	-27	18
7450	-10	14
8940	-20	-4
10430	-23	-10
11920	-31	22
13410	-33	-5
14900	-18	-9
16390	12	-15
17880	2	-4

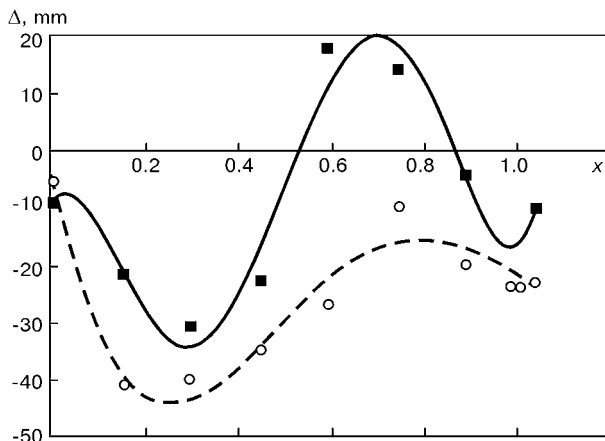


Figure 5. Curves of smoothing the measured deviations Δ of the wall: hatched line — wall section 1; solid line — wall section 2

Figure 5 shows the curves, plotted from these equations. It was assumed that the actual surface that deviated from an ideal cylindrical shell, is given by the following equations in the cylindrical system of co-ordinates:

$$\rho = 19950 + \Delta(x)\sin^2 [\pi S/L],$$

where ρ is the co-ordinate of a point on the wall surface; S is the co-ordinate along an arc; L is the arc length of the disturbance zone (with averaging, $L = 2500$ mm is assumed).

A schematic of this surface significantly distorted along the radial co-ordinate (wall section 2) is shown in Figure 6.

All the calculations were made under the condition of the shell loading by filling it with water up to the height of 17 m, this corresponding to the maximal design filling level in tank service. Calculations were first performed with geometrical parameters of wall sections 1 and 2 in the linear definition, i.e. without allowing for values of the second order. It turned out that the thus derived radial displacements are quite significant (up to 500 mm). Higher displacement values were indicative of the need to perform calculations in the geometrically non-linear definition. In this case the derived displacement values were approximately

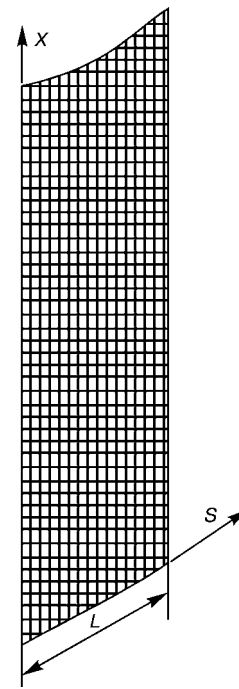


Figure 6. Schematic (development) of wall deflection surface (wall section 2)

by an order of magnitude smaller, than in linear calculation. The obtained values agree well with the actual measurements. The wall stressed state changed by 5 – 40 %. Figure 7 shows the qualitative pattern of hoop stress distribution in wall sections 1 and 2. It follows from calculation that the maximal stresses in wall section 1 are equal to 202.4 and in wall section 2 to 329.6 MPa, i.e. do not exceed the standardised σ_y values of the material of the wall 16 mm thick (09G2S steel). Equivalent stresses (by the 4th theory of strength), rise up to σ_t values. It should, however, be taken into account, that σ_t values were derived in the assumption that the specified deflections are present also at design filling of 17 m height. As shown by observations, already at filling 3 to 4 m higher, than the level of the assumed deflection location, the wall shape becomes close to the design shape, and the deflection values are reduced 2 to 3 times. This allows satisfying just the proposed $\sigma_{h,1} < \sigma_y$ condition.

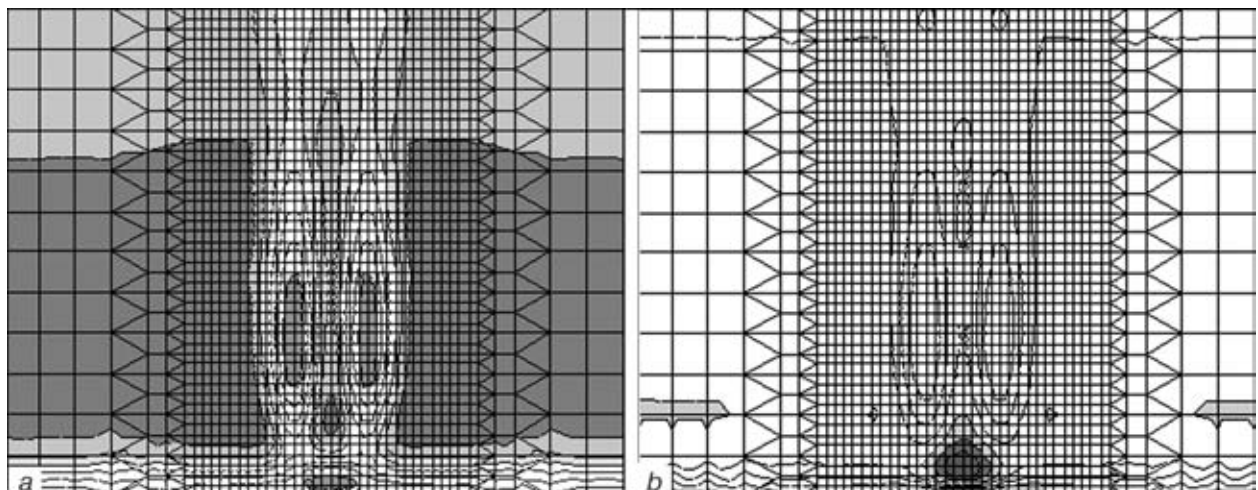


Figure 7. Distribution of hoop stresses in non-linear computation in wall sections 1 (a) and 2 (b)



Results of the performed investigations allowed a realistic evaluation of the influence of local deflections from the design shape on the tank wall stressed state and assigning tolerances for them in development of the contractor design for butt joint repair.

REFERENCES

1. Rayevsky, G.V. (1952) *Fabrication of vertical cylindrical steel tanks by the coiling method*. Moscow-Leningrad: Gosoptekhizdat.
2. Biletsky, S.M., Golinko, V.M. (1983) *Production-scale fabrication of oversized welded sheet structures*. Kyiv: Naukova Dumka.
3. Biletsky, S.M., Chkalin, V.B., Golinko, V.M. *et al.* (1997) Problems of construction of tank fleet. *Budivn. Ukrainy*, **3**, 29 – 31.
4. RD 39-30-1331-85 (1985) Instructions on reinforcement of vertical erection joints in the walls of RVS-20000 tanks. Intr. from 01.01.86 till 01.01.91. Moscow.
5. VSN 311-81 (1982) Instructions on fabrication and mounting of vertical cylindrical tanks. Moscow.
6. Biletsky, S.M., Golinko, V.M., Barvinko, Yu.P. (1990) Methods for improvement of operational reliability of welded cylindrical tanks, made of coiled blanks. *Avtomaticheskaya Svarka*, **3**, 50 – 52.
7. API-650 (1980) Welded steel tanks for oil storage. Washington.
8. Popovsky, B.V., Dzhur, Yu.F. (2000) Stages of solving the problem of assembly of vertical butt joints in tank walls. *Montazhn. i Spets. Raboty v Stroitelstve*, **10**, 4 – 7.
9. Barvinko, Yu.P., Biletsky, S.M., Golinko, V.M. *et al.* (1991) On tolerances for angular deformations of vertical welded butt joints in 10000 – 50000 m³ tanks for storage of oil and petroleum products. *Avtomaticheskaya Svarka*, **4**, 20 – 23.
10. Popovsky, B.V., Ritchik, G.A., Barvinko, Yu.P. *et al.* (1991) On tolerances for angular deformations of vertical welded butt joints of oil tank walls. *Montazhn. i Spets. Raboty v Stroitelstve*, **5**, 11 – 12.
11. VSN 311-89 (1990) Mounting of vertical cylindrical steel tanks of 100 up to 50000 m³ volume for storage of oil and petroleum products. Moscow: Minmontazhspeksstroj SSSR.
12. Barvinko, A.Yu., Barvinko, Yu.P., Golinko, V.M. *et al.* (1999) On performance of 50000 m³ vertical cylindrical tanks of 16G2AF steel. *Truboprovodn. Transp. Nefti*, **9**, 24 – 27.
13. TP 704-1-171-84 (1983) Album VI: Specification for mounting operation performance. Mounting of a tank. Intr. 23.05.83. Moscow.
14. Lyalin, K.V. (1997) Some aspects of improvement of the design and technology of assembly and welding of cylindrical tanks. *Montazhn. i Spets. Raboty v Stroitelstve*, **7**, 10 – 13.
15. BVN B.2.2-58.2-94 (1994) Vertical steel tanks for storage of oil and petroleum products with not more than 93.3 kPa pressure of saturated vapours. Kyiv: Derzhkomnaftgaz.



EFFECT OF PARAMETERS OF ASYMMETRIC AND MODULATED CURRENTS ON QUALITY OF ALUMINIUM ALLOY WELDED JOINTS

A.G. POKLYATSKY and A.A. GRINYUK

The E.O. Paton Electric Welding Institute, NASU, Kyiv, Ukraine

ABSTRACT

The effect of parameters of the asymmetric and modulated currents on the length of oxide film inclusions in the welds and porosity of the joints in alloys AMg6, 1420 and 1460 produced by a pulsed-arc TIG welding is considered. The use of the asymmetric current allows a decrease of 3 times in the relative length of the oxide film inclusions in the AMg6 alloy welds and reduces the probability of whisker inclusions in the welds. Efficient degassing of the molten pool metal is achieved in the case of using the modulated current with a modulation frequency of 5 Hz.

Key words: *pulsed arc, asymmetric current, modulated current, non-consumable electrode, aluminium alloys, inclusions of oxide film, pores*

In non-consumable electrode welding of aluminium alloys the inclusions of oxide film are often observed in welds [1 – 3]. In addition, the Li-containing alloys are characterized by an increased susceptibility to the pore formation [4, 5].

The welding methods, based on intensification of metal stirring, promote its degassing, refining of oxide inclusions in the bottom part of weld pool and their escape to the surface for direct action of the arc [6 – 10]. The effective stirring of the molten metal over all the volume of the weld pool is provided in a non-consumable electrode pulsed-arc welding. Here, the pulsating force action of the arc occurs as a result of changing the amplitude values of current of straight and reverse polarity (asymmetric current) or large drops in amplitude during the period of a pulse and pause (modulated current) [11]. As the arc pressure is proportional to the square of amplitude value of current and «reacts» almost instantaneously on its change, then the periodic increase in current contributes to the increase in a depth of arc immersion into the molten metal and its stirring, providing the destroying of oxide films and escape of gas bubbles [12].

The aim of the present work is to determine experimentally the parameters of asymmetric and modulated currents at which the most effective destroying of oxide film and removal of gas bubbles from the molten metal of the weld pool is attained. The automatic single-pass non-consumable electrode welding of butt joints was performed in argon by a stationary and pulsating arc using asymmetric and modulated currents from the power sources ISVU-315 (Russia), I-126 (Ukraine) and MW-450 (Austria). Weld beads were formed on stainless steel base metal with a groove of a semispherical shape. Standard wire Sv-AMg6 (Al-6.2Mg) was used as a filler in welding sheets of alloy AMg6, Sv-AMg63 (Al-6.3Mg) – for alloy 1420

(Al-Mg-Li) and Sv-1201 (Al-Cu) for alloy 1460 (Al-Cu-Li). The sheets being welded and filler materials were subjected to the chemical etching using the generally-accepted technology. To evaluate the effect of current parameters on the formation of the oxide film inclusions in welds of alloy AMg6 the butt joints of 6 mm thick sheets were assembled with a guaranteed gap $b = 1.2$ mm [13]. The butts of sheets of 6 mm thick alloys 1420 and 1460 were assembled without a gap, because the long whisker oxide inclusions, typical of Li-containing alloys, are formed in welds also in conventional conditions of assembly. Just before welding, the edges of sheets being welded were machined from three sides for the depth of not less than 0.1 mm. The length of defects was measured on longitudinal fractures of welds. The relative length

Table 1. Effect of parameters of asymmetry of variable polarity current of square shape on relative length of oxide film inclusions in AMg6 alloy welds

$I_{str},$ A	$I_{rev},$ A	$\tau_{str},$ ms	$\tau_{rev},$ ms	$f,$ Hz	$l_{rel},$ mm/lin. m	$l_{max},$ mm
290	290	4.6	4.6	109	78	9
		8.0	8.0	63	86	10
		10.4	10.4	48	102	12
		8.0	12.8	48	73	9
		4.6	8.0	79	65	9
		6.1	12.8	53	64	8
		4.6	10.4	67	59	8
		440	220	4.6	4.6	109
440	220	8.0	8.0	63	67	9
		10.4	10.4	48	79	9
		8.0	12.8	48	47	6
		4.6	8.0	79	40	6
		6.1	12.8	53	38	5
		4.6	10.4	67	31	5
300*	300	10.0	10.0	50	125	21

*Welding with a stationary arc.

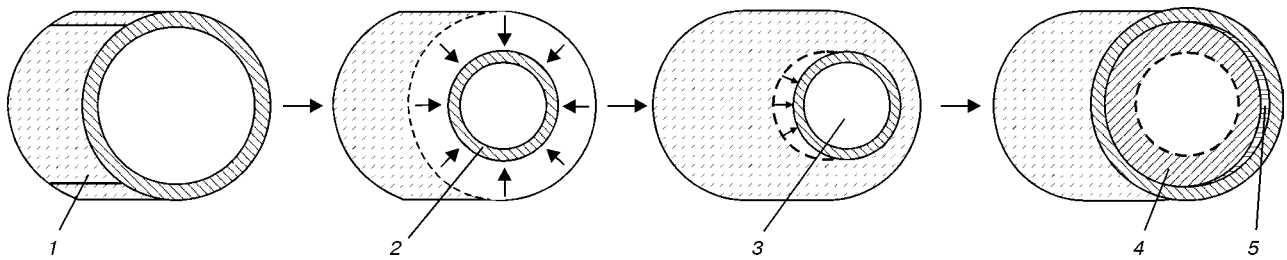


Figure 1. Scheme of cathode destroying of oxide film in a modulated current welding: 1 – oxidized surface of remelted weld metal; 2 – zone of cathode cleaning; 3 – surface of molten weld metal; 4, 5 – oxidized surface, melted at the moment of a pulse action (4 – weld; 5 – butt ahead of weld pool)

of inclusions of oxide film in welds l_{rel} was determined as a total length of defects per 1 linear meter of weld. As in critical structures the length of separate defects is limited, then in each variant the maximum length, l_{max} , of separate oxide inclusions in welds was measured.

To evaluate the porosity of welds in welding alloys 1420 and 1460 only face and lateral surfaces of edges being welded were machined. The surface layer from lower edges was not removed in order to examine the behaviour of gas bubbles forming in the weld pool lower part. The porosity of welded joints was evaluated from X-ray photograph: number of pores of different diameter was calculated per 100 mm of weld and then their total volume was calculated, assuming pores spherical.

The analysis of longitudinal fractures of welds of alloy AMg6 showed that the relative length of inclusions depends on amplitude values and time of current passing at straight, τ_{str} , and reversed, τ_{rev} , polarities (Table 1). Increase in τ_{rev} and decrease in τ_{str} contribute to the activation of processes of a cathode destroying of oxide film during welding and to reduction of length of defects in welds. Amplitude asymmetry of welding current causes the intensive vibrations of the molten metal in change of the polarity at the expense of abrupt drops of the arc pressure. During the period of straight polarity current passing the force action of the arc provides increase in steepness of the pene-

tration front and depth of arc immersion into the weld pool crater. This results in destroying of the oxide film in the bottom part and its separate undestroyed particles are escaped by the molten metal flows to the surface and enter for the direct action of the arc. Therefore, the use of the asymmetric current with $I_{str} = 2I_{rev}$ and $2\tau_{str} = \tau_{rev}$ allows a 3 times decrease in length of oxide film inclusions of weld and 3 – 4 times decrease in maximum length of separate defects in welds of alloy AMg6.

In addition, the use of current with a predominance of τ_{rev} improves the cathode cleaning of filler wire entering the weld pool. As the insufficient destroying of the oxide film at the filler surface is one of main causes of formation of long whisker oxide inclusions in welds during non-consumable electrode welding of Li-containing aluminium alloys the intensive cathode cleaning of the filler wire promotes the improvement of the weld quality. Thus, in a pulsed-arc welding with asymmetric current ($I_{str} = 2I_{rev}$; $2\tau_{str} = \tau_{rev}$) as compared with welding with a conventional sinusoidal current the probability of producing defect-free welds of alloys 1420 and 1460 is 3 times increased.

The use of current, asymmetric in amplitude, improves the conditions of degassing of the molten metal at the expense of its vibrations occurring due to abrupt changes of the force action of arc at the polarity change. As a result, the pores remain only in zones of welds fusion with the parent metal in welded joints of Li-containing alloys 1420 and 1460. In addition, the volume of voids is decreased by 60 – 70 % as compared with a symmetrical current (Table 2).

To intensify the vibrations of the molten metal and its stirring over all the volume of the weld pool is possible in a pulsed-arc welding with a modulated current. At the modulation frequency $f_m = 1 - 4$ Hz a mechanical destroying of long oxide film inclusions occurs due to abrupt vibrations of molten metal, thus leading to the decrease in l_{max} . Here, the relative length of oxide film in welds l_{rel} depends greatly on ratio of duration of pulses τ_{pulse} and pauses τ_{pause} of welding current (Table 3). This is stipulated by different conditions of oxidation of the molten metal and cathode destroying by it of oxide film at the moments of pulses and pauses of the welding current. During pauses the effectiveness of the cathode is reduced greatly due to decrease in the current level, while a process of oxidation of metal melted by a previous pulse of current is activated. Therefore, the

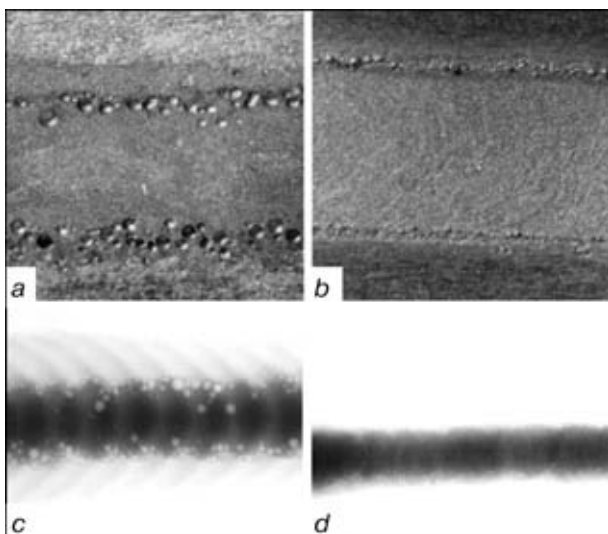


Figure 2. Macrosections of weld root with a removed bead (a, b) ($\times 2$) and X-ray photographs of welds of alloy 1420 (c, d); welding with a pulsed arc at $f_m = 1$ (a, c) and 5 (b, d) Hz

Table 2. Porosity of 1420 alloy welded joints made in welding with symmetrical and asymmetric current

I_{str}, A	I_{rev}, A	τ_{str}, ms	τ_{rev}, ms	Number of pores per 100 mm of weld, pcs, dia., mm			Total amount of pores, pcs	Volume of pores per 100 mm of weld, mm ³	Pores location
				0.1 – 0.3	0.4 – 0.7	0.7 – 1.0			
<i>Symmetrical current</i>									
260	260	10.4	10.4	255	38	27	320	12.2	Weld and fusion zone
<i>Asymmetric in amplitude</i>									
360	180	10.4	10.4	212	26	19	257	8.7	Fusion zone
170	340	10.4	10.4	219	19	15	253	7.0	Same
<i>Asymmetric in duration</i>									
260	260	11.4	6.0	221	29	21	271	9.6	Weld and fusion zone
250	250	7.0	14.0	208	17	18	243	7.8	Same

Table 3. Effect of parameters of modulation of variable polarity current of a square shape on relative length of oxide film inclusions in AMg6 alloy welds

I_{pulse}, A	I_{pause}, A	τ_{pulse}, ms	τ_{pause}, ms	$\frac{\tau_{pause}}{\tau_{pulse} + \tau_{pause}}, \%$	f_m, Hz	$l_{rel}, mm/lin. m$	l_{max}, mm
365	110	87.5	37.5	70	8	116	18
445	135	125.0	125.0	50	4	119	16
365	110	175.0	75.0	70	4	103	12
340	100	200.0	50.0	80	4	85	8
445	135	250.0	250.0	50	2	137	9
365	110	350.0	150.0	70	2	107	8
340	100	400.0	100.0	80	2	82	7
445	135	500.0	500.0	50	1	194	11
365	110	700.0	300.0	70	1	95	8
340	100	800.0	200.0	80	1	90	8

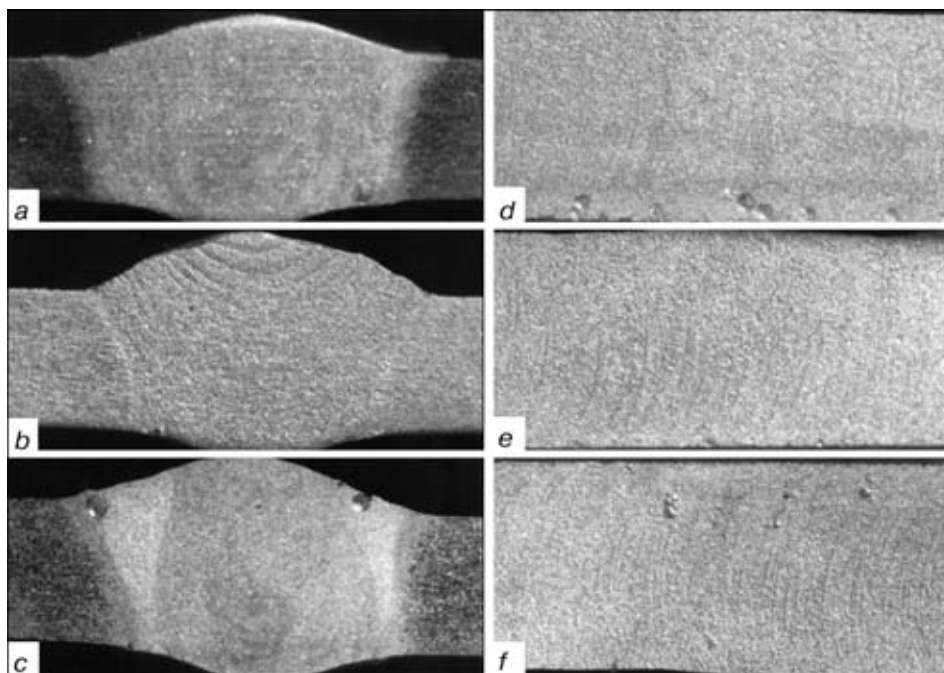


Figure 3. Pores on transverse (a – c) (x3) and longitudinal (d – f) (x4) macrosections from the fusion zone of welded joints of alloy 1420; welding with a stationary (a, d) and pulsed arc at $f_m = 5$ (b, e) and 10 (c, f) Hz (reduced by 2/3)

Table 4. Porosity of 1420 alloy welded joints made in welding with a modulated current

f_m , Hz	$\tau_{\text{pulse}} / (\tau_{\text{pulse}} + \tau_{\text{pause}})$, %	I_{pulse} , A	I_{pause} , A	Number of pores per 100 mm of weld, pcs, dia., mm			Total amount of pores, pcs	Volume of pores per 100 mm of weld, mm ³	Pores location
				0.1 – 0.3	0.4 – 0.6	0.7 – 1.0			
				1	50	400			
	80	305	90	255	52	38	345	16.7	Same
2	50	400	120	241	35	29	305	12.6	»
	80	305	90	231	30	24	285	10.6	»
5	50	400	120	206	9	0	215	1.5	Fusion zone
	80	305	90	215	5	0	220	1.3	Same
10	50	400	120	215	27	8	250	5.2	»
	80	305	90	206	29	5	240	4.4	»

next current pulse with a low frequency of modulation and a high duration of the pause does not provide a complete cathode destroying of the formed oxide film (Figure 1). Increase in τ_{pulse} and decrease in τ_{pause} of the modulated current at the same frequency of modulation promote the improvement of the cathode cleaning and reduction in intensity of oxidation of metal melted by the arc. The relative length of inclusions of oxide film in welds of alloy AMg6 produced in welding with a modulated current at $f_m = 1 - 4$ Hz and duration of current pulses equal to 70 – 80 % of the cycle duration, is by 20 – 25 % less than that in welding with a symmetrical sinusoidal current. At $f_m > 4$ Hz the effectiveness of a dynamic action of the arc on the molten metal is decreased.

The frequency of current modulation also influences greatly the processes of degassing of metal being melted by arc (Table 4). At a long duration of pulses and pauses of the modulated current ($f_m = 1 - 2$ Hz) a large amount of pores of diameter of up to 1 mm is observed in root of welds and zones of its fusion with the parent metal. Their total volume is 10.6 – 16.7 mm³ (see Figure 2, a, c). Increase in modulation frequency to 5 Hz creates favourable conditions for the intensive escape of gas bubbles to the weld pool surface. As a result there are no pores in the weld metal, and in the fusion zone their diameter does not exceed 0.3 mm at the 1.2 – 1.5 mm³ total volume of voids (Figure 2, b, d).

At the further increase of modulation frequency the number and diameter of pores in the fusion zone are increased. The gas bubbles, trying to escape, are not managed to reach the weld pool surface and remain in the solidifying metal (Figure 3).

CONCLUSIONS

1. In non-consumable electrode pulsed-arc welding of aluminium alloys the length of oxide film and porosity of welded joints is decreased as compared with welding using a stationary arc.

2. The use of asymmetric current (with $I_{\text{str}} = 2I_{\text{rev}}$ and $2\tau_{\text{str}} = \tau_{\text{rev}}$) promotes the intensification of stirring of the molten metal and activation of processes of cathode destroying of the oxide film. This decreases

the relative length of oxide film inclusions by 3 times in welds of AMg6 and also probability of formation of long whisker inclusions in welds of Li-containing alloys 1420 and 1460.

3. Abrupt changes in force action of arc during pulses and pauses of the modulated current with $f_m = 5$ Hz also provide the most favourable conditions for removing the gas bubbles from the weld pool melt. Here, the total volume of voids in welded joints of alloys 1420 and 1460 (6 mm thick sheet) is 7 – 10 times decreased as compared with a stationary arc welding at a conventional sinusoidal current.

REFERENCES

- Moiseenko, I.G., Stolbov, V.I., Turchenko, M.A. (1968) Oxide inclusions in welding alloy AMg6. *Svarochnoye Proizvodstvo*, **5**, 23 – 24.
- Moiseenko, I.G., Lukashin, N.V. (1969) Towards the problem of improvement the air-tightness of alloy AMg6 welded vessels. *Ibid.*, **8**, 31 – 32.
- Lukianov, V.F., Fomin, V.N., Moiseenko, V.P. et al. (1970) Effect of oxide inclusions on strength of welded joints of AMg6 alloy pressure vessels. *Ibid.*, **6**, 24.
- Ishchenko, A.Ya., Chayun, A.G., Beletsky, V.M. et al. (1977) Peculiarities of fusion welding of aluminium alloy 01420. *Avtomaticheskaya Svarka*, **3**, 38 – 41.
- Barabokhin, N.S., Bushuev, Yu.G., Shulgina, E.V. et al. (1999) Technological peculiarities of welding high-strength aluminium alloy 1460. *Svarochnoye Proizvodstvo*, **11**, 12 – 14.
- Shiryayeva, N.V., Ovchinnikov, V.V., Gabidullin, R.M. (1987) Pore formation in welding alloy of aluminium-magnesium-lithium system. *Avtomaticheskaya Svarka*, **3**, 16 – 18.
- Oboturov, V.I., Tolkachev, Yu.N. (1973) Some peculiarities of formation and destroying of oxide films in argon-arc welding of aluminium alloys. *Svarochnoye Proizvodstvo*, **11**, 22 – 24.
- Sushkov, V.N., Skachkov, Yu.N., Novikov, O.M. et al. (1975) Susceptibility of light alloys to the oxide inclusions formation during welding. *Ibid.*, **5**, 23 – 24.
- Chayun, A.G., Syrovatka, V.V., Matyash, V.I. (1981) Arc welding of aluminium alloy 01420 using EMP. *Avtomaticheskaya Svarka*, **6**, 19 – 21.
- Ishchenko, A.Ya., Chayun, A.G., Ilyushenko, R.V. (1985) Weldability and technology of arc welding of alloy of aluminium-magnesium-lithium system. *Ibid.*, **10**, 47 – 49.
- Poklyatsky, A.G., Ishchenko, A.Ya., Bessonov, A.S. et al. (1991) Prevention of oxide film formation in welds during a pulsed-arc welding aluminium alloys. *Ibid.*, **7**, 43 – 47.
- Maruo, H., Hirata, Yo., Makino, H. (1989) Rectangular wave AC TIG arc welding of aluminium alloy. *Q. J. of JWS*, **1**, 63 – 69.
- Ishchenko, A.Ya., Poklyatsky, A.G., Yavorskaya, M.R. (1989) Prevention of oxide film inclusions in welds in argon-arc welding of aluminium alloys. *Avtomaticheskaya Svarka*, **6**, 38 – 41.



APPLICATION OF ACTIVATORS FOR TIG WELDING OF STEELS AND ALLOYS

K.A. YUSHCHENKO, D.V. KOVALENKO and I.V. KOVALENKO

The E.O. Paton Electric Welding Institute, NASU, Kyiv, Ukraine

ABSTRACT

The E.O. Paton Electric Welding Institute developed a new generation of activating fluxes. Data are given on the application of the aerosol activating fluxes (activators) of the PATIG series intended for welding stainless steels of the 300 (301, 304, 316, 320, etc.) and 400 (401, 416, etc.) grades, duplex steels, nickel alloys of the Nimonic, Hastelloy and Inconel types, and heat-resistant and high-temperature steels. Technological and economical advantages of manual and mechanized welding of thin and thick metal in making butt, corner, overlap and T-joints in the form of different structures are presented.

Key words: TIG welding, penetration, activating flux, steels, nickel alloys

In 1965 a team of scientists of the PWI published the pioneering data on the results of investigation into the effect of activating fluxes in argon-arc tungsten-electrode welding of titanium [1]. In the years that followed scientists of the PWI and a number of other organizations studied the effect of the activating fluxes on processes occurring in the arc column, behaviour of molten metal in the pool, penetration and formation of the weld metal [2 – 10].

The Presentation-Conference of the E.O. Paton Electric Welding Institute (6 – 14 October, 1993, TWI, Abington, Cambridge, Great Britain) [11, 12] and results of the joint project performed in 1994 – 1996 in collaboration with TWI [13] gave a new impetus to development of the investigations in this area. These investigations confirmed that the activating fluxes led to a substantial increase in penetration and productivity in welding low-alloy (50D and 43A) and stainless (304L and 316L) steels, independently of the degree of their purity in respect to sulphur and oxygen, as well as of the method used for their production. In the last years the investigations were conducted in the following areas:

- development of the new types of the activating fluxes in composition and application methods;
- widening of the range of structural materials, which can be welded using the activating fluxes, and types of joints;
- accumulation of experience in commercial application of the activating fluxes for fabrication of actual welded structures;
- investigation of processes occurring in the welding arc and weld pool under the effect of the activating fluxes, working out of theoretical principles of the process;
- identification of the new fields of application of the activating fluxes for various welding methods.

Materials and investigation results. Traditionally, the activating fluxes consist of dispersed powders

of metal oxides and halides. The so-called brush or wet wad methods, where a thin layer of the mixture consisting of a powdered flux and solvent is applied to the surface, are used for a uniform deposition of the activating fluxes. Good results are achieved in spraying of a suspension consisting of the same main components.

The activating fluxes in the form of crayons also find their way into application. Each of the application methods, as well as materials, have both advantages and disadvantages.

The main advantage of the activating fluxes in the form of aerosols (activators) is a uniform covering along the length of the weld and through thickness of the deposited layer, better practicability and convenience in the application, as well as an extended shelf life in the form ready for use [14, 15].

Figure 1 shows a flow diagram of the process of TIG welding of steel 304L (FeCr-18Ni-10) 6 mm thick and macrosections made without and with an activator. The latter case is characterized by a weld shape peculiar of this process and by an increased penetration.

The PWI developed activating fluxes of the PATIG series for welding different grades of alloyed and stainless steels – fluxes of the PATIG S type, and for welding Ni-base alloys – fluxes of the PATIG N type. Below we describe investigations of the technological capabilities and properties of welded joints made using aerosol (A) activators PATIG S-A and PATIG N-A. In all the cases the use was made of the TIG welding equipment.

Investigated was the possibility of joining metal 1 – 25 mm thick. Macro- and microstructures of the weld metal were analysed. In a number of cases chemical composition and mechanical properties of the weld metal were determined. Choice of the composition of an activator was based on the system of alloying of the base metal. Welding was performed without a filler wire at a DCSP. The automatic welding heads and argon as a shielding gas were used. Both automatic and manual welding was performed. The special con-

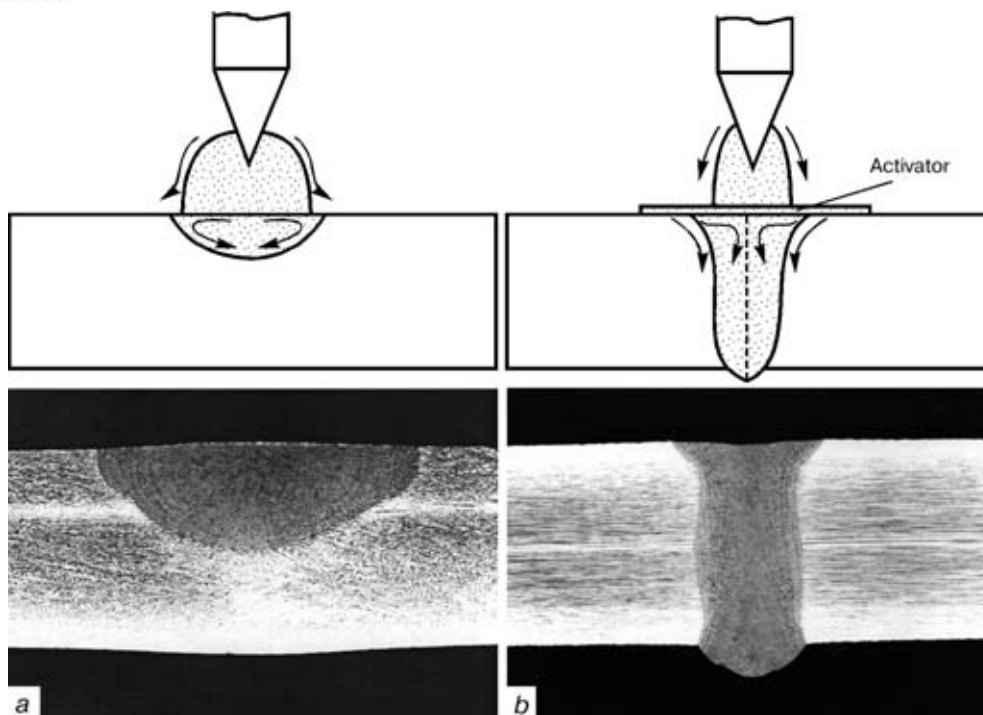


Figure 1. Flow diagram of the arc welding processes and macrosections of welded joints in steel 304L 6 mm thick made by the TIG (a) and A-TIG (b) welding methods

sideration in single-pass welding was given to providing a maximum penetration and weld of a preset geometry.

Types of joints. Table 1 gives examples of the joints which can be made in practice. As it follows from the Table, the use of the activators has no limitations as to types of the joints and spatial position of the weld. The following extra requirements are imposed in this case:

- uniform application of the activator to the surfaces welded;
- retention of a large volume of the molten metal from flowing out in free weld formation.

Such requirements arise when surface tension of the molten metal is insufficient to retain the weld pool, which is usually characteristic of low-alloy and stainless steels in welding metal more than 6 – 7 mm thick using no backing plate or backing gas. If a backing plate is used, thickness of the metal which can be welded in a single pass amounts to 10 – 12 mm, while in performing two-pass two-sided welding it is possible to produce a butt joint up to 25 mm thick (Figure 2). Naturally, this can be achieved also in making corner and T-joints. Like in the case of conventional TIG welding, A-TIG welding process can be performed in a groove, including using a filler wire.

The PATIG S-A activators give good results in A-TIG welding of Fe-base steels with a normal carbon content (0.08 – 0.25 C), additionally alloyed with manganese, silicon, chromium, nickel, molybdenum, vanadium, niobium, nitrogen and tungsten in moderate amounts. In welding these steels, the quality of the welds depends upon the carbon equivalent. Extra hardening of the weld and HAZ metal has been fixed.

The required metal properties are achieved due to appropriate heat treatment. In welding steels containing a low amount of deoxidizers, pores are detected in the welds. The use of a filler wire with an increased content of manganese and silicon allows elimination of this drawback.

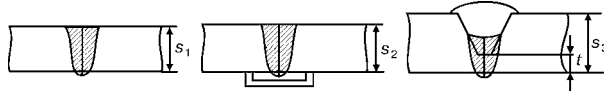
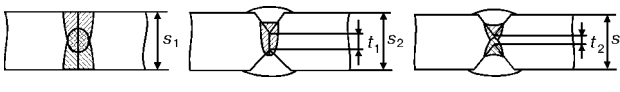
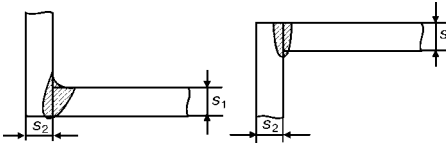
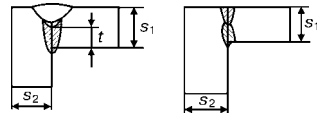
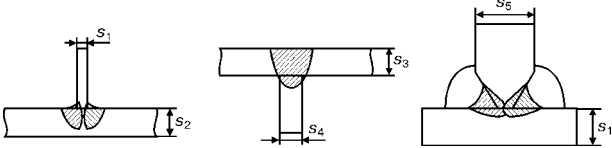
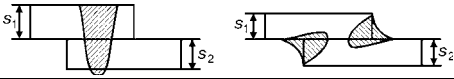
Chemical compositions of typical representatives of low-carbon and low-alloyed steels, as well as stainless steels, on which the sound welds were produced by welding using the PATIG S-A activators, are given in Table 2.

Analysis of mechanical properties of the weld metal on Cr-Ni steels of the austenitic grade of the FeCr-18 – 20Ni-9 – 13 system shows that they are identical in full to those of the welds produced without the activators. Mass fractions of the basic alloying elements (chromium, nickel, manganese, silicon, etc.), including gases, in the metal of both welds do not change.

Steels of the chrome-nickel austenitic-martensitic grade of the FeCr-16Ni-4 type exhibit the same peculiarities. The welds are well formed in the thickness range investigated (up to 20 – 25 mm). After welding, steels of this type should be subjected to standard tempering. This provides full-strength welded joints with good ductility and toughness of the weld metal.

Duplex Cr-Ni-Mo steels of the FeCr-18 – 30Ni-4 – 8MoTi system can also be well welded using the activators. Since in this case the weld cooling conditions change (more intensive heat transfer to the base metal across the weld section at a lower welding heat input), redistribution of the ratios of the austenitic and ferritic phases may occur in the weld. Optimization of phase composition of the weld metal is achieved in welding in a mixture of argon with small additions

Table 1. Examples of the joints which can be made by the A-TIG welding method

Types of joints	Character of making a weld	Shape of the weld cross section	Limits of the values of thickness S and root faces t , mm
Butt	One-sided		$S_1 = 1 - 8$ $S_2 = 8 - 12$ $S_3 = 9 - 25$ and more $t = 5 - 8$
	Two-sided		$S_1 = 8 - 16$ $S_2 = 16 - 25$ $t_1 = 5 - 8$ $S_3 = 16 - 25$ and more $t_2 = 8 - 12$
Corner	One-sided		$S_1 = 1 - 8$ $S_2 = 3 - 20$ and more
	Two-sided		$S_1 = 5 - 20$ and more $S_2 = 5 - 60$ $t = 3 - 6$
T	-		$S_1 = 3 - 6$ and more $S_2 = 3 - 6$ and more $S_3 = 4$ $S_4 = 5$ $S_5 = 6$
Overlap	-		$S_1 = 1.5 - 3.0$ $S_2 = 1.5 - 3.0$

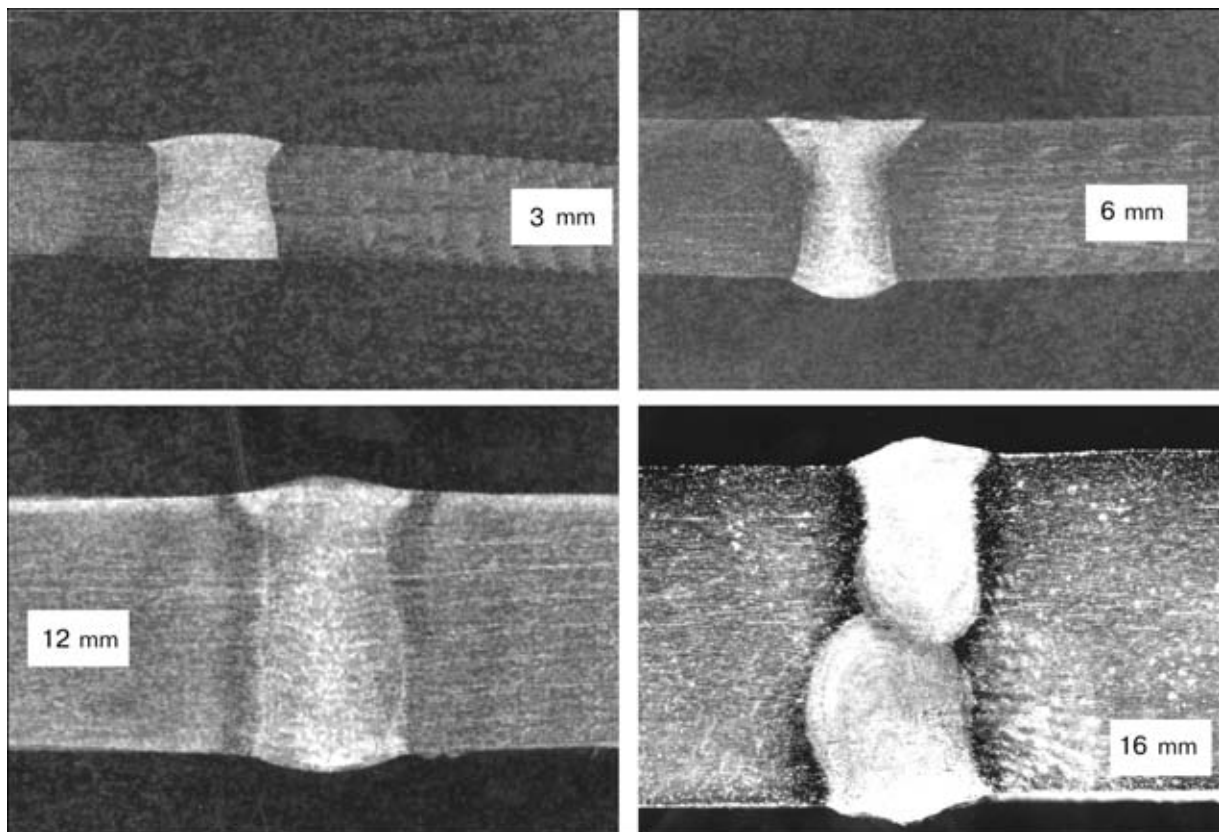


Figure 2. Macrosections of the A-TIG welded joints in steel 301L of different thickness

Table 2. Chemical composition of materials welded by the A-TIG welding method

Steel (alloy) class	Grade	Content of elements, wt. %							
		C	Si	Mn	Cr	Ni	Mo	Ti	Al
Stainless	304L	0.07	0.6	1.7	19.5	9.0	0.45	< 0.10	–
	316L	0.017	0.75	1.9	18.5	13.0	2.75	< 0.12	–
	321	0.17	0.62	1.63	17.4	9.67	0.27	0.15	–
Duplex	23Cr-6Ni	0.03	0.3	1.5	23.0	6.0	–	–	–
	Avesta SAF2205	0.02	0.41	1.65	22.3	5.7	3.09	–	–
Austenitic-marten- sitic	16Cr-6Ni	0.043	0.14	0.6	16.06	6.0	–	–	–
Martensitic	16Cr-4Ni	0.04	0.33	0.5	15.33	4.65	0.14	–	–
Ferritic-martensitic	12Cr-Mo	0.1	0.28 – 0.32	0.47 – 0.57	11.5 – 11.9	0.44	0.42	< 0.01	0.012 – 0.030
Chrome-molybde- num	2.25Cr-1.0Mo	–	–	–	2.25	–	1.0	–	–
Carbon-manganese	50D	0.13	0.63	1.07	0.01	0.01	< 0.005	< 0.002	0.052
	43A	0.1	0.19	0.52	0.01	0.01	< 0.005	< 0.002	0.07
Nickel alloys	Inconel 600	0.032	0.29	0.27	16.0	74.45	–	–	–
	Inconel 690	–	–	–	29.0	61.5	–	–	–
	Inconel 718	0.01 – 0.05	0.75	0.5	17.0 – 21.0	50.0 – 55.0	2.8 – 3.3	0.3 – 1.3	0.2 – 1.0
	Inconel 738LC	–	–	–	16.0	54.0	1.75	3.45	3.45
	Inconel 939	0.15	–	–	22.4	47.0	–	3.7	1.9
	Nimonik-75	0.14	0.14	0.39	21.0	74.6	–	0.28	–
	Hastelloy X	0.1	–	–	22.0	46.5	9.0	–	–
	Hayness 230	0.05	0.5	0.65	23.0	59.1	2.0	–	0.35

Table 2 (cont.)

Steel (alloy) class	Grade	Content of elements, wt. %							Other
		Fe	Co	P	S	W	O		
Stainless	304L	–	0.062 – 0.21	0.009 – 0.031	0.002 – 0.1	–	0.005	0.07 – 0.16Cu 0.02 – 0.08V 0.032 – 0.056 N 0.08 – 0.35Cu	
	316L	–	–	0.017 – 0.032	0.001 – 0.004	–	0.0045 – 0.0085	0.04 – 0.07V 0.02 – 0.073N	
	321	–	0.11	0.002	0.002	–	–	0.41Cu 0.011N	
Duplex	23Cr-6Ni	–	–	–	–	–	–	N (not determ.)	
	Avesta SAF2205	–	0.08	0.021	–	–	–	0.18Ni 0.14Cu	
Austenitic-marten- sitic	16Cr-6Ni	–	–	–	0.001	–	–	0.22Cu	
Martensitic	16Cr-4Ni	–	–	0.02	0.01	–	–	–	
Ferritic-martensitic	12Cr-Mo	–	–	0.013 – 0.019	0.001 – 0.014	–	0.002 – 0.003	0.00005 – 0.0023Ca 0.016 – 0.036N	
Chrome-molybde- num	2.25Cr-1.0Mo	Balance	–	–	–	–	–	–	
Carbon-manganese	50D	Same	< 0.005	0.014	0.011	–	0.0018	0.025Nb 0.01Cu	
	43A	»	–	0.011	0.012	–	0.0015	0.04Cu	
Nickel alloys	Inconel 600	8.3	–	–	0.004	–	–	0.09Cu	
	Inconel 690	9.0	–	–	–	–	–	–	
	Inconel 718	Balance	–	–	0.03	–	–	0.75Cu	
	Inconel 738LC	Same	8.5	–	–	2.6	–	1.75Ta 0.85Nb	
	Inconel 939	–	19.0	–	–	2.0	–	1.4Ta 1.0Nb	
	Nimonik-75	3.4	–	0.008	0.001	–	0.0175	–	
	Hastelloy X	18.5	1.5	–	–	0.6	–	–	
Hayness 230	–	–	–	–	–	–	0.028La		

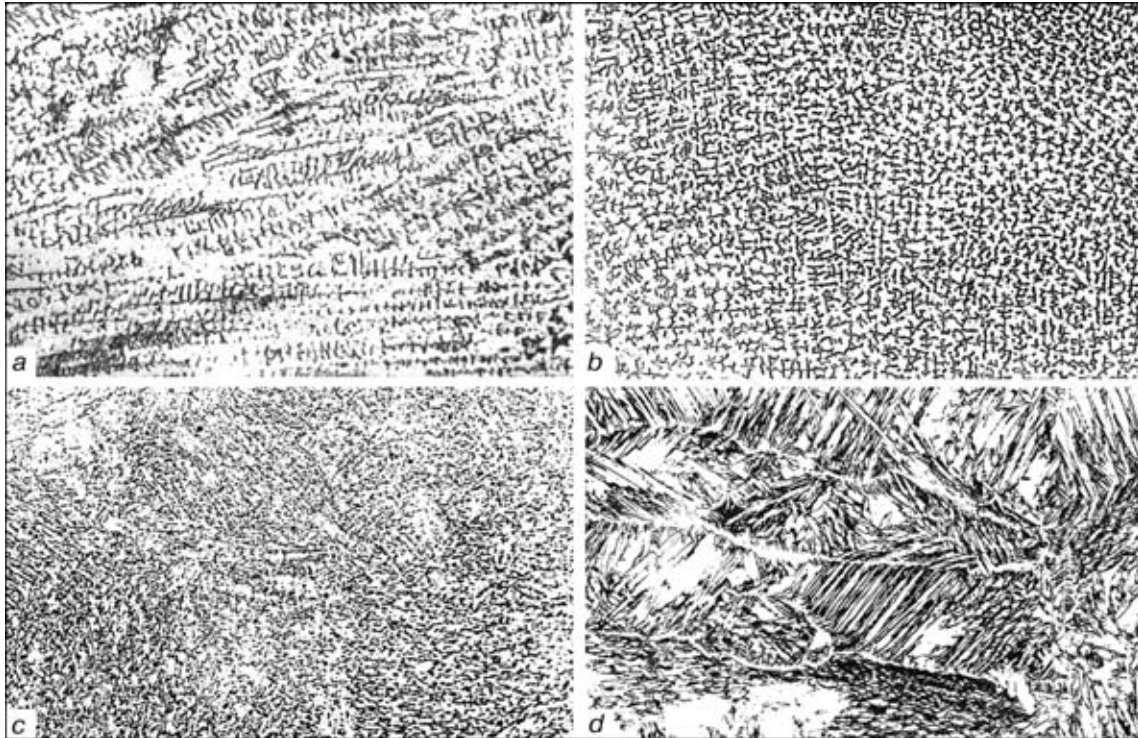


Figure 3. Microstructures of A-TIG weld metal on different steels: *a* – Fe-19Cr-9Ni (304L); *b* – Fe-18Cr-13Ni (316L); *c* – Fe-16Cr-4Ni; *d* – Fe-23Cr-6Ni-MoTi



Figure 4. Microstructures of A-TIG weld metal on different nickel alloys: *a* – Nimonic-75; *b* – Inconel 600; *c* – Hastelloy X

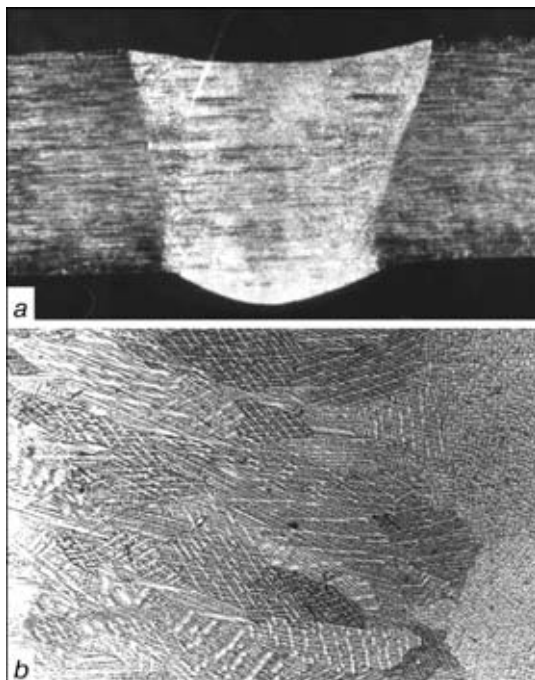


Figure 5. Macrosection (*a*) and microstructure (*b*) of A-TIG weld metal on Cu-Ni alloy Cu-70Ni-30, 5 mm thick

of nitrogen ($\approx 2 - 4 \%$), which has no effect on the process stability and weld shape.

Similar results using the activators are obtained also on other Fe-base steels of different alloying systems. Peculiarities of their structural state may affect mechanical properties of the weld (especially in the case of welding without a filler). As it has been mentioned above, the appropriate heat treatment provides mechanical properties of the weld metal and joint as a whole identical to those of the base metal. This was confirmed in welding chromium ferritic steels of the

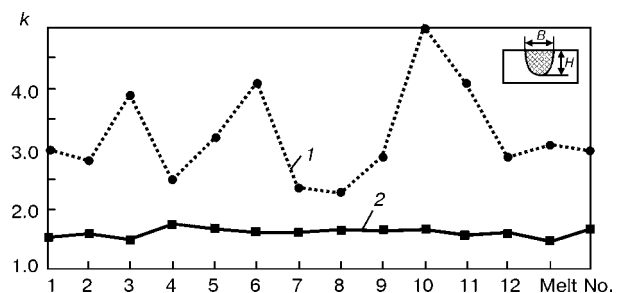


Figure 6. Variations in the weld aspect ratio ($k = B/H$, where B is the weld width and H is the penetration depth) in argon-arc welding of 14 different melts of stainless steel 304L: 1 – TIG; 2 – A-TIG

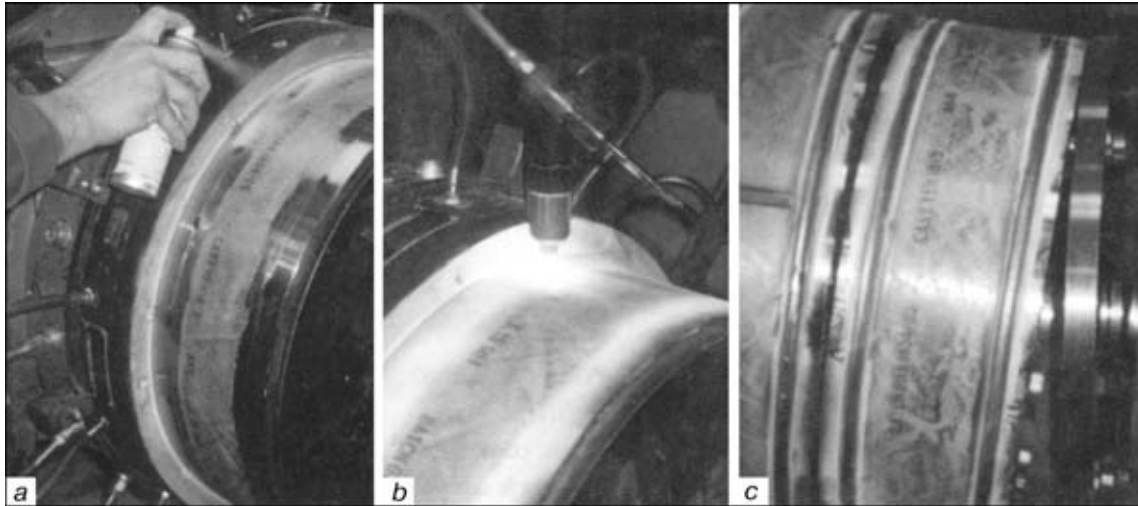


Figure 7. A-TIG welding of a component of the gas turbine engine cylindrical casing made from nickel alloy Nimonic-75, 3.25 mm thick [16]: *a* – manual application of the aerosol activator to a joint prior to welding; *b* – mechanized A-TIG welding; *c* – weld

Fe17 – 28Cr type, martensitic-ferritic steels of the Fe9 – 14Cr type, as well as low-alloy steels of the bainitic and martensitic grades.

Microstructures of the weld metal produced by A-TIG welding of some steels are shown in Figure 3. They are typical for this type of materials.

Nickel alloys have a somewhat different behaviour in A-TIG welding, which is associated with their low thermal conductivity and, in a number of cases, with an increased content of special alloying elements (titanium, aluminium). Alloys of the Cu–Ni system, on the contrary, have a very high thermal conductivity, which affects penetration and weld formation.

Table 2 gives chemical compositions of a number of nickel alloys for which the PATIG N-A series activators were developed. Figure 4 shows typical microstructures of the weld metal on a number of nickel alloys. In all the cases we achieve the main benefits of the use of an activating flux: increase in penetration (hence, productivity), decrease in the number of passes and decrease in heat input.

Main difficulties for welding arise in the case of materials with a high thermal conductivity (aluminium, copper and alloys on their base). As to the latter case, we managed to develop activating fluxes for this grade of materials. So far, the effect here is not that substantial as in the case of welding of Fe- and Ni-base alloys. Nevertheless, penetration has been

almost doubled. Figure 5 shows macro- and micro-structure of the weld metal on alloy Cu–70Ni–30.

Experiments allow a conclusion of the possibility of making activating fluxes which could provide an increase in penetration (or decrease in heat input) and suit many methods of welding and types of materials, provided that an appropriate arc contraction concentration of energy released at the anode and convective flows in the weld pool are achieved.

A distinctive feature of welding using activators is that this process provides almost identical weld shape for similar types of steels, i.e. metal received from different suppliers and manufactured by different technological processes (melting in arc or induction furnaces, vacuum of electroslag vacuum-arc or electron-beam remelting), and behaves similarly in terms of penetration and weld formation.

Figure 6 shows the data on variations in the weld shape in TIG and A-TIG welding for different melts of stainless steel of the 304L grade (FeCr–18Ni–10). It is apparent that the activator levels the effect of the metal manufacturing method, which is especially important for fabrication of critical structures in terms of guaranteed reproducibility of the welding technology and weld quality.

Cost effectiveness of application of the activators is very high. It is provided due to the following factors:

Table 3. Comparison of cost effectiveness of A-TIG and conventional TIG welding methods

Welding method	Technology	Welding speed, mm/min	Costs, US \$/m					
			Gas	Wire	Salaries	Production costs	Power	Total
TIG	4 passes (1 – root weld, 2 – 4 – filling welds, TIG + wire)	55	3.53	3.02	79.25	0.79	0.13	86.72
A-TIG	1 pass (A-TIG welding without wire)	80	0.90	–	13.61	0.13	0.01	14.65

Notes. 1. Calculation was made for welding of 316L stainless steel pipes 100 mm dia. with wall thickness of 5.7 mm. 2. All calculations were made using the WELDCOST software developed by TWI (Great Britain), where the salary is assumed to be US \$ 40 per hour. 3. The saving achieved from use of one can of the aerosol activator PATIG S-A, intended for a running weld length of 10 – 15 m, is about US \$ 700 – 1000.

- decrease in the number of passes;
- decrease in the amount of the deposited metal through avoiding groove preparation;
- elimination of the need to use a filler wire;
- reduction of labour costs for performing, grooving and repeated welding of the root weld;
- decrease in overall power and labour consumption.

Table 3 shows a comparative analysis of cost effectiveness of the TIG and A-TIG welding methods by an example of making circumferential welds on pipes. The data of this analysis prove the efficiency of use of the activators.

One should note a substantial commercial experience accumulated in using the aerosol activators PATIG in Great Britain by ABB Alstom Power UK, Ltd. [16]. This Company, in collaboration with the PWI, conducted the work on making and utilization of the activators for English carbon steels and nickel alloys [17]. Figure 7 shows an example of A-TIG welding of circumferential welds on a cylindrical casing of the gas turbine power plant made from nickel alloy Nimonic-75, 3.25 mm thick [16].

The many-year experience is indicative of considerable advantages of using activators for the fabrication of structures in heat and nuclear power generation, chemical, oil, aerospace engineering, ship building, food processing machine-building, boiler construction and other industries, as well as in the manufacture of tubes and pipes and their products.

CONCLUSIONS

1. The PWI developed new types of activating fluxes of the PATIG series for welding different grades of steels and some Ni-base alloys. The aerosol activator has been developed and validated for the fabrication of actual welded structures.

2. The range of structural materials and types of joints which can be welded using the aerosol activators has been widened.

3. The use of the activators allows an increase of 2 – 4 times in the penetration depth, minimizing or elimination of the effect of cast-to-cast variation on penetration, single-pass welding of butt joints up to 10 – 12 mm thick without groove preparation, elimination of different types of defects (pores, cracks, lack of penetration, etc.) by remelting the metal to a depth of down to 12 mm without machining of

defects, reduction in welding strains, increase in productivity of welding operations by a factor of 2 to 7 and decrease of 3 – 6 times in the materials and labour consumption.

REFERENCES

1. Gurevich, S.M., Zamkov, V.N., Kushnirenko, N.A. (1965) Increase in efficiency of penetration of titanium alloys in argon-arc welding. *Avtomaticheskaya Svarka*, **9**, 1 – 4.
2. Simonik, A.G., Petriashvili, V.I., Ivanov, A.A. (1976) Effect of the arc discharge contraction in adding electrically negative elements. *Svarochnoye Proizvodstvo*, **3**, 49 – 51.
3. Ostrovsky, O.E., Kryukovsky, V.N., Buk, B.B. *et al.* (1977) Effect of activating fluxes on penetrating power of the welding arc and concentration of the energy in the anode spot. *Ibid.*, **3**, 3 – 4.
4. Paton, B.E., Makara, A.M., Medovar, B.I. *et al.* (1974) Weldability of structural steels subjected to refining remelting. *Avtomaticheskaya Svarka*, **6**, 1 – 4.
5. Savitsky, M.M., Leskov, G.I. (1980) Mechanism of the effect of electrically negative elements on penetrating power of the arc with a tungsten electrode. *Ibid.*, **9**, 17 – 22.
6. Paton, B.E., Zamkov, V.N., Prilutsky, V.P. *et al.* (2000) Contraction of the welding arc caused by the flux in tungsten-electrode argon-arc welding. *The Paton Welding J.*, **1**, 5 – 11.
7. Savitsky, M.M., Kushnirenko, B.N., Olejnik, O.I. (1999) Peculiarities of tungsten-electrode welding using an activating flux (A-TIG process). *Avtomaticheskaya Svarka*, **12**, 20 – 29.
8. Eriksson, J., Limu, H., Hannerz, N. *et al.* (1997) Welding tests on stainless steel with the Paton A-TIG method. In: *Proc. of the 5th World Conf. on Duplex Stainless Steel*, Maastricht, Oct. 21 – 23. Maastricht.
9. Paskell, T., Lundin, C., Castner, H. (1997) GTAW flux increases weld joint penetration. *Welding J.*, **4**, 57 – 62.
10. Perry, N., Morya, S., Soutif, E. (1998) Study and development of flux enhanced GTA penetration in a commercial grade titanium. In: *Proc. of the 5th Int. Conf. on Trends in Welding Research ASM/AWS*, Pipe Montain, Georgia, June 1 – 5. Georgia.
11. Yushchenko, K.A., Kovalenko, D.V. (1994) Collaboration between TWI and PWI. *Avtomaticheskaya Svarka*, **1**, 54 – 55.
12. Yushchenko, K.A., Savitsky, M.M., Kovalenko, D.V. (1993) A-TIG welding of carbon-manganese and stainless steel. In: *Proc. of Conf. on Welding Technology of PWI*, Abington, Oct. Abington.
13. Lucas, W., Howse, D. (1996) Activating flux – increasing the performance and productivity of the TIG and plasma processes. *Welding and Metal Fabrication*, **1**, 11 – 17.
14. Stankevich, I.Ya., Dmitriev, V.I., Karida, V.L. *et al.* (1982) Application of the activating flux for automatic welding of the nuclear power plant pipings. *Energetich. Stroitelstvo*, **10**, 19 – 20.
15. Yushchenko, K.A., Kovalenko, D.V., Kovalenko, I.V. (1998) Aerosol activator PATIG S-A for A-TIG welding of steels. *Svarshchik*, **3**, 21 – 22.
16. Lucas, W. (2000) Activating flux – improving the performance of the TIG process. *Welding and Metal Fabrication*, **2**, 7 – 10.
17. Yushchenko, K.A., Kovalenko, I.V., Kovalenko, D.V. *et al.* (2000) A-TIG welding of nickel alloy Nimonic-75. *Svarshchik*, **4**, 26 – 27.

AUTOVACUUM BRAZING OF STEEL IMPELLERS OF CENTRIFUGAL COMPRESSORS

V.N. RADZIYEVSKY, G.G. TKACHENKO and Yu.F. GARTSUNOV
 VNIImkompessormash, Sumy, Ukraine

ABSTRACT

It is shown that argon-arc welding combined with brazing to form a large fillet of a metal powder can provide a reliable T-joint in hard-of-access channels in the centrifugal compressor impellers. Simple-to-perform autovacuum heating applied for brazing allows cleaning of surfaces prior to melting of a brazing filler alloy, promotes formation of the frame of a powder in a large fillet and creates conditions for formation of a composite metal structure with required mechanical properties.

Key words: *argon-arc welding, brazing, autovacuum heating, surface cleaning, structurization, formation of a fillet, formation of a frame, impeller, T-joint, metal powder, brazing filler alloy*

Reliability and durability of a centrifugal compressor depend in many respects upon the fatigue strength of the most loaded component, i.e. impeller. High-capacity compressors include the closed-type impellers (Figure 1) consisting of two disks (main and covering), which are connected to each other by blades. The blades are milled in a body of one of the disks or formed separately from a plate and then joined to the disks by welding or brazing. Outside diameter of the impeller is 200 – 1200 mm and the width of a channel on the outside diameter is 5 – 60 mm. The impellers are manufactured from strong steels with a yield point of more than 800 MPa. Providing that the channel is sufficiently wide, a T-joint between the disk and the blade is made by two-sided welding with a required leg of the fillet weld. If the channels are narrow, welding is difficult to perform. So, in this case joining is done through slots made in the disk. This adds complexity to the welding process because of the necessity to achieve a guaranteed penetration to form fillets of a molten or close to molten metal in a T-joint.

As shown in [1], it is best to use simultaneously EBW and brazing to achieve the guaranteed formation of the quality fillets. For this a strip of a brazing filler

alloy is placed in a gap between workpieces and then the electron beam is used to penetrate the disk and partially the blade. EBW causes the strip to melt and form fillets under the effect of capillary forces.

A reliable and strong joint between the disk and the blades is ensured by the brazing process performed in vacuum using a high-strength Pd-based filler alloy [2 – 5]. However, in T-joints, where a fillet is formed by the molten filler alloy under the effect of capillary forces, the radius of the fillet is no more than 1 mm. At $R = 2S$ (R is the radius of the fillet and S is the tee wall thickness), the fillet is known to induce no concentration of stresses. Normally the blades and disks are not less than 4 mm thick. Therefore, the fillet with a radius of 1 mm acts as a substantial stress raiser and leads to fatigue fracture of the disks. In this case the fatigue strength of a T-joint is almost half of that of the base metal.

It is shown in [6] that fatigue strength of a brazed T-joint can be brought up to the level of the base metal by formation of a required size of the fillet from a metal powder impregnated with the brazing filler alloy melt during vacuum heating. Along with advantages, the brazing technology involving formation of large-radius fillets has a serious drawback. The fillet is formed from a paste which consists of a metal powder bonded by a copolymer solution. After evaporation of a solvent and solidification of the paste, the impeller is heated in a furnace to the brazing temperature, at which the molten filler alloy impregnates the fillet to join it to the base metal. Nonuniform heating of the impeller components associated with their different thickness, as well as phase transformations of the metal structure, result in a deformation which changes the gap size, this leading to fracture of the fillets formed of a metal powder. They are cracked or separate from the base metal. Cracks are not filled with the molten filler alloy during brazing, because the melt does not flow from the microcapillary channels between particles of the powder to wider channels formed by the cracks.

Of interest is fixation of the impeller components by fusion welding prior to formation of the large-ra-



Figure 1. Centrifugal compressor impeller

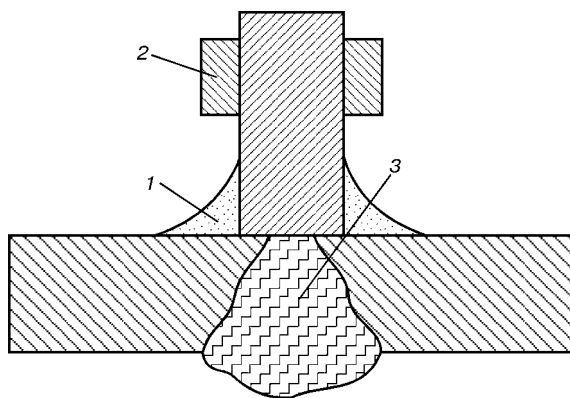


Figure 2. Schematic of the braze-welded T-joint: 1 – braze joint fillet; 2 – brazing filler alloy; 3 – weld

dus fillets from a metal powder (Figure 2). Argon-arc welding performed through slots in a cover disk, combined with subsequent brazing using autovacuum heating, shows promise for this application (Figure 3) [7]. A sorbent of powders of reactive metals creates vacuum with a low partial oxygen pressure in a cavity of the impeller sealed by welding of the process plugs and shroud. These conditions provide a quality impregnation (comparable with brazing in vacuum furnaces) of the weld fillets formed of a metal powder by the molten brazing filler alloy. The welds constituting 50 – 70 % of the blade length provide a reliable elimination of the risk of fracture of the fillets made from a powder in heating to the brazing temperature.

The blade is welded through its entire thickness to the disk to form a defect-free combined T-joint. In this case probable laps and deformation of the surface in a corner of the T-joint are not discarded, as all the shape defects are repaired by subsequent formation of the powder fillet.

In welding through thickness of the blade, the metal surface in the HAZ is oxidized. This zone is located in places of formation of the braze joint fillets. Therefore, removal of an oxide film from the surface is a necessary condition to achieve the quality brazing. No abrasive grinding or etching is permitted, as they cause contamination of the brazing gaps. The efficient method is «self-cleaning» of the metal surface from the oxide film in autovacuum heating [8]. It is shown in [9] that in autovacuum heating to 900 °C the oxide film of a blue-violet colour, 60 – 70 μm thick, formed on carbon steel (such a film is formed in the weld zone on the impeller) is reduced to pure iron to form a rough surface, which promotes wetting and spreading of the molten brazing filler alloy. Therefore, no difficulties associated with surface cleaning arise in autovacuum brazing of steel T-joints in the impellers of structural carbon steels. However, the impellers are made mainly from alloyed steels (07Kh16N6 (C – 0.07; Cr – 16.0; Ni – 6.0 wt.%; Fe – balance), 13KhGMRB (C – 0.12; Cr, Mn, Mo – up to 1.0; Ni – up to 0.2 wt.%), 14Kh2GMR (C – 0.14; Cr – 2.0; Mn, Mo – 1.0; W – 0.4 wt.%), 20KhN3FA (C – 0.2; Cr – 1.0; Ni – 3.0; V – 0.3 wt.%)). «Self-cleaning» from the oxide film on the above steels has a bit different character

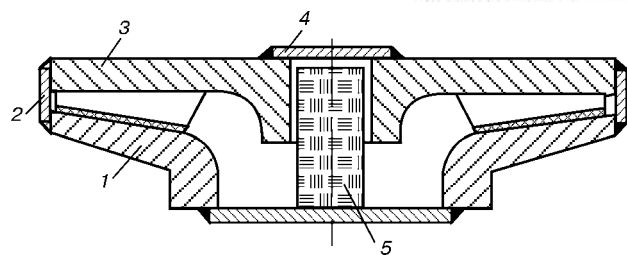


Figure 3. Schematic of the process of autovacuum brazing of the impeller: 1 – disk; 2 – shroud; 3 – disk with blades; 4 – process plug; 5 – cartridge with a sorbent and activator

and ends at a temperature of above 1000 – 1100 °C, depending upon the steel composition. This may lead to formation of a defective brazed joint, as the selected brazing temperature for a number of reasons is 900 – 1050 °C. In this case the molten brazing filler alloy impregnates the powder fillets, while the base metal remains uncleaned from the oxide film. This joint fractures by a brittle mechanism directly in the joining zone. To provide the guaranteed cleaning of the oxidized surface, it is necessary that a halide-containing salt, whose vapours activate the deoxidation process, be added to the sorbent composition [10].

Special powders meeting a number of requirements should be used for formation of a brazed joint. Firstly, they should form, with a copolymer solution, a plastic paste which would allow formation of a smooth fillet in the T-joint, characterized by a gradual transition to the base metal. This characteristic depends both upon size and shape of the powder particles. Secondly, in heating the powder should help retain the shape of the fillet and its bonding to the base metal. Thirdly, size and shape of the powder particles should provide formation of the microcapillary channels to ensure their reliable filling with the brazing filler alloy melt. Fourthly, the powder composition should be selected so that an active mutual diffusion of components occurs in the process of interaction of the brazing filler alloy with the melt to cause an isothermal solidification of the weld metal and increase in its mechanical properties. Powders of Fe–Ni alloys, i.e. permalloys, meet these requirements.

In selection of the powder composition, it is necessary to take into account the peculiarity of autovacuum heating. At the first stage of heating to 500 – 600 °C, oxidation of the sorbent is accompanied by oxidation of the base metal and powder in the fillets. At a temperature above 600 °C the partial pressure of oxygen is drastically decreased, and cleaning of the surfaces from the oxide film begins. A rough film of the reduced metal, promoting formation of a diffusion bond at the contact points, is formed on the surface of the powder particles (Figure 4). The formed frame of the joined particles maintains the shape of the fillet in its impregnation by the molten brazing filler alloy. Activity of the process can be controlled by selection of a proper powder composition.

It is indicated to perform autovacuum brazing of the impeller at a minimum possible temperature, at which the required mechanical properties of a brazed

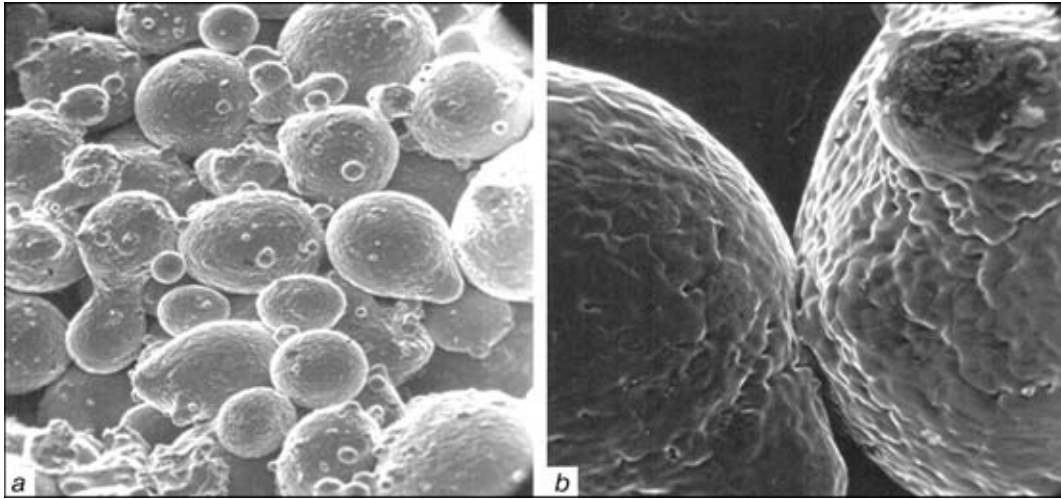


Figure 4. Fractogram of fracture of the fillet frame formed from the permalloy powder (*a* – $\times 1500$; *b* – $\times 3000$) (reduced by 4/5)

joint are ensured. An increase in temperature in autovacuum heating requires an increase in technological allowances on the outside surfaces of the disks to avoid their deformation under the effect of the atmospheric pressure, whereas an increase in thickness of the disks is undesirable because it makes welding in deep slots more difficult. In addition, an increase in temperature favours growth of grain in the metal and oxidation of the grain boundaries on the outside surface of the disks. Temperature within a range of 900 – 1050 °C seems optimal, as it is at this temperature that normalizing, hardening or austenization of steels used for the fabrication of the impellers occur. Since the steel impellers are not designed for compression of aggressive gases, the brazing filler alloys on a Cu–Mn base are most suitable for the techno-

logical process under consideration. Alloying of the Cu–Mn base with nickel and dispersing elements allows selection of the filler alloy with a required melting point to ensure desirable mechanical properties of the joints in diffusion interaction with the powder [11].

According to the process conditions, the powder particles should be 50 – 150 μm in size. The weld metal formed by impregnation of the powder with this size of the particles by the Cu–Mn brazing filler alloy melt has low ductile properties at a short-time holding under the brazing temperature conditions. At a long isothermal holding the liquid phase in contact of the particles is solidified and the molten filler alloy causes dispersion of the powder particles in gaps between the particles [12]. Holding for 40 – 60 min leads to formation of a homogeneous brazed joint metal, which consists of an alloyed Cu–Mn–Ni matrix reinforced with spheroidal particles 2 – 20 μm in size formed from the powder (Figure 5). Metal with such a homogeneous equilibrium fine-dispersed structure is characterized by the following mechanical properties: $\sigma_y = 340 \text{ MPa}$, $\sigma_t = 640 \text{ MPa}$, $\delta = 30 \%$, $\psi = 60 \%$, $KCU = 120 \text{ J/cm}^2$ and $HB 160$. The above properties provide the T-joint metal in the impeller with strength equal to that of the base metal, providing that the size of the fillet is properly selected.

One should note the advantage of autovacuum heating during the process of formation of the brazed joint metal structure. Brazing is characterized by a short-time holding, during which a structurally heterogeneous joint is formed as a rule. An extension of holding for the diffusion processes occurring during brazing in an atmosphere is not indicated because of the risk of oxidation, whereas in vacuum brazing with a continuous evacuation of gases it is intolerable because of the risk of evaporation of elements with a high vapour pressure. In this case properties of the brazing filler alloy and conditions of formation of a joint change to a considerable degree. Autovacuum heating leads to formation of a neutral low-rarefaction atmosphere, in which an equilibrium pressure of va-

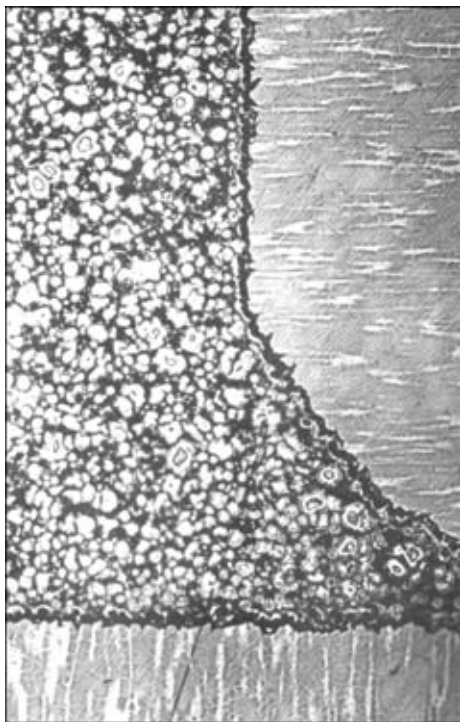


Figure 5. Microstructure of the composite weld metal formed using an alloyed copper-manganese brazing filler alloy and permalloy powder ($\times 50$) (reduced by 4/5)



pours of metal and reactive compounds is established. This allows addition of readily evaporating metals to the brazing filler alloys and an active salt — to the sorbent to create optimal conditions for formation of the joints.

The technology of autovacuum brazing of combined T-joints was tested in the fabrication of impellers with channels 8 to 60 mm wide. Full-scale tests of the braze-welded impellers proved reliability of the resulting joints.

The development results make it possible to consider this technology of the fabrication of the impellers to be promising, as its implementation requires no expensive materials and no special equipment. It can be applied using insignificant capital expenses in mass or customized production for the fabrication, repair and upgrading of centrifugal compressors.

CONCLUSIONS

1. The use of argon-arc welding with through penetration of a blade via a slot in the disk, combined with brazing to form large-radius fillets from a metal powder, leads to elimination of drawbacks characteristics of each of the methods of making T-joints in impeller components.

2. Autovacuum heating used during brazing creates optimal conditions for formation of a joint at all its stages: surface preparation, formation of a frame from particles and structurization of the weld metal. Physical-chemical and metallurgical processes occurring at all the stages of formation of a joint can be controlled

through selection of a required composition of the process consumables.

REFERENCES

1. Myers, L.W., LaFlamme, G. (1998) Electron beam braze welding of compressor impellers. *IIW Doc. IV-732-98*.
2. Radziyevsky, V.N., Bondarev, A.A., Rymar, V.I. (1971) Brazing of centrifugal machine impellers. *Svarochnoye Proizvodstvo*, **3**, 40 – 41.
3. Radziyevsky, V.N., Lotsmanov, S.N., Rymar, V.I. (1974) Braze centrifugal compressor impellers of low-alloyed steels. *Khim. i Neft. Mashinostroyeniye*, **8**, 3 – 8.
4. Radziyevsky, V.N., Rymar, V.I., Chernov, V.Yu. (1976) Technology for fabrication of all-braze centrifugal compressor impellers. *Ibid.*, **12**, 10 – 12.
5. Radziyevsky, V.N., Rymar, V.I. (1978) Vacuum brazing of centrifugal compressor impellers of steel 07Kh16N6. *Ibid.*, **5**, 9 – 11.
6. Radziyevsky, V.N., Rymar, V.I., Beshpalov, V.K. (1991) Vacuum brazing of T-joints with a large fillet of a powder. *Svarochnoye Proizvodstvo*, **8**, 5 – 6.
7. Rymar, V.I., Lotsmanov, S.N., Radziyevsky, V.N. *et al.* (1973) Interaction of manganese, chromium and titanium with air under conditions of autovacuum heating during brazing. *Ibid.*, **11**, 6 – 8.
8. Kuchuk-Yatsenko, S.I., Kharchenko, G.K., Falchenko Yu.V. *et al.* (1998) Self-cleaning of the mating surfaces from oxides in solid-state welding using heating. *Avtomaticheskaya Svarka*, **2**, 16 – 23.
9. Radziyevsky, V.N., Gartsunov, Yu.F. (1990) Cleaning of surface of carbon steel from an oxide film in autovacuum heating. *Svarochnoye Proizvodstvo*, **5**, 31 – 33.
10. Rymar, V.I., Radziyevsky, V.N. *Sorbent for autovacuum brazing of hard-to-braze materials*. USSR author's certificate **803962**, Int. Cl. B 01 J 1/22, B 23 K 35/22. Publ. 15.02.81.
11. Radziyevsky, V.N., Gartsunov, Yu.F., Tkachenko, G.G. (1997) Brazing of steel using copper-manganese cored filler alloy in a wide gap. *Avtomaticheskaya Svarka*, **11**, 18 – 21.
12. Radziyevsky, V.N., Gartsunov, Yu.F., Tkachenko, G.G. (1997) Effect of dispersion of the iron powder core by a copper filler alloy on properties of the braze joint. *Ibid.*, **8**, 18 – 22.